Dissertation
zur
Erlangung des Doktorgrades
der Naturwissenschaften
(Dr. rer. nat.)

Modeling and Simulation of Non-Equilibrium Effects in Modern Semiconductor Nanostructures

dem
Fachbereich Physik
der Philipps-Universität Marburg
vorgelegt von

Ada Bäumner

aus Herdecke/Ruhr
Marburg/Lahn (2016)

Vom Fachbereich Physik der Philipps-Universität Marburg
als Dissertation angenommen am: 19.07. 2016

Erstgutachter: Hr. Prof. Dr. S.W. Koch
Zweitgutachter: Fr. Prof. Dr. K. Volz

Tag der mündlichen Prüfung: 21.07. 2016

Hochschulkennziffer 1180

Zusammenfassung

Die Entwicklung immer effizienterer und leistungsfähigerer Computersysteme ermöglicht immer neue Dimensionen des Experimentierens mit komplexen Modellen. In der Wissenschaft motiviert die steigende Rechenleistung und zunehmende Geschwindigkeit, mit der Rechenprozesse ablaufen können, in den unterschiedlichsten Fachrichtungen den Ausbau einer vergleichsweise jungen Disziplin: rechnergestützte Modellierung und Simulation. Computer-Modelle unterscheiden sich dabei deutlich von den traditionellen Modellen der Wissenschaft, wie sie sich über Jahrhunderte bewährt haben. Sie sind häufig deutlich komplexer, oft wesentlich abstrakter und immer dynamisch. Eben diese in mathematischen Gleichungen steckende Dynamik des Modells ist es, die eine Berechnung erforderlich macht. Die mathematischen Gleichungen, auf denen das Modell basiert, repräsentieren den Zusammenhang der verschiedenen modellrelevanten Parameter und Variablen. Verändert man eine Größe und löst daraufhin die entsprechende Gleichung oder das Gleichungssystem, wird man herausfinden, wie diese Veränderung sich auf das Gesamtergebnis auswirkt. In den meisten Fällen, wird eine solche Rechnung die menschliche Rechenleistungsfähigkeit übersteigen. Aber mit den heutigen Supercomputern wird das Problem lösbar und Experimente mit komplexen dynamischen Modellen, d.h. Simulation, werden möglich. Ein interessantes Beispiel in diesem Zusammenhang ist die Modellierung und Simulation moderner Halbleiterlaserstrukturen.

Sowohl für die Konstruktion neuartiger Bauelemente als auch für die Optimierung bestehender Konfigurationen ist es entscheidend ein umfassendes Verständnis der dem Laserbetrieb zu Grunde liegenden physikalischen Prozesse und ihrer Wechselwirkung zu erlangen. Da ein experimenteller Zugang zu relevanten Schlüsselparametern nicht immer einfach ist und in der Regel auch bereits im Designstadium vor der Fabrikation des ersten Prototypes ein Grundverständnis der genauen Funktionsweise und Zusammenhänge unumgänglich ist, kann ein geeignetes Lasermodell oftmals sehr nützlich und hilfreich sein. So kann ein Modell, das ein quantitatives Verständnis der inneren Funktionsweise eines Lasersystems liefert, die Optimierung des Designs im Hinblick auf Leistung, Kompaktheit, Robustheit und Kosten anstoßen. Bei Problemen im Experiment kann ein Modell einen entscheidenden Beitrag bei der Analyse und dem Auffinden funktionierender Lösungen leisten. Außerdem kann ein Modell dazu herangezogen werden zu prüfen, ob bestimmte verdächtigte Effekte für ein beobachtetes Missverhalten verantwortlich sein können und eine Simulation kann zeigen, ob eine vermutete Verbesserung tatsächlich greift und welche Nebenwirkungen sie eventuell mit sich bringt. Ein Lasermodell macht es desweiteren möglich, Ideen zu testen und somit ein vertieftes Verständnis der relevanten physikalischen Mechanismen und Prozesse zu erlangen.

Grob unterteilt kann man festhalten, dass es zwei verschiedene Arten von Laser-Modellen gibt: Material-Modelle, die die physikalischen Zusammenhänge auf mikroskopischer Grundlage beschreiben und Prozessmodelle die die Funktionsweise oder Eigenschaften des Bauteils beschreiben. In unseren hier zusammengestellten Untersuchungen nutzen wir idealisierte Modelle sowohl für das Material als auch die Funktionalität die es uns ermöglichen die methodische Herangehensweise zu demonstrieren und Licht auf die Vor-und Nachteile der Halbleiterlasermodellierung und -Simulation zu werfen. Zusätzlich erlauben unsere Modellstudien Untersuchungen interessanter und aktueller Fragestellungen der Forschung auf dem Gebiet moderner Halbleiterheterostrukturen. So analysieren wir als erstes Beispiel ein Modell eines optisch gepumpten Oberflächen-emittierenden Lasers mit vertikal angeordneter externer Resonatorstruktur (englisch: vertical external cavity surface emitting laser, (kurz : VECSEL)) im extremen Parameterbereich jenseits des Quasi-Gleichgewichtes [5], [56]. Die Berücksichtigung der damit einhergehenden Nicht-Gleichgewichtseffekte erfordert eine vollständig mikroskopische Beschreibung der Dynamik der elektronischen Ladungsträgerverteilungen im Modell. Anders im zweiten Beispiel der elektrisch gepumpten Halbleiterlaserdiode nahe an der Laserschwelle, bei der die Annahme eines Quasi-Gleichgewichtes der direkt am Laserprozess beteiligten Ladungsträger aufrecht erhalten werden kann. Nicht-Gleichgewichtseffekte kommen hier nur durch ausgleichende Ladungsträger in den höheren Energiezuständen zum Tragen und können

auf Ratengleichungsebene berücksichtigt werden [4].

Die systematische Modellierung moderner Halbleiterlaserstrukturen stellt eine bedeutende Herausforderung für die Formulierung einer physikalisch motivierten Lasertheorie dar, bei der die Beschreibung mikroskopischer Prozesse im Vordergrund steht und nicht das phänomenologische Widerspiegeln empirischer Beobachtungen. Dies gilt insbesondere für VECSEL Anwendungen deutlich oberhalb der Laserschwelle. Unter den verschiedenen Halbleiterlasersystemen hebt sich der VECSEL aufgrund seines einzigartigen Designs mit der externen Resonatorstruktur deutlich hervor. Diese externe Resonatorstruktur kann einerseits als mechanisch unhandlich betrachtet werden, da sie die Laseraufbauten deutlich verkompliziert und im Gegensatz zu einfachen monolithisch integrierten Kanten- oder Oberflächen-emittierenden Halbleiterstrukturen mehr Montage- und Justagearbeiten erfordert. Andererseits jedoch vermittelt die externe Resonatorstruktur VECSEL Anwendungen und Funktionen eine hohe Flexibilität und Einsatzvielfalt. Insbesondere erlauben Anordnungen mit externem Resonator die anpassungsfähige Integration von optischen Elementen wie spektralen Filtern für die Kontrolle der Lasermoden, sättigbaren Absorberkomponenten zur Modenkopplung und Erzeugung ultrakurzer Pulse und nichtlinearen Kristallen zur Frequenzmischung. Darüberhinaus weist der VECSEL aufgrund seiner externen Resonatorstruktur und der damit verbundenen relativ geringen Lichtverstärkung über einen Hin- und Rücklauf im Vergleich zum Beispiel mit gewöhnlichen Kantenemittern deutlich andere Betriebsbedingungen mit deutlich höherer Feldintensität auf, da vergleichsweise stark angeregt werden muss und die Resonatorspiegel eine sehr hohe Qualität haben müssen, um ausreichend Verstärkung zu erzielen.

Da die Emissionscharakteristik des VECSEL-Systems stark von der eigentlichen Geometrie des Aufbaus, den Materialparametern sowohl der dielektrischen Struktur als auch des optisch aktiven Materials und den Anregungsbedingungen abhängt, ist die mikroskopische Modellierung und Simulation der Eigenschaften einer solchen Struktur ein absolut nicht triviales Problem. Während es in vielen Situationen angemessen ist anzunehmen, dass die hohen Ladungsträgerdichten und damit verbundenen schnellen Streuprozesse zwischen den Ladungsträgern unter Laserbedingungen zu einer ausreichend schnellen Thermalisierung des Ladungsträgersystems führen, ist so eine Annahme unter typischen VECSEL Anwendungsbedingungen zumeist nicht gerechtfertigt. In diesen Systemen können die Ladungsträgerverteilungen mitunter stark von den Fermi-Dirac Verteilungen des thermalisierten Quasi-Gleichgewichtes abweichen, da stimulierte Emission hier dazu neigt, in der energetischen Umgebung des Laserübergangs kinetische Löcher in die Ladungsträgerverteilungen zu brennen [6]. Eine der Simulation von Nicht-Gleichgewichtseffekten zugrundeliegende Theorie muss daher in der Lage sein, die zeitliche kinetische Dynamik der Ladungsträger des optisch aktiven Materials zu verfolgen. Der Betrieb moderner Halbleiterheterostrukturlaser im extremen Parameterbereich wird somit durch ein kompliziertes Zusammen- und Wechselspiel einer Vielzahl an Prozessen bestimmt, die sich auf verschiedenen Zeitskalen abspielen. So liegt die charakteristische Zeit für optisches Dephasieren und Ladungsträgerstreuung im Sub-Picosekunden-Bereich, während sich stabile Laseroszillationen über einige Nanosekunden aufbauen und thermische Effekte bis zu wenigen Mikrosekunden beanspruchen können. Dieses Multi-Zeitskalen Problem erfordert Lasermodelle, die eine Brücke schlagen zwischen mikroskopischer und makroskopischer Physik und die numerisch anspruchsvolle Simulation von Halbleiterlaserexperimenten praktikabel machen. Die größte Herausforderung dabei ist es die richtige Balance zu finden zwischen einer mikroskopischen physikalisch motivierten Charakterisierung und einer rein phänomenologischen Beschreibung der Eigenschaften, um alle relevanten Informationen zu integrieren und gleichzeitig die numerischen Kosten gering zu halten.

Vollständig mikroskopische Modelle lösen die zeitliche Dynamik der Streuprozesse auf und sind damit geeignet für die Analyse von Nicht-Gleichgewichtseffekten. Sie sind jedoch sehr rechenintensiv und erlauben in der Regel nur sehr kurze Simulations-Zeiten, so dass sie insbesondere zum Beispiel für die Untersuchung von Anschwingvorgängen des Lasers praktikabel und bereichernd sind [12]. Für Studien über längere Simulationszeiten ist eine Theorie entwickelt worden, die die vollständig mikroskopische Beschreibung der Streuprozesse in der Berechnung der Lasereigenschaften und -funktionalität durch effektive Streuraten annähert, die vorab

berechnet und für die Simulation bereitgestellt werden [69, 70]. Die mikroskopische Konsistenz einer solchen Theorie erfährt dadurch zwar einen Bruch, der aber durch die Berechnung parametrischer Streuraten abhängig von beispielsweise Temperatur, Dichte und Anregungsenergie auf mikroskopischer Grundlage weitgehend geschlossen werden kann.

Der den hier zusammengestellten Untersuchungsergebnissen zugrundeliegende Modellansatz basiert auf solch einer effektiven Streuraten-Näherung. Das Lasersystem besehend aus Halbleiterverstärkungsmedium, dielektrischer Resonatorstruktur und Lichtfeld wird im Rahmen der semi-klassischen Maxwell Halbleiter Bloch Gleichungen beschrieben [42]. Vielteilchen Coulomb-Effekte werden auf der Ebene der Hartree-Fock Näherungen integriert. Um unser Modell zu testen und die Relevanz von Nicht-Gleichgewichtseffekten zu studieren, wählen wir das Beispiel eines traditionellen VECSEL Bauelementes, das Zwei-Farben Emission aufweist [15], sowie das Beispiel der Erzeugung ultrakurzer Pulse durch passive Modenkopplung in einem VECSEL System [63]. Für den Zwei-Farben Betrieb präsentieren wir eine Modellstudie, die deutlich macht, dass unsere weiter oben kurz umrissene Lasertheorie auf Grundlage der MSBE sehr gut für die Beschreibung von Hochleistungslaseranwendungen geeignet ist bei denen Nicht-Gleichgewichtseffekte zunehmend an Bedeutung gewinnen. Zusammengefasst geben unsere mikroskopische Simulationen die erste numerische Bestätigung, dass dynamische stabile Zwei-Farben Emission von Halbleiterlasern erfolgen kann, wenn die Modenkopplung zwischen den beiden relevanten Wellenlängen schwach ausgeprägt ist, wie in dem Artikel *Non-Equilibrium Analysis of the Two-Color Operation in Semiconducor Quantum-Well Lasers* [5] näher erläutert. Durch diese Ergebnisse motiviert nutzen wir den selben Modellansatz um eine erste numerische Simulation von Modenkopplung in einer einfachen VECSEL Struktur durchzuführen und die Rolle der angeregten Ladungsträgerverteilungen zu analysieren, wie ausführlich im Artikel *Non-Equilibrium and Thermal Effects in Modelocked VECSELs* [56] dargestellt.

Die Studien des Einflusses der Ultrakurzzeit-Ladungsträgerdynamik auf den Zwei-Farben Laserbetrieb und die Erzeugung kurzer Pulse in Hochleistungslaseranwendungen mögen als Beispiel dienen für die Tatsache, dass Modellierung und Simulation helfen können, aktuelle Fragestellungen der Forschung darzustellen, zu analysieren und zu beantworten. Als Interessantes Beispiel für die Tatsache, dass Modellierung und Simulation auch dazu dienen kann Arbeitshypothesen zu verifizieren, kann das Problem der Ladungsträgerdynamik in elektrisch gepumpten Halbleiterheterostrukturen herangezogen werden, das wir in dem Artikel *Charging Dynamics in Electrically Pumped Quantum Wells* [4] vorstellen. Hierin haben wir erstmals die häufig genutzte doch bis dahin nicht bewiesene Annahme der Ladungsneutralität der aktiven Region elektrisch gepumpter Halbleiterquantenfilmlaser als gerechtfertigt belegen können. Betreibt man einen Halbleiterquantenfilmlaser elektrisch, wird durch das Einfangen von hochangeregten Barrieren-Ladungsträgern in der aktiven Quantenfilm Region Besetzungsinversion aufgebaut. Die Einstreuraten für Elektronen und Löcher sind dabei aufgrund ihrer in der Regel unterschiedlichen effektiven Massen in den Valenz-und Leitungsbändern des aktiven Halbleitermaterials nicht gleich, so dass sich unterschiedlich viele positive und negative Ladungsträger im Quantenfilm sammeln können und die Ausbildung einer elektrischen Nettoladung in diesem Bereich wahrscheinlich wird. Als direkte Folge dieser durch elektrisches Pumpen induzierten elektrischen Ladung des Quantenfilmes erwartet man die Ausbildung eines statischen Feldes, dessen Auswirkungen auf die optischen Eigenschaften des Bauteils signifikant sein sollten. Wie weiter oben bereits erwähnt, hängen die optischen Eigenschaften eines Halbleiterlasers stark von seinem genauen strukturellen Design ab, das nicht nur durch seine Herstellung definiert ist, sondern auch noch nachträglich durch variable Einflüsse wie externe Felder verändert und manipuliert werden kann. Da jedoch im Vergleich von experimentellen und theoretisch vorhergesagten Quantenfilmverstärkungsspektren keine durch evtl. Nettoladungen der Quantenfilmregion hervorgerufenen Modifikationen berücksichtigt werden müssen, um sehr gute Übereinstimmung zu erhalten, wird üblicherweise geschlossen, dass in experimentellen Aufbauten keine Ladungseffekte auftreten und somit auch in der Modellierung der optischen Eigenschaften elektrisch gepumpter Halbleiterquantenfilmstrukturen diese vernachlässigt werden können. Diese eindeutige Diskrepanz von Erwartung und Beobachtung legt die Frage nahe, was die Vernachlässigung der Ladungseffekte rechtfertigt. Um dieser Frage nachzugehen, führen wir eine

vergleichende Modellstudie einer Quantenfilmlaserstruktur mit und ohne elektrische Nettoladung innerhalb der gebunden Zustände des Quantenfilmes durch. Wir zeigen, dass typische durch elektrisches Pumpen induzierte Nettoladungswerte das optische Absorptionsspektum des Quantenfilmes deutlich beeinflussen. Um der tatsächlichen Abwesenheit einer solchen Nettoladung Rechnung zu tragen, erweitern wir unser Lasermodell dahingehend, dass es auch die Dynamik der Ladungsträger in den ungebundenen energetisch höher liegenden Zuständen die nicht direkt am Laserübergang beteiligt sind berücksichtigt. So präsentieren wir eine phänomenologische Theorie auf Grundlage mikroskopischer Überlegungen die die Abwesenheit einer Nettoladung im Bereich des Quantenfilmes durch eine dynamische ausgleichende Umverteilung der Barrieren-Ladungsträger erklärt. Darüberhinaus stellen wir fest, dass es bei der ausgleichenden Dynamik zu kollektiven Ladungsträger Oszillationen kommen kann, die als Quelle von THz Strahlung fungieren könnten.

Das vorliegende Manuskript ist im Rahmen einer kumulativen Dissertation mit dem Titel Modeling and Simulation of Non-Equilibrium Effects in Modern Semiconductor Heterostructures am Fachbereich Physik der Philipps Universität Marburg entstanden. Entsprechend der Promotionsprüfungsordnung sind dafür hier im Anschluss an eine Zusammenfassung der Beiträge in deutscher und englischer Sprache die originalen Artikelbeiträge zusammengetragen und durch eine Einführung und Diskussion ergänzt. Um die Inhalte in Zusammenhang zu bringen und einen besseren Lesefluss zu gewährleisten, sind die Artikelbeiträge dabei in logischer Folge und teilweise nicht vollständig im Fliesstext wiedergegeben. So habe ich beispielsweise versucht, Redundanzen in der Darstellung der zugrundeliegenden Theorie zu umgehen, in dem ich den Artikeln *Non-Equilibrium Analysis of the Two-Color Operation in Semiconducor Quantum-Well Lasers* [5] und *Non-Equilibrium and Thermal Effects in Modelocked VECSELs* [56], die auf gleichen Modellannahmen basieren, eine vereinheitlichte Übersicht über die relevanten Bewegungsgleichungen und deren numerische Umsetzung voranstelle. Desweiteren habe ich Textpassagen, zu deren Inhalt ich keinen wesentliche Beitrag geleistet habe, wie die experimentellen Aspekte des Artikels *Ultrafast Non-Equilibrium Carrier Dynamics in Semiconductor Laser Mode Lockings* [56] nicht in die vorliegende Niederschrift integriert. Um Missverständnisse zu vermeiden und eine eindeutige Zuordnung von Manuskriptabschnitten auf Grundlage von Artikelbeiträgen zu garantieren, sind entsprechende Abschnitte durch eine Referenznummer in der Überschrift gekennzeichnet, die auf den zugehörigen originalen Beitrag verweist. Die vollständigen Artikel finden sich im Anhang zusammen mit einer kurzen Erläuterung meines Anteils an den präsentierten Ergebnissen.

Das vorliegende Manuskript ist wie folgt aufgebaut: In Kapitel 1 wird allgemein in das Thema der Modellierung und Simulation moderner Halbleiterlaserstrukturen eingeführt. Daran anschliessend sind im ersten grösseren Block des Manuskriptes die in den Artikeln *Non-Equilibrium Analysis of the Two-Color Operation in Semiconducor Quantum-Well Lasers* [5] und *Ultrafast Non-Equilibrium Carrier Dynamics in Semiconductor Laser Mode Lockings* [56] dargestellten Ergebnisse unserer Studien zu den optisch gepumpten Hochleistungs VECSEL Anwendungen zusammengefasst und in einen etwas umfassenderen Kontext gesetzt. Nachdem in Kapitel 2 zunächst die genaue Fragestelllung und Motivation dieser Studien umrissen und die wesentlichen Begrifflichkeiten erläutert werden, folgt in Kapitel 3 eine Beschreibung der Modellannahmen sowie eine Übersicht über die dem Modell zugrunde liegenden Gleichungen und deren numerischer Umsetzung. Die eigentlichen Forschungsergebnisse, wie sie in den oben genannten Artikeln bereits veröffentlicht sind, sind in Kapitel 4 wiedergegeben und werden in Kapitel 5 abschliessend reflektiert. Kapitel 6 eröffnet mit einer genauen Problemdefinition und Diskussion der Fragestellung zur Ladungsträgerdynamik in elektrisch gepumpten Halbleiter Quantenfilm Lasern den zweiten grösseren Block dieses Manuskriptes. Die Forschungsergebnisse des Artikelbeitrages *Charging Dynamics in Electrically Pumped Quantum Wells* [4] sind darauf folgend in Kapitel 7 dargestellt.

Abstract

In laser physics, for the construction of new devices as well as the command and optimization of established configurations, it is crucial to properly understand the interplay between the different physical effects underlying the laser operation. In many cases, it may be rather difficult to experimentally access relevant key parameters. Furthermore, a decent understanding of the operation principles may be required already in the design stadium before the fabrication of the first prototype. Hence, an appropriate laser model is highly desirable since it allows for the simulation and analysis of important aspects of the laser performance. Modeling and simulation may help to represent or characterize, understand or analyze, asses or solve research problems encountered in experiments and verify assumptions made in theoretical investigations.

As a rough classification, on can say that there are two different kind of models related to semiconductor lasers: material models which describe the physical interactions in the semiconductor and process models which describe the device functionality or behavior. In our studies presented here, we use idealized models for both the material and the functionality that allow us to demonstrate the methodical approach and shed some light on the benefits and drawbacks of laser modeling and simulation. In addition, these model studies allow for interesting and timely research investigations.

As examples, we first analyze a model for an optically pumped vertical cavity surface emitting laser (VECSEL) – also called disk laser – operating in the extreme parameter regime far beyond the quasi-equilibrium situation such that the full microscopic carrier dynamics needs to be included in the model approach. As the second example, we investigate the case of an electrically pumped semiconductor laser diode near threshold where the quasi-equilibrium situation of the charge carriers directly involved in the lasing process is still pretty well realized and the non-equilibrium effects enter only via the dynamics of the carriers in higher level energy states.

The operation of modern microcavity lasers is governed by a complicated interplay of a variety of interaction processes. The systematic modeling of such devices therefore poses a significant challenge to the formulation of a physics driven laser theory based on the description of microscopic processes rather than on phenomenological approaches that mimic empirical observations. Especially, this applies to the modeling of high power VECSEL applications in extreme parameter regions well above the threshold. Since the emission characteristics of the laser systems is strongly dependent on the actual geometry of the setup, on the material parameters of both the dielectric structure and the gain region, and on the actual excitation state of the optically active material, the simulation of the experimentally observed features poses a highly non-trivial problem. While in many situations, it is sufficient to assume that the high carrier densities and the related fast carrier-carrier scattering effects in lasers lead to a sufficiently fast thermalization of the carrier system [43, 57], under high power VECSEL operation conditions, such an assumption is usually not satisfied. In these systems, the carrier distribution in the valence and conduction bands may deviate significantly from Fermi-Dirac functions provided by the quasi-equilibrium conditions of a thermalized carrier system as the stimulated emission tends to burn kinetic holes into the carrier distributions leading to gain modifications[59] which affect the emission characteristics of the device. A theory appropriate for the simulation of non-equilibrium laser performance, therefore, must be able to closely track the quantum kinetic carrier dynamics in the optically active material. This implies that for the simulation of the VECSEL performance a model has to be used that allows for the monitoring of the carrier dynamics on a microscopic time scale (i.e. a few femtoseconds) for macroscopic time periods (i.e. several nanoseconds) corresponding to the build up of stable laser oscillations - all the while being computationally thus feasible that even parametric studies do not become impractical.

Fully microscopic non-equilibrium models resolve the scattering dynamics and are thus appropriate for the analysis of non-equilibrium effects. However, they are computationally very demanding and do not yet allow for acceptable simulation times. Consequently, a theory has been developed that replaces the fully dynamic treatment

of the scattering processes in the computation of the laser performance by effective scattering rates. These rates are parametrically dependent e.g. on temperature, density and excitation energy, and have to be computed for the appropriate conditions before the laser simulation.

In our approach, the system consisting of semiconductor gain medium and laser field is described within the context of semi-classical laser theory by the Maxwell-semiconductor-Bloch equations (MSBE) [10, 22]. Many-body Coulomb effects are included at the level of the screened Hartree–Fock approximation, and the effective relaxation rate approximation is used to account for the effects of carrier–carrier and carrier–phonon collisions. Here, we follow this approach to analyze the dominant non-equilibrium effects in the multimode operation of VECSEL devices under high excitation conditions.

To test our model and to study the relevance of non-equilibrium effects, we pick the examples (i) of a traditional device configuration that exhibits dual-mode emission [15] and (ii) of ultrashort pulse generation via modelocking in a VECSEL [35]. For the two-color operation, a model study is presented demonstrating that the non-linear laser theory on the basis of the MSBE is fully adequate for the description of high power applications where non-equilibrium effects gain increased importance. Altogether, our microscopic simulations give the first numerical verification that dynamically, stable two-wavelength oscillation of a semiconductor laser can occur when the mode coupling between two wavelengths is weak as we point out in the paper *Non-Equilibrium Analysis of the Two-Color Operation in Semiconducor Quantum-Well Lasers* [5]. Using the same model approach, we further carry out the first microscopic simulations of modelocking in a simple VECSEL configuration as presented in the paper *Non-Equilibrium and Thermal Effects in Modelocked VECSELs* [56]. Thus, we present a preliminary analysis of ultrafast mode-locking in order to expose the role of hot carrier distributions in establishing this feature.

The study of the influence of the ultrafast carrier dynamics on two-color laser operation and the generation of short pulses in high power laser applications may serve as an example for the fact that modeling and simulation may help to represent or characterize, understand or analyze, asses or solve research problems encountered in experiment. As an interesting example for the fact that modeling and simulation may help to verify assumptions made in theoretical investigations, we analyze the problem of the charging dynamics in electrically pumped quantum well lasers. This work is presented in the paper *Charging Dynamics in Electrically Pumped Quantum Wells* [4]. Here, we could verify that the frequently used but not yet proven assumption of charge neutrality in the active region of electrically pumped quantum well lasers is actually justified. Operating a quantum-well laser device by electric pumping, population inversion is obtained by the capture of barrier electrons and holes into the quantum well, i.e. into the active region of the laser.

When modeling the capture process, one has to account for the Fermionic nature of electrons and holes leading to the well-known Pauli blocking of the occupied states. Since typically the holes have a significantly larger effective mass than the electrons, this phase space effect is more prominent for the electrons than for the holes giving rise to a reduced capture probability for the electrons such that injection pumping of quantum well lasers can be expected to lead to charging of the active region.To investigate the significance and consequences of this effect, the consequences of electrical pumping and the associated charging phenomena have been investigated microscopically. The analysis reveals the necessity to include the extended barrier states energetically above the band edge in addition to the quantum-confined well states. Furthermore, we find that the replenishing of stimulated carrier recombination under CW laser operation causes persistent charge oscillations at the plasma frequency.

This thesis is in partial fulfillment of the requirements of a cumulative dissertation at the department of physics of the Philipps University Marburg. As the dissertation rules require, in this manuscript preceding the original paper contributions a summary of the presented research results in English and German is submitted as well as an introduction to the topic and a final discussion of the findings. To place everything in the right context, I structured the presentation of the results in a logical order and not according to their actual publication dates. Moreover, before the presentation of the original model exercises and simulation results, I present a unified review of the

underlying laser theory. Furthermore, whenever it seems appropriate, I present some interim conclusions. To avoid misunderstandings and to assure the clear identification of manuscript sections and original paper contributions, sections that foot on the latter are marked by an upper index number.

Overall, this thesis is organized into two main parts. In the first part on high power laser applications, the results of the paper contributions *Non-Equilibrium Analysis of the Two-Color Operation in Semiconducor Quantum-Well Lasers* [5] und *Non-Equilibrium and Thermal Effects in Modelocked VECSELs* [56] are summarized. In detail, in Chapter 1, we introduce the problem of modeling and simulation of modern semiconductor laser structures from a general point of view. Subsequently, in Chapter 2 we dive more into the details giving a precise problem definition of non-equilibrium effects in high power laser applications and explanation of the relevant terms in this context before, in Chapter 3, we highlight the model assumptions and briefly review the underlying laser theory. The research results as originally presented in the paper contributions of Ref. [5] and Ref.[56] are stated in Chapter 4 and reflected upon in Chapter 5.

The second part of this thesis focuses on the charging dynamics, and summarizes the results presented in the paper contribution *Charging Dynamics in Electrically Pumped Quantum Wells* [4] . In detail, Chapter 6 opens with a problem defintion and short disussion of the issue of charging dyanmics in electrically pumped semiconductor quantum-well lasers. The research results of the corresponding original paper contribution Ref. [4] are pointed out in Chapter 7.

Acknowledgement

The research presented in this work has been carried out in the context of a dissertation of the author at the department of Physics and Material Science at Philipps university Marburg. The path towards this doctoral thesis spans several years of work full of success and failures, frustration and acceptances and many other typical highs and lows characteristic of such a time. From an organizational point of view, somewhat uncommon in this work, however, is a relatively wide gap in time between the actual project handling and composition of this written record as I come back to it after almost two years of absence caused by a parental leave after the birth of my second daughter and an excursion into private enterprise as I felt the need to indulge my curiosity and explore the world outside the university. While on the one hand this gap in time makes it difficult for me to recall the subtleties of the research project and slows down the writing progress notably, on the other hand, this gap makes it much easier for me, to get an objective assessment of the findings, for two reasons. The first reason relates to the practical problem of being able to recognize the limits of what is feasible for oneself to do and to admit these limits to oneself, the second to the fact that motivated by the project findings scientific research has progressed and is about to overcome the difficulties I faced once by joint effort of different research fields as pointed out below.

Many people have been involved and contributed to the presented ideas and understanding gained. Heartily, I acknowledge my debt to those who have helped along the way and influenced the formation of the understanding of and the approach to the non-equilibrium effects in modern semiconductor micro-cavities presented here. First and foremost, I wish to express my gratitude to my supervisor, Professor Dr. Stephan W. Koch for his continued encouragement, guidance and invaluable suggestions during this work. It has been an honor to be his PhD student for almost eight years and have his trust all the time. His immense knowledge, patience and motivation makes him an outstanding mentor. In my gratitude I also like to include Prof. Dr. Mackillo Kira, who guided me closely as an advisor during my undergraduate career and in the first years of my doctoral study. I owe to him a high degree of initiative, responsibility and creative thinking. Furthermore, I am deeply indebted both to my colleagues at the physics institute that have provided the environment for lively exchange and thoughtful discussion and to former group members as W.Hoyer, B. Pasenow, C.Bückers, E. Kühn and B. Bredderman that have become friends and never stopped sharing their experiences about the problem issues involved. In this context, special mention should be made of Professor. Dr. Peter Thomas who made me feel always at home in Marburg and Dr. Hanno Steiner who taught me self-critic and self-confidence more than anybody else. I would specially like to thank my colleagues and co-authors M. Wichmann, M. Scheller and I. Kilen for their extremely valuable experiences, support, and insights. The experiments on the two-color operation of Vecsels in the group of Martin Koch and program optimization in the group of Prof. Dr. Jerome V. Moloney with focus on applied mathematics helped to increase the computational speed of the computer program underlying the simulation of high power laser application decisively and made me in the end report of my findings with motivation and concentration. Sincere thanks also go to Renate Schmid, Linda Grigat and Annegret Webel without whose support the organizational performance of my studies would have been much more troublesome to me. I gratefully acknowledge a most stimulating collaboration with a large number of mentors and colleagues in the interdisciplinary research training group Functionalization of Semiconductors supported by the Deutsche Forschungsgemeinschaft (DFG). I would also like to acknowledge Angela Thränhardt for carefully proofreading the manuscript, Prof. Dr. Kerstin Volz for providing her evaluation of this work and Dr. Habil. Sangam Chatterjee for being member of the examination commission. Finally I want to thank my family. The encouragement and support from my beloved husband Robin and our always positive and true children Enna and Winnie is a powerful source of inspiration, energy and self-confidence. A special thought is devoted to my parents for never-ending support, belief and allowing me to grow as I am.

Contents

1. Contextual Background

Modeling and Simulation Discipline

The availability of more and more efficient computing power makes new dimensions of experimentation with complex models possible and thus motivates in science further the emergence of a modeling and simulation discipline. The term modeling, thereby, refers to the activity of creating an object, i.e. a model, that is afterwards used as a tool for experimentation. This experimentation with the model, in turn, is described by the phrase simulation and carried out typically by a computer program. Through increasingly more powerful computers and with progress in software development, an analysis technology thus arises, which can handle problems of growing complexity. An interesting problem in this context is the modeling and simulation of modern semiconductor laser devices where the accurate description of the structure details and the material properties are particularly critical and complex.

Advances of Laser Modeling and Simulation

In laser physics, for the construction of new devices as well as the analysis and optimization of established configurations, it is crucial to achieve a profound understanding of how various physical effects underlying the laser operation interact. Given the fact that sometimes it may be rather difficult to obtain experimental access to relevant key parameters, and a decent understanding of the operation principles may be required already at the time of designing before the fabrication of the first prototype, an appropriate laser model will be rather useful, allowing for the simulation and analysis of certain aspects of the functionality of a laser. Thus, a model providing a quantitative understanding of the inner workings of a laser can trigger the optimization of the device designs with respect to

performance, component costs, compactness, robustness, etc. In the case of problems, a model can produce essential insight to analyze the cause and to find a working solution. Besides, a model may be used, e.g., to check whether certain suspected effects can be responsible for observed misbehavior, and a simulation can show whether a conceived remedy would be sufficiently effective and which side effects it may have. A laser model also makes it possible to check certain beliefs and can thus make an essential contribution to improve the level of understanding and to obtain a thorough insight into the relevant physical mechanisms.

Laser Fundamentals

In short, a laser is an externally pumped self-sustained oscillator that exists in various realizations all of which consist of a gain medium that is placed inside an optical cavity to provide the necessary feedback. Superficially, these various laser realizations differ only in the choice of a suitable gain material, the pumping mechanism, the resonator configuration and the thermal management. However, despite the generic common features of different kinds of lasers, in the details of operation they may differ decisively. Hence, while for example the gain medium of a gas laser is modeled as a collection of independent two level atoms or molecules, in a semiconductor laser, due to the delocalized nature of the electronic states in the energy band, the electrons interact with each other via intraband collision processes and should be treated collectively in modeling the fundamental laser aspects of spontaneous emission, absorption and stimulated emission [1]. Moreover, the semiconductor laser in itself is as versatile as the material from which the devices are made such that semiconductor lasers exist in numerous configurations. Thus, in the past decades, the concept of the semiconductor laser has evolved into a class of robust, reliable devices of small compact size and with long operation lifetimes that owe their popularity to their outstanding laser properties such as high individual conversion efficiencies, continuous output powers of several kilowatts, modulation rates of several tens of gigahertz, and wavelengths from 0.4 to beyond 2 μm [23, 47, 62, 73] .

Consequently, it is not surprising, that semiconductor lasers play an ever increasing role in our modern world. The application of these light sources in communication, sensor and medical technologies as well as entertainment electronics is well known. But also in the fields of optical storage technologies, material processing and as pumping source laser of other laser types does the semiconductor laser replace traditional light sources. Naturally, the different fields of application imply different specifications of the semiconductor laser as it would be hardly possible to reconcile all good laser characteristics in a single device. Depending on the specific usage, a semiconductor laser will be needed with predefined qualities in terms of wavelength, threshold current, beam quality, spectral purity and so forth.

Effect of Quantization

Advances in epitaxial growth techniques as molecular beam epitaxy (MBE) allow for the fabrication of multilayered heterostructures of different semiconductor materials with precisely controlled composition profiles. These compounds can serve as artificial materials, whose electronic and optical properties deviate fundamentally from those of natural materials. In principle, the large number of feasible alloy compositions introduced

during epitaxial growth makes it possible to design arbitrary energy-band diagrams. The main building-blocks of these so-called bandgap-engineered structures are potential energy wells, which are formed by embedding an ultrathin layer of a low band-gap material into wider gap semiconductors. Since they allow for confinement of both carriers and light waves in the cavity, these double heterostructures consisting of a light amplification layer, with subsequent cladding layers on either side of it are the core component of a semiconductor laser device. When the thickness of the well layer, i.e. the optically active region, becomes comparable to or smaller than the carrier de-Broglie wavelength, quantum mechanical effects occur, which can be observed in the absorption and emission characteristics of the quantum-well structure. A prominent application of an optical device whose principle of operation is based on the quantum-size effect is the semiconductor quantum-well laser. Typically, the energy difference between the smaller bandgap of the quantum-well material and the larger bandgap of the barriers on either side of it causes a confinement potential for both positive and negative charge carriers, i.e. electrons and holes. Since modern epitaxial growth techniques allow the fabrication of heterojunctions with atomically abrupt interfaces, the potential jump occurs within one atomic layer, so that one can model the confinement as a one-dimensional box potential. Conceptually, the quantum-well corresponds to the well-known elementary example of quantization in a box treated in quantum mechanical textbooks. The quantum confinement, therefore, introduces energy subbands, which are characterized by discretization of the energy values for the motion perpendicular to the quantum well and the continuum of energy states for the motion in its plane. Most semiconductor quantum-well lasers are diode lasers that use different heterojunctions to achive simultaneous carrier and photon confinement in the active region. Current is injected via two electrodes on the top and at the bottom of the resulting heterostructure. A sketch of a simplified geometry of a semiconductor laser diode mounted on a heat sink is presented in Figure 1.1.

Laser Model Exercise: optical, electrical and thermal phenomena

As a common feature, the behavior of semiconductor lasers is not simple since optical, electrical, and thermal phenomena are present at the same time. Put in a nutshell, the operation of semiconductor lasers involves a complicated interplay of these phenomena, which can affect a variety of important performance parameters of the laser device. For example, the material is optically nonuniform and the propagation of waves and formation of cavity modes is complex. In consequence, the designed laser frequency is essentially influenced by thermal lensing, misalignment of components, and thermal expansion. Furthermore, the process of shaping optical pulses under the influence of laser gain, chromatic dispersion and nonlinearities can be manifold and closely interrelated. And, to cite another example, the charge carrier concentrations of both electrons and holes are high and various recombination processes need to be taken into account.

As in most lasers, in a semiconductor laser the basic prerequisite for lasing processes is population inversion. This means that in order to obtain amplification of light by stimulated emission, the number of particles in an excited state has to exceed the number of particles in the ground state. In this condition, not only absorption of incident light can

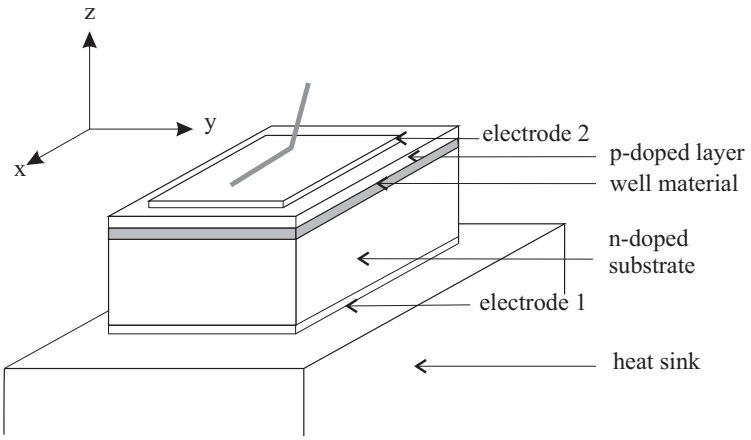

Figure 1.1: Schematic diagram of the layer system of a semiconductor quantum-well laser device. The active region is highlighted by the shaded area. The coordinate axes identify the direction in space. So, in this investigation, the z direction always indicates the direction perpendicular to the active region. [cf. [10]]

occur. Emission of light will stimulate the system to release energy. A single photon might trigger an avalanche of further light quanta from the excited particle system and thus cause gain for the optical wave. However, thermodynamical arguments show that in thermal equilibrium the vast majority of atoms in a crystal are in the ground state. According to a Boltzmann distribution the population of a lower-lying electronic state outweighs the population of a higher one. Therefore, by the process denoted as pumping one has to make sure that energy is stored in the system such that more atoms are in an excited state than in the ground state.

The pump energy is usually provided as light or electric current. While optical pumping is based on lifting electrons into higher energy levels by electromagnetic radiation, in case of electrical pumping carriers are injected directly via an external power supply. Typically, the pumping process excites electrons in an energy level well above the electronic energy states that participate in the lasing process such that carrier relaxation mechanisms and scattering events become important for the laser behavior. Furthermore, good heat dissipation and heat sinking are critical for high-power operation of all semiconductor lasers. Without these, the temperature of the active region would rise and excited carriers would escape thermally from this area into the adjacent layers, thus depleting laser gain and turning the laser off in a thermal rollover process.

Laser Model Exercise: Multi-Time Scale Problem

The dynamical behavior of the coupled carrier-photon system from a starting of the pump process over the onset of laser action to the stationary situation is characterized by an interplay of processes acting on very different time-scales. The Coulomb scattering and, under extremely high power conditions, the stimulated recombination are the fastest processes acting on sub-picosecond time scales. Cooling and equilibration of the carrier system takes place within several picoseconds and spontaneous emission has

characteristic times of some hundreds of picoseconds up to nanoseconds. Following this line of reasoning, it is clear that the operation of modern semiconductor laser systems involves a complicated interplay of many processes which span over time scales from tens of femtoseconds for optical dephasing and carrier scattering events to several nanoseconds for the build up of stable laser oscillations up to some microseconds for thermal effects. This multi-scale problem necessitates laser models that bridge the gulf between microscopic and macroscopic physics and make the computationally demanding simulation of semiconductor laser-device experiments feasible. Clearly, the main challenge one faces in modeling such a complex problem is to achieve the right balance between an elementary microscopically motivated physics driven characterization and a purely phenomenological description of the processes involved to catch all relevant information while simultaneously holding the numerical costs down.

Laser Model Categories

The laser models are almost as numerous as the laser configurations itself ranging from simple rate equation models to highly sophisticated models taking into account the fully microscopic theory [24, 32, 45, 76]. In general, a model contains some number of variables and parameters, related to physical quantities and properties, and a number of assumptions which may or may not always be very well fulfilled in reality and should always be made explicit, therefore, to avoid misunderstandings. Laser models, in particular, contain mathematical relations as essential ingredients which connect different model variables with each other and can sometimes be solved by analytical means, whereas in other cases numerical methods have to be used depending on the level of complexity of the approach. Typically, in the latter case, some computer software is required. Particularly, this holds in case of microscopic laser models that go beyond a rate equation approach for the description of the relevant laser dynamics and necessitate the implementation of many-body techniques that demand state of the art supercomputers [12] .

Laser Model Equations

Formally, the potential distribution, the carrier concentrations, and the current densities are linked through Poisson's equation, current equations and continuity equations, respectively [2]. The latter needs to take into account absorption and recombination phenomena, meaning that the net gain or loss and also the power density of the optical fields appear in these equations. The net gain as well as the refractive index change depend on the carrier density and are relevant for the description of the wave propagation and the cavity resonance. For the coupled carrier-photon system a quantum mechanical non-equilibrium theory has to be applied to analyze the laser dynamics and stationary emission properties [42]. Electrical and optical heat dissipation may be introduced into a heat diffusion model yielding the temperature increase which affects most material parameters.

Semiclassical Approach

A laser model on the basis of the fully microscopic theory is a representative example of an approach too sophisticated to be numerically feasible. Depending on the phenomena of interest, therefore, typically some requirements of the rigorous model have to be relaxed and the approach has to be reduced in complexity via appropriate assumptions and approximations. For example, being interested in the laser behavior well above threshold, it is common practice to reduce the fully microscopic approach to a semi-

classical description where the optical material properties as the refractive index and the optical gain correctly follow from the semiconductor Bloch equations of many-particle quantum mechanics [22]. Propagation effects then enter via Maxwell's equations.

Process Models and Material Models

In general, there are two different kind of models related to semiconductor lasers. On the one hand, there are material models which describe the physical interactions in the semiconductor. On the other hand, there are process models which describe the device functionality or behavior. Motivated by recent experiments [15, 27] and a long time experience in modeling and simulating semiconductor laser aspects in the team of Prof. Dr. S.W. Koch [22, 40, 42], we pick an example study for each of these kind of laser models. We show that, whereas in the one case a complex laser model may be the essential tool for understanding the principle of operation and its limitations, in the other case modeling on the basis of simpler design rules is fully sufficient and makes a sophisticated model obsolete. In detail, we first pick the example of the optically pumped VECSEL operating in the extreme parameter regime far beyond the quasi-equilibrium situation such that the full microscopic carrier dynamics need to be included in the model approach. Second, we analyze the example of an electrically pumped semiconductor laser diode near threshold where the quasi-equilibrium situation of the charge carriers relevant for the lasing process might still be assumed and non-equilibrium effects enter only via the dynamics of the charge carriers in higher level energy states. Together these examples do not only demonstrate characteristically the methodical approach, the benefits and drawbacks of laser modeling and simulation but, in addition are supposed to show examples of interesting and current research subjects.

Part One: High Power Laser Applications

2. Problem Definition

Semiconductor lasers are as versatile as the material from which they are made. Moreover, compared to other laser families, in several aspects the inner workings of the semiconductor laser differs decisively from that of a conventional laser such as a gas or solid-state laser, making it a perfect candidate to trigger further innovations in laser design and usage.

Unique Design of VECSELs

Among the different semiconductor laser systems, VECSELs have a unique design due to their external cavity configuration. On the one hand, the realization of the external optical cavity might be viewed as mechanically cumbersome, making these lasers more complex and requiring assembly and alignment as compared with the simple integrated edge-emitting and surface-emitting semiconductor lasers. On the other hand, however, such an external cavity gives tremendous versatility to VECSEL device configurations and functions. In particular, the external cavities allow for the flexible insertion of intracavity optical elements reaching from spectral filters (birefringent filters, etalons) for laser mode control over saturable absorber components to achieve laser passive mode locking with picosecond and subpicosecond pulse generation all the way to nonlinear crystals to generate intracavity frequency mixing. To dive into the details of the characteristics and functionality as well as the benefits and drawbacks of VECSEL configuration, we highly recommend the review article [47] by M. Kuznetzov, the pioneer of this class of devices.

Operating Conditions of VECSELs

For the following, it is particularly relevant that, in comparison to conventional edge-emitting semiconductor lasers, VECSELs exhibit quite different operating conditions. The resonant periodic gain medium typically consists of 8 - 12 quantum wells which have to be

pumped relatively hard to provide suitable amplification of the light field in the resonator. In addition, the rather small round-trip gain demands a sufficiently high quality of the resonator to allow for stable VECSEL operation. As a consequence, the intracavity field intensity is dramatically increased relative to conventional edge-emitting semiconductor lasers.

Non-Linear Optical Effects

Clearly, such a configuration leads to questions concerning the relevance of strong non-linear optical effects which appear at high optical power densities. Thus, other than in conventional experimental situations where the Coulomb intraband scattering in the excited electron-hole plasma is fast enough to establish a quasi-equilibrium within the bands in which the electrons and holes are distributed according to Fermi functions, for optical transitions stimulated by intense laser light, the Coulomb scattering will no longer be able to resupply fast enough the carriers which where lost by stimulated recombination. To properly model these situations one has to go beyond the quasi-equilibrium approximation where only the total number of electrons (or holes) has to be calculated and take into account the momentum resolved carrier dynamics on a microscopic level.

Non-Equilibrium Charge Carrier Distributions

In particular, the analysis of semiconductors interacting resonantly with strong light fields requires the calculation of charge carrier non-equilibrium distributions in the conduction and valence bands. Above the lasing threshold, the carrier distributions typically extend over energy ranges that are broader than the homogeneous width of the laser transition. On the one hand, therefore, in a semiconductor laser stimulated emission depletes the populations in electron and hole states that have transition energies lying within the homogeneous lineshape function of the laser transition and thus removes charge carriers from the associated excited states. On the other hand, these states are refilled by the fast intraband carrier–carrier scattering processes.

Kinetic Hole Burning

If the refilling rate outweighs the stimulated emission rate, the efficient carrier-carrier Coulomb scattering leads to carrier redistribution in the form of quasi- equilibrium Fermi-Dirac distributions, but it does not dissipate kinetic energy from the carrier system. The resulting state is therefore a non-equilibrium state where the carrier temperature differs from that of the crystal lattice. Moreover, if the stimulated emission rate outweighs the refilling rate, a net depletion of the charge carrier population of the involved laser states occurs giving rise to the formation of a hole in the charge carrier occupation probability distribution around the wavenumber at which the resonance with the laser light occurs. Considering the typical carrier scattering times and the non-equilibrium electron-hole-plasma dynamics, VECSEL configurations with a strong intracavity laser field, therefore, should involve significant kinetic holes in the carrier distribution functions.

Spectral Hole Burning

This kinetic hole burning, in turn, may lead to a spectral hole in the gain characteristics if the dephasing of the polarization does not destroy the one-to-one correspondence between momentum values and transition energies and introduce an homogeneous broadening of each transition. By analogy with the term kinetic hole burning, the term spectral hole burning thereby, describes a drop in the gain spectrum induced by stimulated emission (see below).

Naturally, the gain must be reduced for high input powers as the radiation intensity in the resonator cannot increase without limits. As the power in the oscillator grows, the carrier concentration in the conduction and valence band decreases significantly and less states satisfy the amplification condition such that the gain is reduced and decreases below its initial value . A stable condition is reached when the reduced gain is equal to the loss. The gain then just compensates the loss such that the cycle of amplification and feedback is repeated without change and steady-state oscillation prevails.

Definition Gain Saturation

The dependence of gain on the field intensity is referred to as gain saturation. Thereby, a distinction is made between homogenous and inhomogeneous gain saturation. While homogenous gain saturation refers to the situation of spectral homogeneity of the emission line where the shape of the gain spectrum is not affected and the carrier distribution functions remain unperturbed, inhomogeneous saturation tends to saturate the gain around the laser wavelength more than the gain at other wavelengths leading to a change in the spectral shape.

Homogeneous vs. Inhomogeneous Gain Saturation

Provided that all modes experience the same losses, in a situation with homogenous broadening, laser oscillation occurs at the mode with maximum gain and forces this to threshold value. As the overall shape of the gain spectrum remains unchanged in this process, the gain level of all other modes falls below the threshold value thus preventing the onset of laser oscillations of neighboring modes. Contrary, inhomogeneous gain saturation enables multi-mode emission: the gain at adjacent modes continues to increase after reaching threshold for the first mode until the threshold for the other modes is reached leading to spectral holes in the gain spectrum for high excitation conditions. As long as the holes occurring in the emission are spectrally sufficiently far apart from each other, a possible mutual interaction is minimized and stable multi-mode emission facilitated. If direct inter-band transitions with the conservation of quasi-momentum are considered, only relaxation can render the emission linewidth homogeneous. Relaxation mechanisms as Coulomb and phonon Scattering couple different momentum states and optical transitions in consequence. Doing so, they prevent each mode from being fed by its own gain reservoir. The weaker the coupling between modes, the less the gain competition and the more inhomogeneous the gain saturation. In a perfect inhomogeneous laser system with fully independent modes, therefore, multimode emission should be favored, while homogenous laser systems with highly interrelated modes should have preferences for single-mode emission.

Multi-Mode Emission

It is well-known that semiconductor lasers allow for the emission of several longitudinal lasing modes that compete for the optical gain and have a frequency spacing related to the laser internal cavity length [51]. The number of spectral lines that a laser is capable of supporting is a function of the cavity structure, the gain material, and the excitation conditions. So, it should be possible for a traditional VECSEL to simultaneously lase at dual wavelengths separated by a few nanometers for the following reasons. First, the quantum well gain spectra have a wide bandwidth with a relatively flat peak leading to a low mode selectivity for devices with large extended cavities since in these configurations,

usually several of the densely spaced cavity modes experience comparable amplification. Second, the VECSEL gain medium is inhomogeneously broadened due to the width and composition fluctuations in multi-quantum wells, as well as material defects. All of these result in low longitudinal mode selectivity of the VECSEL such that VECSEL well above threshold tend to oscillate in multi-longitudinal modes with an envelope of a few nanometers.

Two-Color Laser Emission

Under most conditions one ideally prefers an efficient conversion of the excited carriers into a single-mode laser field such that multi-mode operation is undesirable. However, the well-defined emission at more than one mode is needed in cases where sum or difference frequency generation is exploited. For example, experimentally dual-mode operation in VECSELs has been taken advantage of to generate light in the terahertz spectral range using either spectrally filtered mirror feedback [27] or a suitable intracavity filter [15] to isolate the required modes. Here, two-color laser operation has been achieved where the two emission wavelengths are separated spectrally by far more than the free spectral range of the cavity. While the realization of stable dual-mode operation using spectrally filtered mirror feedback is based on a complex design and critical epitaxial growth of the VECSEL chip, the realization using an intracavity filter is based on a traditional device structure with an etalon as additional optical element and is, therefore, of special interest for an analysis of the physical principles underlying stable dual-mode emission of a regular VECSEL.

Generally, optical etalons in the form of transparent plan-parallel plates with reflecting surfaces belong to the family of Fabry-Perot interferometers. When inserted into a laser cavity, an etalon acts as an additional resonator that may limit the number of cavity modes to the number of modes that simultaneously fulfil the resonance condition of the cavity and the etalon. With weighting provided by the gain spectrum of the laser material, the emission spectrum of the laser system follows. Depending on the position of the etalon resonance relative to the gain spectrum, single-mode or multi-mode emission becomes possible (cf. Section 4.1.3).

Despite the experimental realizations, a full theoretical understanding of the conditions under which semiconductor lasers can oscillate simultaneously and stable at two different frequencies is still missing. Since the emission characteristics of the laser systems is strongly dependent on the actual geometry of the setup, the material parameters of both the dielectric structure and the gain region and the actual excitation state of the optically active material, the analysis of the different lasing regimes that might be encountered in experiments establishes a highly non- trivial problem. So far, scientific research did not provide final answers to the questions occuring in the discussion following the observation of stable two-color operation of VECSELs. In particular, the questions of which processes may lead to a stable two-color operation and for what parameters such a situation may be realized are still not fully resolved. Furthermore, the full analysis of the temporal multi-mode emission dynamics and its influence on the process of frequency conversion still constitute an open problem.

On the experimental level the work of M.Wichmann. et al. [74] revealed several important insights in this field. Four important experiments have been performed which allow for important insights into the power dependent emission bandwidth of the VECSEL device as well as on the temporal dynamics of the two-color emission. In detail, the experiments cover (i) a study of the spectral composition of the laser emission, (ii) a statistical investigation of the two-color emission, (iii) an analysis of the anti-phase dynamics related to the two-color operation and (iv) tests linked to the VECSEL-based THz-source. On the level of modeling and simulation, previous studies used quasi-equilibrium gain configurations in order to study two-color laser systems based on semiconductor laser devices and simulated the spectrally filtered feedback to characterize the dynamic regimes [52].

Modelocking Dynamics

Just like two-color laser operation, modelocking in VECSELs is a feature of multimode dynamics. So, the laser output spectrum is far more complicated to obtain than the simple weighting of the cavity longitudinal mode structure with the laser gain bandwidth by a simple multiplication. Each mode represents a separate laser oscillation with its own frequency that competes with the other modes for the gain, respectively inversion.

The total field is the coherent sum of all modes, i.e. a complex superposition such that without a well defined phase relation between the different modes, a chaotic, irregular dynamics follows. For a fixed phase relation, however, pulsed time behavior may be observed due to mode-locking. In most but not all cases, the pulse duration achieved is governed by a balance of pulse shortening through the modulator and pulse broadening via other effects, such as the limited gain bandwidth. In the stationary mode-locking situation, the various effects influencing the circulating pulse are in a balance so that the pulse parameters are unchanged after each completed round trip, or often even nearly constant throughout each round trip. Each time the pulse hits the output coupler mirror, a usable pulse is emitted, so that a regular pulse train leaves the laser. If the modulation is synchronized with the resonator round trips, this can lead to the generation of ultrashort pulses, usually with picosecond or even sub-picosecond pulse durations.

Active Modelocking

Generally, the technique of mode locking encompasses a group of methods to obtain ultrashort pulses from lasers [34]. Thereby, the laser resonator contains either an active element (an optical modulator) or a nonlinear passive element (a saturable absorber), which favors the formation of an ultrashort pulse circulating in the laser resonator. In particular, active mode locking involves the periodic modulation of the resonator losses by an external signal that is applied to an optical loss modulator typically using the accousto-optic or electro optic effect. When such an electronically driven loss modulation runs according to a sine function with a period given by the cavity round-trip time, the saturated gain at steady state only supports net gain around the minimum of the loss modulation and therefore only supports pulses that are significantly shorter than the cavity round trip time.

Passive Modelocking

For passive modelocking, a saturable absorber, i.e. a material that has decreasing light absorption with increasing light intensity, is used to obtain a self-amplitude modulation of the light inside the laser cavity. Such an absorber introduces some intracavity loss which

is relatively large for low intensities but can be saturated to become significantly smaller for a short pulse with high intensity. Thus, a short pulse then produces a loss modulation because the high intensity at the peak of the pulse saturates the absorber more strongly than its low intensity wings. This results in a loss modulation with a fast reduction of the loss and typically a somewhat slower recovery. While the fast reduction of the loss is determined by the pulse duration, the slower recovery depends on the detailed mechanism of the absorption process in the saturable absorber.

Semiconductor Saturable Absorber Mirror

Properly designed, systems utilizing passive mode locking with a saturable absorber can generate much shorter pulses than actively modelocked systems. Basically, a saturable absorber driven by already short pulses can modulate the resonator losses much faster than an electronic modulator. The system provides a positive feedback loop since the shorter the pulse becomes, the faster the loss modulation occurs, provided that the absorber has a sufficiently short recovery time. The most important type of absorber for passive mode locking is the semiconductor saturable absorber mirror, called SESAM, that operates in reflection, as the reflectivity increases with higher incoming pulses. A semiconductor absorbs light when the photon energy is sufficient to excite carriers from the valence band to the conduction band. Under conditions of strong excitation, the absorption is saturated because possible initial states of the pump transition are depleted while the final states are partially occupied. Subsequently, on a femtosecond time scale, the carriers in each band thermalize thus giving rise to a partial recovery of the absorption. Semiconductor saturable absorber mirrors are a compact semiconductor devices, the parameters of which can be adjusted in very wide ranges, so that appropriately designed SESAMs can be used to mode-lock very different kinds of lasers, in particular solid-state lasers, including different kinds of semiconductor lasers, as VECSELs. The research area of femtosecond pulsed mode-locking in VECSELs is a relatively young field despite the many successes demonstrated to date [26, 63, 75, 77].

Non-Equilibrium Effects on Laser Performance

The extent to which non-equilibrium effects such as kinetic and/or spectral hole burning actually affect the laser performance is determined by the complex interplay of the various interaction processes taking place within the carrier system including the pumping process (i), the intra-band relaxation process of the pump-injected carriers (ii) and the inter-band recombination process by spontaneous and stimulated emission (iii). A non-linear laser theory that allows for the description of high power applications of VECSELs, therefore, requires a close tracking of the dynamics of the carrier distributions and thus renders a microscopic laser theory necessary. Furthermore, typically, the non-equilibrium effects not only lead to deviations of the carrier distribution from a Fermi-Dirac function but additionally involve carrier and eventually even lattice heating. The overall temperature change in the device, in turn, results in a shift of the designed laser frequency which is determined by the sub-cavity resonance of the laser setup. Thermal management, therefore, becomes critical for high-power operation of VECSELs as well. In experimental configurations often it can not be avoided that a detuning emerges between the temperature-dependent sub-cavity resonance and the temporally changing gain maximum of the

quantum-well active layers. This detuning clearly affects the laser performance such that an appropriate laser theory must allow for a wide range of thermal and spectral parametric dependencies in the computation of the emission characteristics of the device.

Non-Equilibrium Laser Theory

We conclude that since both intrinsic properties of the quantum-well active material (as carrier relaxation) and design properties of the resonator structure (as the detuning of the laser frequency) are decisive for the VECSEL performance, a laser theory that aims to describe the optical properties of these systems must be able to specify the non-linear coupling of a propagating light field to the active medium polarization as well as the quantum kinetic carrier dynamics. This implies that for the simulation of the VECSEL performance a model has to be used that allows for the monitoring of the carrier dynamics on a microscopic time scale (i.e. a few femtoseconds) for macroscopic time periods (i.e. several nanoseconds) corresponding to the build up of stable laser oscillations - all the while minimizing the computational cost such that even parametric studies do not become impractical. It is well-known that numerous models exist that apply to either of these requirements. These models range from simple rate equation approximations for the total carrier density and the laser field to highly sophisticated models taking into account the full microscopic theory.

The different approaches for the microscopically-based modeling of micro-cavity lasers range from quasi-equilibrium approaches for the carrier system where only the total density varies with the laser field all the way to highly sophisticated non-equilibrium theories taking into account the full quantum dynamics. These different approaches have their particular advantages and disadvantages and are therefore most suitable for particular operation conditions. The quasi-equilibrium models rely on sufficiently fast inter-band relaxation processes to eliminate the medium polarization adiabatically and approximate the carrier distributions by quasi-equilibrium Fermi-Dirac functions. This way, one can perform efficient long-time simulations, however, the fast quantum kinetic carrier dynamics and the related non-equilibrium effects are neglected. In contrast, the full microscopic non-equilibrium models resolve the scattering dynamics and are thus appropriate for the analysis of non-equilibrium effects. However, they are computationally very demanding and typically do not allow long-time simulations. To bridge the gap between both approaches, a theory has been developed that replaces the fully dynamic treatment of the scattering processes in the computation of the laser performance by effective scattering rates. These rates are parametrically dependent e.g. on temperature, density and excitation energy, and have to be computed for the appropriate conditions before the laser simulation [69, 70]. The results depend on intrinsic material properties such as temperature and carrier density and on the excitation conditions. While it is more rigorous to describe collisional effects using quantum kinetic equations, the relaxation rate approach is numerically less demanding, for example, in terms of the number of momentum-points necessary to ensure particle and energy conservation in intraband interactions. This relaxation of computational requirements allows for the inclusion of other details of the laser configuration in the model or for the simulation of longer

periods in time. Here, we follow this effective rate approximation approach to analyze the dominant non-equilibrium effects in the multimode operation of VECSEL devices under high excitation conditions. A fully microscopic theory that abstains from the effective rate approximation is applicable to study, for example, to simulate single-pass experiments and laser start-up behavior[6, 20, 31].

Formulation of Reseach Problem

This work aims to build on the experience gained in the past with modeling and simulation of laser applications in the semi-classical limit [7, 8, 9, 46] and further expand the underlying model to effectively include microscopic carrier dynamics and non-linear light propagation effects. In order to enable the simulation of non-equilibrium effects in laser devices on timescales ranging from picoseconds to a few nanoseconds, we work directly with momentum-resolved carrier distributions. Taking into account that the term modeling does not only refer to the process of constructing a model but also implies testing and application, motivated by recent experiments [15, 27] we perform a model analysis of the non-linear dynamics in vertical external cavity surface emitting lasers devices. In detail, our study focuses on the formation of stable dual-wave length laser operation on the one hand and the generation of ultrashort pulses via mode-locking on the other aiming at an interpretation of the interplay of microscopic effects as hole burning on these macroscopic multi-mode features.

3. Theoretical Footing

3.1 Non-Linear Laser Modeling

3.1.1 Equations of Motion

Microscopic Description of Macroscopic Quantities

In order to analyze the non-equilibrium effects in high power applications as VECSELs, we need to model the propagation of the light field inside the laser cavity and its non-linear interaction with the optically active gain region, i.e., the QW layers. As the light field E(z, t) leads to a material polarization P(z, t) which in turn affects the light field, a basic building block of any laser theory is a self-consistent set of equations for these quantities. In this approach, the requirement of a non-linear description of the material response may be accounted for by including the polarization dynamics on a microscopic level. The laser field can be described classically, however, as our interest is in laser dynamical behavior far above the lasing threshold such that the quantum fluctuations are small. To this purpose, we apply a semi-classical theory where we treat the field-induced optical excitations of the gain material microscopically, while we deal with the dynamics of the light field on the level of the classical Maxwell equations. Such a theory naturally involves the complex interplay of the relevant interaction processes and dynamics that are decisive for the VECSEL performance ranging from the detailed properties of the resonator structure and the propagating light field to the intrinsic properties of the quantum-well (QW) active material.

Wave Equation

In detail, we solve the transversal wave equation for the propagating light field $\mathrm{E}(z,t)$

that excites the polarization $\mathrm{P}(z,t)$ at the QW position. Assuming that the cavity light-field circulates in z-direction perpendicular to the QW plane, this equation may be cast into the following form

$$\left[\frac{\partial^2}{\partial z^2} - \frac{n^2}{c_0^2}\frac{\partial^2}{\partial t^2}\right]\mathrm{E}(z,t) = \mu_0 \frac{\partial^2}{\partial t^2}\mathrm{P}(z,t) \tag{3.1}$$

where, the constants n and c_0 are the background refractive index and the vacuum velocity of light and μ_0 denotes the vacuum permeability, respectively. The relation between the macroscopic polarization $\mathrm{P}(z,t)$ entering the wave equation Eq.(3.1) and the relevant microscopic quantities is established by the summation of the so-called microscopic polarizations $\mathrm{p}_{\lambda,v,\mathbf{k}}$, i.e., the probability amplitudes for the excitation of an electron from a valence-band state $(v,\mathbf{k})$ into an empty conduction-band state $(\lambda,\mathbf{k})$ of equal crystal momentum $\mathbf{k}$ in the plane of the QW

$$\mathrm{P}(t) = \sum_{\lambda,v,\mathbf{k}} (d_{\mathbf{k}}^{\lambda,v})^{\star}\mathrm{p}_{\lambda,v,\mathbf{k}} + \mathrm{c.c.}. \tag{3.2}$$

Here, the sum is weighted with the dipole-matrix element d_{cv} which is characteristic of the optically active material.

Semiconductor Bloch Equations

The dynamics of the transition amplitude $\mathrm{p}_{\lambda,v,\mathbf{k}}$ introduced above as essential component in the microscopic description of macroscopic observables follows from the multiband semiconductor Bloch equations (SBE) [22] that describe the optical response of semiconductors excited by coherent classical light sources

$$\begin{aligned}\frac{\partial}{\partial t}p_{\lambda,v,\mathbf{k}} = &-\frac{i}{\hbar}\sum_{\lambda_1,v_1}\left(e^{e}_{\lambda,\lambda_1,\mathbf{k}}\delta_{v,v_1} + e^{h}_{v,v_1,\mathbf{k}}\delta_{\lambda,\lambda_1}\right)p_{\lambda_1,v_1,\mathbf{k}} \\ &-i(\mathrm{n}^{\mathrm{e}}_{\lambda,\mathbf{k}} + \mathrm{n}^{\mathrm{h}}_{v,\mathbf{k}} - 1)\Omega_{\lambda,v,\mathbf{k}} + \Gamma_{\lambda,v;\mathrm{deph}} + \Lambda^{\mathrm{p}}_{\mathrm{spont}}\end{aligned} \tag{3.3}$$

$$\frac{\partial}{\partial t}\mathrm{n}^{\mathrm{e(h)}}_{\lambda(v),\mathbf{k}} = -2Im\left(\Omega_{\lambda,v,\mathbf{k}}(p_{\lambda,v,\mathbf{k}})^{\star}\right) + \Gamma^{e(h)}_{\lambda(v);\mathrm{scatt}} + \Lambda^{\mathrm{n}}_{\mathrm{spont}} + \Pi_{\mathrm{pump}}. \tag{3.4}$$

These equations couple the dynamics of the microscopic polarization $\mathrm{p}_{\lambda,v,\mathbf{k}}$ and the occupation functions $\mathrm{n}^{\mathrm{e(h)}}_{\lambda(v),\mathbf{k}}$ determining the probability that a state $\mathbf{k}$ in the conduction band λ (valence band v) is occupied by an electron (hole).

Hartree-Fock Approximation

In the well-known Hartree-Fock approximation [22], the renormalized single-particle energies are given as

$$e^{e}_{\lambda,\lambda_1,\mathbf{k}} = \varepsilon^{e}_{\lambda,\mathbf{k}}\delta_{\lambda,\lambda_1} - \sum_{\lambda_2,\mathbf{q}} V^{\lambda,\lambda_2,\lambda_1,\lambda_2}_{|\mathbf{k}-\mathbf{q}|}\mathrm{n}^{\mathrm{e}}_{\lambda_2,\mathbf{q}} \tag{3.5}$$

$$e^{h}_{\nu,\nu_1,\mathbf{k}} = \varepsilon^{h}_{\nu,\mathbf{k}}\delta_{\nu,\nu_1} - \sum_{\nu_2,\mathbf{q}} V^{\nu,\nu_2,\nu_1,\nu_2}_{|\mathbf{k}-\mathbf{q}|}\mathrm{n}^{\mathrm{h}}_{\nu_2,\mathbf{q}} \tag{3.6}$$

and the renormalized Rabi frequency is

$$\Omega_{\lambda,\nu,\mathbf{k}} = \omega_{\mathrm{R}} + \frac{1}{\hbar}\sum_{\lambda_1,\nu_1,\mathbf{q}\neq\mathbf{k}} V^{\lambda,\nu_1,\nu,\lambda_1}_{|\mathbf{k}-\mathbf{q}|}\mathrm{p}_{\lambda_1,\nu_1,\mathbf{q}}. \tag{3.7}$$

Here, $V^{\lambda_1,\lambda_2,\lambda_3,\lambda_4}_{|\mathbf{k}-\mathbf{q}|}$ is the Coulomb potential, [22]

$$V^{\lambda_1,\lambda_2,\lambda_3,\lambda_4}_{|\mathbf{k}-\mathbf{q}|} = \sum_{n,n'}\int dz\,dz' V(|\,\mathbf{k}-\mathbf{q}\,|)e^{-|\mathbf{k}-\mathbf{q}||z-z'|}\zeta^{\star}_{\lambda_1,\mathbf{k},n}(z)\zeta^{\star}_{\lambda_2,\mathbf{k},n'}(z')\zeta_{\lambda_3,\mathbf{q},n'}(z')\zeta_{\lambda_4,\mathbf{q},n}(z) \tag{3.8}$$

with the band and momentum dependent confinement functions $\zeta_{\lambda,\mathbf{k},n}(z)$. The unrenormalized single-particle energies of electrons and holes $\varepsilon^{e(h)}_{\lambda(\nu),\mathbf{k}}$ are defined by the band dispersion of the valence and conduction bands, respectively. In the momentum range relevant for optical transitions, i.e. in close proximity of the Γ-point at $\mathbf{k}=0$, this dispersion can be computed using the well-known $\mathbf{k}\cdot\mathbf{p}$-theory [22]. The unrenormalized Rabi frequency $\omega_{\mathrm{R}} = \frac{d^{\lambda,\nu}_{\mathbf{k}}\mathrm{E}(z,t)}{\hbar}$ is the basic light-matter coupling parameter. In the semi-classical limit and in dipole approximation it is determined by the product of the exciting light field $\mathrm{E}(z,t)$ at the QW position and the dipole-matrix element $d^{\lambda,\nu}_{\mathbf{k}}$. Contributions to the SBE that go beyond the Hartree-Fock approximation describe correlation effects such as dephasing of the polarization (Γ_{deph}), carrier scattering (Γ_{scatt}), and Coulomb screening. The accuracy of the theory, therefore, depends strongly on the treatment of these contributions. Detailed experiment-theory comparisons [7, 8, 21] show that a description of the correlation effects on the level of a second-Born Markov approximation is well suited to realistically model semiconductor QW lasers with emission wavelengths from the visible to the near- and mid-infrared regions of the electromagnetic spectrum. In this approximation, the correlation effects add contributions to the polarization equation of motion [32] Eq.(3.3)

Beyond Hartree-Fock Approximation

$$\Gamma_{\lambda,\nu;\mathrm{deph}} = i\left(\Gamma^{\lambda}_{d}+\Gamma^{\nu}_{d}\right)p_{\lambda,\nu,\mathbf{k}} - i\sum_{\mathbf{q}}\left(\Gamma^{\lambda}_{nd}(\mathbf{k},\mathbf{q})+\Gamma^{\nu}_{nd}(\mathbf{k},\mathbf{q})\right)p_{\lambda,\nu,\mathbf{k}+\mathbf{q}} \tag{3.9}$$

that may be subdivided into terms diagonal (d) and non-diagonal (nd) in the momentum index of the microscopic polarization. Here, Γ_d and Γ_{nd} are complex quantities whose real

parts describe a correction to the Hartree-Fock renormalization of the single-particle energies and whose imaginary parts represent the actual dephasing of the polarization. In the equation of motion for the carrier distributions Eq.(3.4), the correlation effects in second-Born Markov approximation lead to Boltzmann type scattering terms [32]

$$\Gamma^{e(h)}_{\lambda(\nu);\mathrm{scatt}} = \Sigma^{in,\lambda(\nu)}_{e(h),\mathbf{k}} \left(1 - \mathrm{n}^{\mathrm{e}(h)}_{\lambda(\nu),\mathbf{k}}\right) - \Sigma^{out,\lambda(\nu)}_{e(h),\mathbf{k}} \mathrm{n}^{\mathrm{e}(h)}_{\lambda(\nu),\mathbf{k}} \tag{3.10}$$

with momentum-dependent in- and out-scattering rates $\Sigma^{in,\lambda(\nu)}_{e(h),\mathbf{k}}$ and $\Sigma^{out,\lambda(\nu)}_{e(h),\mathbf{k}}$, respectively.

Effective Rate Approximation

Since the numerical evaluation of the microscopic scattering terms Eqs.(3.9)-(3.10) in each time step of a numerical laser-dynamics simulation is excessively CPU-time demanding, it is often necessary to include the correlation effects on the level of effective rates expressing the net effect of the underlying microscopic processes. In this limit, the dephasing of the polarization is described by a simple decay contribution with the characteristic dephasing time τ_{deph} [10, 13]

$$\Gamma_{\lambda,\nu;\mathrm{deph}} = -\frac{1}{\tau_{\mathrm{deph}}} \mathrm{p}_{\lambda,\nu,\mathbf{k}}. \tag{3.11}$$

Similarly, the carrier-scattering contribution modeling the equilibration of the carrier system follows from [10]

$$\Gamma^{e(h)}_{\lambda(\nu);\mathrm{scatt}} = -\frac{1}{\tau_{\mathrm{scatt}}} \left(\mathrm{n}^{\mathrm{e(h)}}_{\lambda(\nu),\mathbf{k}} - \mathrm{f}^{\mathrm{e(h)}}_{\lambda(\nu),\mathbf{k}}\right) \tag{3.12}$$

where τ_{scatt} governs the characteristic time scales of scattering events. Here, we have to distinguish between Coulomb scattering, which conserves the energy of the carrier system, and phonon scattering, which dissipates energy to the lattice. Thus, due to Coulomb scattering, the occupation probability $\mathrm{n}^{\mathrm{e(h)}}_{\mathbf{k}}$ develops into Fermi-Dirac distributions $\mathrm{f}^{\mathrm{e(h)}}_{\mathbf{k}}$ which yield the same total density and kinetic energy as the respective non-equilibrium distributions. As a result of phonon scattering, the occupation probability $\mathrm{n}^{\mathrm{e(h)}}_{\mathbf{k}}$ develops into Fermi-Dirac distributions $\mathrm{f}^{\mathrm{e(h)}}_{\mathbf{k}}(\mathrm{T_{lat}})$ at the lattice temperature $\mathrm{T_{lat}}$, conserving the total number of electron-hole pairs in the process. We note that as electrons and holes are excited at different energies due to their different dispersion relation, generally the electronic temperatures of electrons and holes differ. In order to keep some level of microscopic consistency, the different rates have to be computed on the basis of the SBE with correlation contributions in second-Born Markov approximation. For example, by monitoring the carrier thermalization process after pulsed excitation and extracting the characteristic time scales for different configurations, relaxation rates may be derived [69, 70]. The results depend on intrinsic material properties such as temperature and carrier

density and on the excitation conditions. To include effects related to the quantization of the light field, such as spontaneous dipole fluctuations ($\Lambda^{\mathrm{p}}_{\mathrm{spont}}$) and loss processes ($\Lambda^{\mathrm{n}}_{\mathrm{spont}}$), we phenomenologically add the appropriate terms in the set of equations Eq.(3.3) and Eq.(3.4). Similarly, we deal with the contributions describing carrier generation via (Π_{pump}) .

To model the effect of continuous carrier injection by optical pumping in Eq. (3.3), we assume a momentum-dependent generation rate

$$\Pi_{\mathrm{pump}}(\mathbf{k}) = -\left(\frac{d_{\mathrm{cv}}}{\hbar}\right)^2 \mid \mathrm{E}_0 \mid^2 (\mathrm{n}^{\mathrm{e}}_{\mathbf{k}}(t) + \mathrm{n}^{\mathrm{h}}_{\mathbf{k}}(t) - 1) \times \left(\frac{2\eta}{(\omega_{\mathbf{k}} - \omega_{\mathrm{pump}})^2 + \eta^2}\right)$$

where the effect of Pauli blocking leads to the factor $(\mathrm{n}^{\mathrm{e}}_{\mathbf{k}}(t) + \mathrm{n}^{\mathrm{h}}_{\mathbf{k}}(t) - 1)$. The quantities E_0, $\hbar\omega_{\mathrm{pump}}$ and η denote the amplitude, the energy, and the spectral width of the continuous pump-light field, respectively. Clearly, the generation rate $\Pi_{\mathrm{pump}}(\mathbf{k})$ yields a Lorentzian distribution of the pump-induced carriers in the bands. [1]

The relevant rate in the discussion of effects related to the spontaneous emission process is the spontaneous emission coefficient Γ_{spont}. In these terms the spontaneous emission contributions in Eq.(3.4) can be modeled according to [25]

$$\Lambda^{\mathrm{n}}_{\mathrm{spont}} = -\Gamma_{\mathrm{spont}}(\mathbf{k})\mathrm{n}_{\lambda\mathbf{k}}\mathrm{n}_{\bar{\lambda}\mathbf{k}} \mathit{and} \Lambda^{\mathrm{p}}_{\mathrm{spont}} = \beta\Gamma_{\mathrm{spont}}(\mathbf{k})\mathrm{n}_{\lambda\mathbf{k}}\mathrm{n}_{\bar{\lambda}\mathbf{k}} \tag{3.13}$$

whith $\lambda = \mathrm{e}$ and $\bar{\lambda} = \mathrm{h}$ and vice versa. Here, we use the Wigner-Weisskopf coefficient

$$\Gamma_{\mathrm{spont}}(\mathbf{k}) = \frac{n^3}{\pi^2\varepsilon_0\hbar^4 c_0^3} \mid d_{\mathrm{cv}} \mid^2 \left(\mathrm{E}_{\mathrm{g}} + \frac{\hbar^2\mathbf{k}^2}{2m_{\mathrm{r}}}\right)^3 \tag{3.14}$$

where the quantities c_0, ε_0, n and m_{r} are constants describing the vacuum velocity of light, the dielectric constant, the background refractive index and the reduced effective mass of electrons and holes, respectively. The spontaneous emission factor β is given by the ratio between the spontaneous emission radiated into the lasing mode and the total spontaneous emission such that it assumes values between zero and one.

Maxwell Semiconductor Bloch Equations

Coupling the Hartree-Fock SBE for the microscopic polarization $\mathrm{p}_{\lambda,\nu,\mathbf{k}}$, Eq. (3.3), and the occupation probabilities for electrons and holes $\mathrm{n}^{\mathrm{e}(h)}_{\lambda(\nu),\mathbf{k}}$, Eq. (3.4), to the transversal wave equation, Eq.(3.1), we have a closed set of equations that allows for the study of non-equilibrium effects in VECSELs and is still numerically feasible. For a discussion of

[1] An analogues model of the effect of electrical pumping is provided in the discussion of charging dynamics in Section 7.2.2.

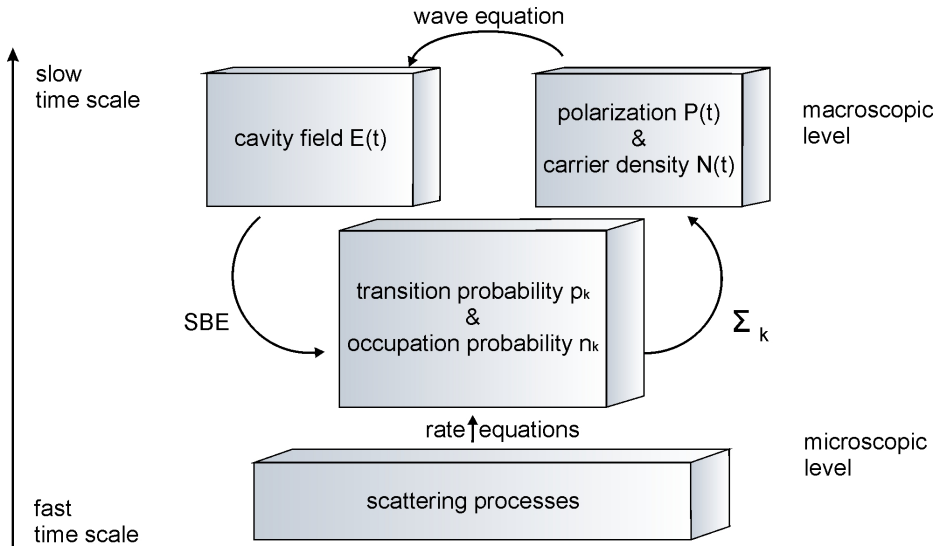

Figure 3.1: Model buliding Blocks.

the numerical implementation of this set of equations that forms the mathematical basis of the model studies performed in the following see Section 3.1.3.

3.1.2 Model Assumptions

Generic Model Description

As a first step towards the complete VECSEL modeling, we want to analyze the regimes where non-equilibrium effects are truly important. Therefore, we use a generic model rather than modeling a real material system as needed for a fully quantitative analysis. For the description of the QW active material, we restrict ourselves to a two-band model, postulating strong confinement of electrons and holes such that only the lowest subbands need to be taken into account. In addition, we limit the consideration to a parabolic band structure where the transition energy is expressible in terms of the effective masses of the electrons, m_e, holes, m_h, and the band-gap energy E_g. More complicated bandstructures may be implemented directly but would lead to increased computational effort only and not contribute to the generic understanding we aim at with our numerical simulations. Finally, in a first approximation, we do not yet implement the microscopic relaxation rate approximation summarized in Section 3.1.1 but use properly chosen phenomenological dephasing rates instead.

3.1.3 Numerical Implementation

Traveling Wave Method

For our model analysis, we solve the semiconductor Maxwell-Bloch equations in the time domain, applying a traveling-wave method based on a direct solution of the wave equation, Eq. (3.1). This method takes advantage of the fact that within each layer of the dielectric structure of the laser device, the light field can propagate freely and may thus be decomposed into forward and backward traveling field components, E^+ and E^-,

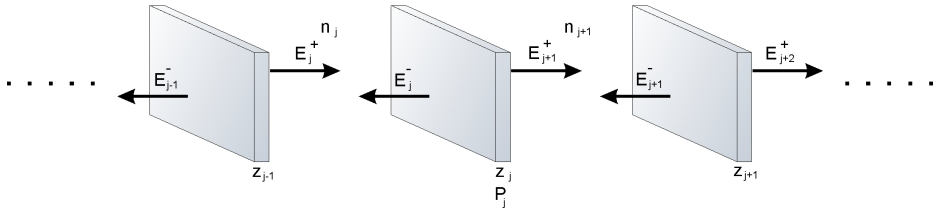

Figure 3.2: About numerical implemenation of the field propagation. A travelling-wave model [36] based on a direct solution of the wave equation is applied to simulate the propagation of the light field inside the laser cavity.

respectively. Typically, the laser wavelength is large in comparison to the QW width such that it is justified to tread the QW as δ-peaks of negligible spatial extension. Hence, the forward and backward traveling field components can be determined via Maxwell's boundary conditions at the layer interfaces. Thus, assuming that the polarization is non-vanishing only at the QW positions, for the cavity field at both sides of the *jth* boundary one obtains [36]

$$\begin{bmatrix} \mathrm{E}^{+}_{j+1}(t-\frac{z_j}{c_{j+1}}) \\ \mathrm{E}^{-}_{j}(t+\frac{z_j}{c_j}) \end{bmatrix} = \begin{bmatrix} \frac{2n_j}{n_j+n_{j+1}} & \frac{n_{j+1}-n_j}{n_j+n_{j+1}} \\ \frac{n_j-n_{j+1}}{n_j+n_{j+1}} & \frac{2n_{j+1}}{n_j+n_{j+1}} \end{bmatrix} \begin{bmatrix} \mathrm{E}^{+}_{j}(t-\frac{z_j}{c_j}) \\ \mathrm{E}^{-}_{j+1}(t+\frac{z_j}{c_{j+1}}) \end{bmatrix} - \frac{\mu_0 c_0}{2n_j} \begin{bmatrix} \frac{\partial}{\partial t}\mathrm{P}_j(t) \\ \frac{\partial}{\partial t}\mathrm{P}_j(t). \end{bmatrix} \tag{3.15}$$

While the first term on the right hand side of the above equation describes reflection and transmission at the interface of the j-th dielectric layer, the second term accounts for the absorption and amplification of the light field. Explicitly, we solve the above equation in the slowly varying envelope approximation and perform a Fourier-transform of the resulting complex field component to analyze the frequency components of the outcoupled laser light field.

Runge-Kutta Algorithm

The time dynamics of the microscopic polarization and carrier distributions follow from a fourth order Runge-Kutta algorithm providing a stable finite difference method for numerical solutions of differential equations in the form of the SBEs [10, 22].

4. Research Results

4.1 Microscopic Analysis of Two-Color Laser Operation (cf. Ref.(5))

4.1.1 Introduction

Motivation

Semiconductor quantum-well (QW) lasers exist in numerous realizations. As a common feature, the gain material in all these systems has a relatively large bandwidth and a rather flat peak. This gain characteristics leads to a low mode selectivity for semiconductor laser devices with large extended cavities. Since these devices involve a very high density of longitudinal modes, usually several of the densely spaced cavity modes experience a comparable amplification. As a consequence, typical QW lasers exhibit a multi-mode emission characteristics. Whereas this multi-mode operation is undesirable in many cases where one ideally prefers an efficient conversion of the excited carriers into a single-mode laser field, the well-defined emission at two laser modes is needed, e.g. in cases where difference frequency generation is exploited to generate light in the terahertz spectral range [15, 27]. Experimentally, such two-color operation has been observed not only in semiconductor QW lasers using spectrally filtered mirror feedback [27], but also in a traditional vertical external cavity surface emitting laser (VECSEL) system [15].

Despite the experimental realizations, a full theoretical understanding of the conditions under which semiconductor lasers can oscillate simultaneously and stable at two different frequencies is still missing. This question establishes a highly non-trivial problem since

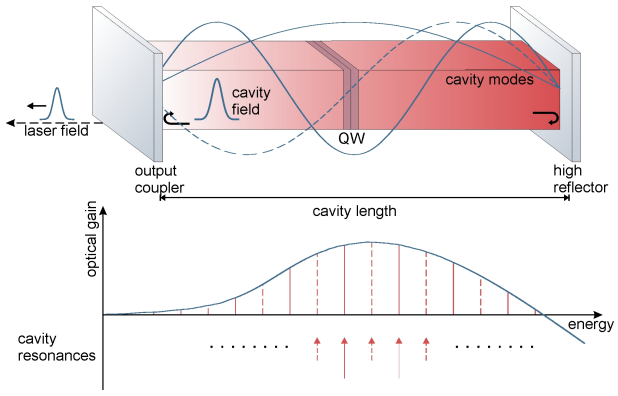

Figure 4.1: Sample setup. The upper plot depicts a schematic sketch of the effective-mirror resonator structure we use in our model calculations. The lower plot shows a typical semiconductor-gain spectrum. The vertical lines indicate the positions of the cavity resonances. While the dashed lines belong to modes leading to negligible modal gain due to the vanishing light -matter coupling, the solid lines correspond to potential lasing modes.

the multi-mode dynamics is determined by a complex interplay of mode competition, gain, and carrier distribution dynamics. Furthermore, the emission characteristic of the laser systems is strongly dependent on the actual geometry of the setup, the material parameters of both the dielectric structure and the gain region and the actual excitation state of the optically active material. In this context, it is an interesting problem, to theoretically analyze the different lasing regimes that might be encountered in experiments and to correlate the observed dynamics to the system configuration in detail. Whereas previous studies [52] used quasi-equilibrium gain configurations, we include the important non-equilibrium effects using a non-linear laser model on the basis of the semiconductor Maxwell-Bloch equations. Such a model is not limited to the dynamics of the macroscopic quantities laser field, polarization and carrier density, which are typically studied in multi-mode problems, but, furthermore, allows insight into the underlying microscopic processes and effects. Thus, it is perfectly suited for an analysis of non-linear processes caused by and associated with non-equilibrium effects as for example kinetic and spectral hole burning.

4.1.2 Model Exercise

Model Setup

To test our model, we set up an effective-mirror resonator structure with appropriate reflective boundary conditions at both ends of a linear cavity (cf. Fig. (4.1)). The cavity length is adjusted to have several cavity modes covered by the semiconductor gain spectrum. In order to obtain maximum overlap between the cavity light-field and the gain material and thus provide maximum light-matter coupling, the QW gain regions are

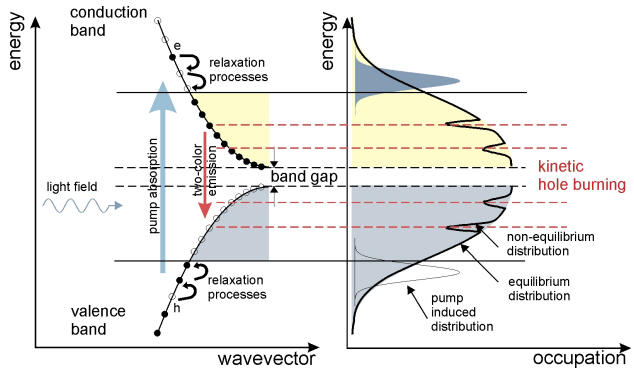

Figure 4.2: Schematic diagram of the excitations in semiconductor materials. The left plot shows the band structure in parabolic approximation. The right plot depicts the microscopic occupation probabilities for the electrons in the conduction band and the holes in the valence band.

positioned in the anti-nodes of the empty-cavity modes. The set of material parameters is chosen such that the cavity including the QW layers consists of a homogenous dielectric structure with constant background refractive index. This way, we avoid additional backscattering effects which may further complicate the dynamics.

4.1.3 Simulation Results

Simulation Results and Condition of Stable Two-Color Laser Emission

Our numerial results show that stable dual-mode operation is achieved for conditions where the mode spacing allows the two modes to burn separate kinetic holes into the occupation probability $n_{\mathbf{k}}^{e(h)}$ as depicted schematically in Fig. (4.2). As can be seen in the upper panels of Fig. (4.3), the amplitude spectrum of the complex laser field clearly displays two dominant peaks at the position of the laser resonances with the maximum modal gain. Clearly, this situation is favored when the two modes have similar modal gain (see lower panels of Fig. (4.3)). Interestingly, even though distinct kinetic holes are seen in the carrier distribution functions, no spectral holes can be seen in the corresponding gain spectra. Due to the dephasing of the polarization there is no one-to-one correspondence between momentum values and transition energies since the dephasing of the polarization leads to an homogeneous broadening of each transition. Consequently, the distinct kinetic holes in the occupation probability only show up as a broadening and flattening of the gain spectrum.

Because of the momentum resolved treatment of the momentum-state occupation dynamics, the different elements of this distribution function are only coupled via the interaction and relaxation processes. Hence, for sufficient mode spacing, the momentum regions into which the separate holes are burned by the two-color laser operation are only weakly coupled and the influence of cross-saturation effects is relatively small. With respect to the gain, this mutual independence implies that the gain saturation caused by the amplification of a given mode reduces the available gain basically for itself and not for all other modes, as would be the case in the homogeneous limit. As a result, the separate holes in the occupation probability can compensate small inequalities in the unsaturated

net gain and thus contribute to the stability of the two-color laser emission.

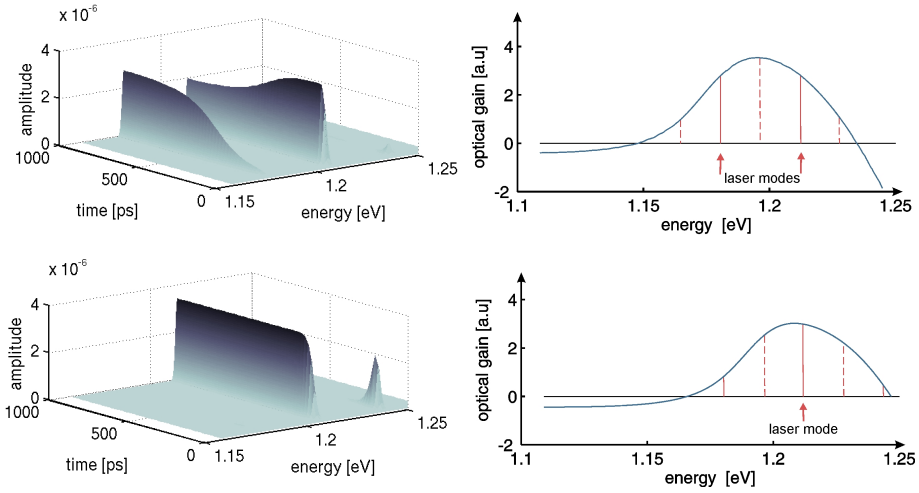

Figure 4.3: Frequency analysis of the laser field. On the left hand side, the amplitude spectrum of the complex laser field is shown in dependence of time for two different sets of material parameters. On the right hand side, corresponding gain spectra are given. For further explanations see text.

4.1.4 Summary

We conclude that taking into account non-equilibrium effects and the corresponding inhomogeneity by coupling the dynamics of the microscopic polarization to the occupation probability is important for a detailed study of the stabilty of multi-mode problems. Laser simulations based on rate equations for the carrier density and the resulting quasi-equilibrium Fermi-Dirac distributions for the occupation probabilities, therefore, are not sufficient for this purpose and may be considered as the homogeneous limit of the more general model introduced here.

4.2 Microscopic Analysis of Mode-Locking Dynamics (cf. Ref.(56))

4.2.1 Introduction

Motivation

Optically-pumped vertical external cavity surface emitting lasers (VECSELs) or disk lasers have been shown to be ideal as wavelength agile, high brightness sources for numerous applications including raw power [23], multi-Watt single frequency [48] and high average power under various mode-locking scenarios. Specifically, mode-locking has been observed with external semiconductor saturable absorber mirrors (SESAM) [26, 63, 75] , with integrated quantum well and quantum dot SESAMS (MIXSEL) [77], with graphene [30, 77] and carbon nanotube [64] saturable absorbers. To our knowledge, the shortest fundamental mode-locked pulse duration to date has been 107 fs albeit at very low average power [39]. While shorter 60fs pulses have been reported [60], these have been harmonically mode-locked transients within longer few picosecond “pulse molecules”. Rate equation level models using parameters extracted from experiment have proved

successful in capturing the mode-locking behavior for longer duration pulses [14]. As typical intraband carrier scattering times are on the order of 100 fs, it is expected that dynamically changing non-equilibrium distributions will not have a chance to relax to quasi-equilibrium Fermi-Dirac distributions during the pulse itself. The complexity of the non-equilibrium many-body dynamics has limited studies to date to a relatively simple one of multiple QW single pass geometries. In this study, we present what to our knowledge is the first attempt to simulate microscopic many body effects in a simple mode-locked geometry by solving the Maxwell - Semiconductor Bloch equations (MSBE) in the Hartree Fock limit using a 2-band model. Our preliminary finding is that sub 100fs mode-locking is feasible in the low gain limit where all carriers are utilized in the pulse forming stage. In higher gain situations unused carriers can destabilize the pulse by providing unused gain in spectral regions that exist external to the interacting non-equilibrium system.

4.2.2 Model Exercise

Model Setup

As a first effort we employ a simple linear one-dimensional VECSEL cavity with a 2 ps round-trip time, with an active mirror consisting of a DBR and a resonant-periodic gain medium on the one end and the SESAM attached to a 1 % outcoupling mirror on the other end. We assume a 3ps (0.5 ps) relaxation time for the QW (SESAM) populations back to a reference 300 K quasi-equilibrium distribution of density 2.0e16 [1/m 2] (5.0e14 [1/m 2]) and InGaAs/AlGaAs bandstructure parameters. The gain medium consists of 10 effective 8nm QWs and the bandgap of the single SESAM QW is energetically 10 meV below that of the gain QWs. To simulate the transverse focusing onto the SESAM used in mode-locking experiments, we use a tenfold field enhancement in the SESAM. With this input, we numerically solved the MSBE starting with a very weak initial pulse of 200 fs duration (FWHM). By changing the initial pulse duration and amplitude, we verified that the results are independent of the initialization details.

4.2.3 Simulation Results

Simulation Results and Modelocking Conditions

An example of the numerical results is presented in Fig.4.4 . The upper left panel shows the reference carrier distribution in the gain QWs together with the non-equilibrium distribution induced by the intra-cavity circulating pulse. We clearly notice the pronounced kinetic hole- burning in the distributions. The corresponding non-equilibrium gain spectrum is shown in the upper right panel of Fig. 4.4. We clearly see a significant gain reduction and flattening in comparison to the quasi-equilibrium gain spectrum of the background distributions. The lower left panel depicts the SESAM carrier distribution induced by the pulse and the stable converged pulse shape is plotted in the lower right panel, respectively. From the insets, we can see that pulse amplitude and FWHM stabilize approximately 2ns after the initialization. The resulting 75 fs FWHM mode-locked pulse has a somewhat complex shape and is clearly not Fourier-transform limited since we did not implement any attempts of round-trip dispersion management. Whereas the chosen

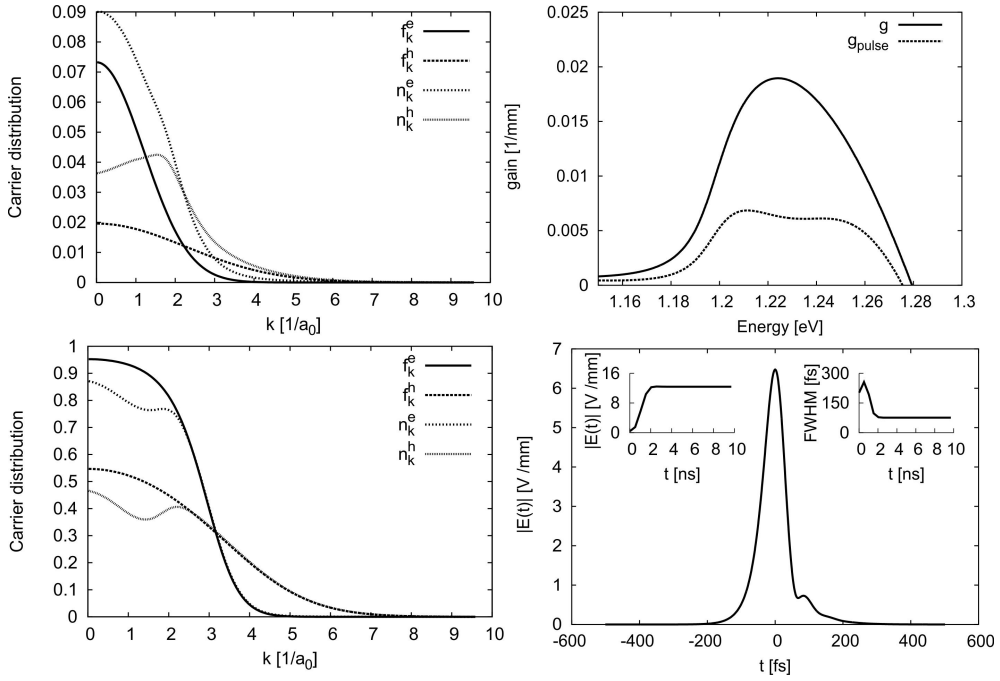

Figure 4.4: Example for the results obtains by numerical solution of the MSBE for mode-locking operation. The upper left panel shows the momentum resolved reference carrier distributions fke(h) in the gain QWs together with the nonequilibrium distribution nke(h) induced by the intra-cavity circulating pulse. The corresponding nonequilibrium gain spectrum is shown in the upper right panel (dotted line) together with the reference gain spectrum of the background distributions (solid line). The SESAM carrier distribution and the converged stable pulse are plotted in the lower left and right panels, respectively. The insets show the temporal stabilization of the pulse amplitude and the FWHM.

example shows a successfully mode-locked configuration, we have encountered many situations with unstable results where the pulse develops complicated multi-peaked shapes or does not reach a stable configuration. We are in the process of mapping the parameter space to identify the best mode-locking conditions and to explore the limitations on achievable pulse durations and intensities.

4.2.4 Summary

In conclusion, we have carried out the first microscopic simulation of mode-locking in a simple VECSEL cavity. Our results indicate that clean sub 100fs pulses can be generated in the low gain limit. At higher gain and consequently higher peak intensities, we have preliminary evidence that unused carriers can destabilize the pulse waveform. The challenge in modeling the latter is the extreme computational complexity of the many-body physics including carrier capture between bands including barrier states and

intraband correlations involving carrier-carrier and carrier phonon scattering. The first simulation presented in this paper, while modest, is a key first step to assessing the role of non-equilibrium processes in limiting pulse duration or maximal achievable intensity or repetition rate. The next step is to move beyond the Hartree Fock limit and study the influence of ultrafast carrier scattering within individual carrier plasmas. Going beyond the Hartree-Fock limit to assess the role of ultrafast correlations in the hot carriers (electron/hole) and carrier capture from the pumped barrier to inverted well states, we expect further pulse-reshaping effects due to kinetic hole filling. However, we anticipate that the generic features observed in the simple two-band model will be preserved in the low-gain limit, due to the presence of shallow kinetic holes, these correlations should not significantly affect the results.

5. Conclusion

Benefits and Challenges of Semiconductor Laser Modeling

Apparently, a laser model can save a lot of time and costly experiments by performing model calculations and numerical experiments to find out, for example, what the driving mechanisms are, how strong certain effects really are, or to what extent improvements can be expected from certain design changes. Thus, for the detailed study of pulse shaping in mode-locked lasers and the stable emission of dual-mode lasers, numerical light propagation modeling on the basis of a microscopic theory for the light-matter interaction may be very usefu. However, both the modeling of pulse shaping mechanisms in a mode locked laser and the mapping of the ocurance of stable two color operation of modern semiconductor heterostructures like VECSELs are numerically very challenging as different time scales are involved in these processes. Thus, these kinds of laser simulations requires the computation of the light matter interaction and propagation through the active and passive medium over numerous roundtrips while at the same time the ultrafast electronic charge carrier dynamics need to be traced closely in order to catch the non-equilibrium dynamics correctly.

Summing up the problem of modeling and simulating the two-color operation and modelocking dynamics in VECSELs, we want to emphasize that a realistic description of multi-mode emission requires the incorporation of the complex interplay of mode competition, gain characteristics and charge carrier dynamics on a microscopic level [36, 78, 79] in the model. Without laser oscillations, the pump-induced charge carrier distributions relax towards Fermi-Dirac distributions via interband scattering processes.

Thus, Coulomb- and phonon-scattering events lead to thermalization of the excited semiconductor material towards a quasi-equilibrium situation. With the onset of laser activity, non-equilibrium effects play an increasing role and the charge carrier distribution may deviate decisively from a quasi-equilibrium Fermi-Dirac distribution. In particular, under high excitation conditions, kinetic holes are burned into the charge carrier distribution as the interband recombination mediated by stimulated emission prevents a thermalization towards a quasi-equilibrium situation. We conclude that taking into account non-equilibrium effects and the corresponding inhomogeneity by coupling the dynamics of the microscopic polarization to the occupation probability is important for a detailed study of the stability of multi-mode problems. Laser simulations based on rate equations for the carrier density and the resulting quasi-equilibrium Fermi-Dirac distributions for the occupation probabilities, therefore, are not sufficient for this purpose and may be considered as the homogeneous limit of the more general model introduced here. Approaching the given problem, therefore, most attention needs to be paid to develop, test and apply models that unite the best of the two fields of laser modeling, i.e. material models which describe the physical interactions in the semiconductor and process models which describe the device functionality or behavior . Thereby whenever possible consistency checks should be carried out comparing the results of the fully microscopic theory to the results of the model exercise to avoid e.g.oversimplification and effectively excluding relevant effects from the model. So, though in the framework of the model presented here we find that for sufficiently large mode spacing two-color emission may emerge naturally in high power applications as VECSELs where several modes experience comparable amplification, in future studies a careful inspection needs to be made of the initial assumptions underlying the model. Especially, the assumption of phenomenological relaxation rates in a problem where special emphasis needs to be placed on homogenizing effects as scattering is questionable. Thus, for example, in a next step of the model approach presented in this work, it seems to suggest itself to carefully check whether beside the prominent Coulomb interaction between the carriers there are further relevant contributions in the microscopic scattering terms that may counteract the kinetic hole burning and thus destabilize related phenomena as modelocking and two color emissions in semiconductor lasers. Another approximation that needs to be reconsidered is the neglection of the fact that, typically, the free spectral range of the laser is by a multiple smaller than the halfwidth of the etalon filter function and often several resonator modes oscillate is doubtful. In reality, furthermore, signal noise as acoustic vibrations or pump-laser fluctuations may occur and disturb the optimum laser performance. Hence, we expect that in reality the mode spacing may not be sufficiently large such that different kinetic holes merge and ultrafast homogenizing scattering processes counteract the hole burning effect which we observe in our recent model study.

Demands and Expectations Placed on Intensified Research Efforts

Intensified research efforts need to find a way to include further aspects of the fully microscopic theory in the model computations - which is a computer-related challenge rather than physically motivated, as by code optimization procedures the runtime needs to

be decreased decisively to go beyond the assumptions made here. The first step into this direction has already been made in the form of passing the program developed for our model calculations to experts in the fields of applied numerically oriented mathematics [37]. Foremost, however, to render consistency checks as well as parametric studies feasible, it is necessary to optimize the model implementation with respect to computational speed. Since both the mode-locking and two-color simulation have to integrate the equations for tens of thousands of timesteps, any small improvements add up to large computing time savings such that more experienced programming knowledge is needed for further improvements. Hence, full of curiosity and expectations, the simulation program has been handed over to the experts in the field of applied mathematics in the research group of Prof. Dr. J.V Moloney and Isak Kilen who already contributed decisively to the results presented in the paper *Ultrafast nonequilibrium carrier dynamics in semiconductor laser mode lockings* [56] (cf. Section 4.2). At this stage, we conclude that a first and relevant step has been made towards an effective non-equilibrium semiconductor laser simulation tool. The overall direction is very promising such that we can expect that numerous further studies will follow.

II Part Two: Charging Dynamics

6. Problem Definition

As mentioned earlier, in laser physics, modeling and simulation may help to represent or characterize, understand or analyze, assess or solve research problems encountered in experiments and verify assumptions made in theoretical investigations. While the study of the influence of the ultrafast carrier dynamics on two-color laser operation and the generation of short pulses in high power laser applications serve as examples for the former aspects, the analysis of charging dynamics in electrically pumped quantum well lasers may be considered as an interesting example for the latter. In the framework of this analysis, we could verify that the frequently used but not yet proven assumption of charge neutrality in the active region of electrically pumped quantum well lasers is actually justified.

Injection Pumped Quantum-Well Laser

To dive into the details of our investigations, we recall that in its simplest form, an injection pumped quantum-well (QW) laser consists of a thin layer of low band-gap material sandwiched between an n-doped substrate and a p-doped layer of high band-gap materials. The difference between the smaller band gap of the well material and the larger band gap of the barriers causes a confinement potential for both electrons and holes. Current is injected into the heterostructure via suitably designed electrodes.

Operating a quantum-well laser device by electric pumping, population inversion is obtained by the capture of barrier electrons and holes in the quantum well, i.e. into the active region of the laser. The relaxation mechanism involved in the carrier-capture process, may induce different dynamics for electrons and holes and thus assign different

roles to positive and negative charge carriers in a quantum-well laser [61, 67] as the following consideration clarify. When modeling the capture process, one has to account for the Fermionic nature of electrons and holes leading to the well-known Pauli blocking of the occupied states. Since typically the holes have a significantly larger effective mass than the electrons, this phase space effect is more prominent for the electrons than for the holes giving rise to a reduced capture probability for the electrons. Charging of the quantum well becomes possible.

Consequence of Electric-Pumping Induced Charging of the Quantum Well

As a direct result of this electric-pumping induced charging of the quantum well, one expects the generation of static fields whose effects on the optical properties of the sample should be significant. The optical properties of a semiconductor quantum-well laser strongly depend on its exact structural design [66], which is defined not by fabrication only but may be changed and manipulated decisively by variable influences as, for example, an applied voltage [3, 53, 54, 55]. However, since in a comparison of experimental and theoretical quantum-well gain spectra for accurate predictions no modifications due to charging have to be considered [11, 58], it has to be concluded that in experimental setups no electric-pumping induced charging effects can be observed. This discrepancy in expectation and observation gives rise to the question by what the neglect of charging is legitimated. It is common practice to ignore the modifications due to charging in modeling the optical properties of an electrically pumped semiconductor quantum-well laser (see Ref. [16, 49, 65, 72]) even though only few studies of the effects of charging on the device characteristics are reported [44, 71]. To address this issue, in this investigation we perform a comparative modeling of a quantum-well laser structure with and without charging of the quantum well. We show that typical values of charging introduced by electric pumping clearly affect the optical absorption spectrum of a quantum-well system. In order to account for the actual absence of electric-pumping induced charging effects, we extend the laser model to also include the dynamics of the carriers in the unconfined states, which do not contribute to the lasing process. Thus, we present a phenomenological theory on the basis of microscopic reflections which explains the lack of an electric-pumping induced positive net-charge by a dynamic redistribution of barrier electrons in the quasi-continuum of states. It is shown that free barrier electrons move in to compensate the charging of the quantum well, yielding an almost vanishing overall charge. Furthermore, from the dynamics of the barrier carriers collective charge-density oscillations with plasma frequency are predicted, which may give rise to terahertz emission.

7. Research Results (cf. Ref.(4))

7.1 Introduction

Motivation

In its simplest form, an injection pumped quantum-well (QW) laser consists of a thin layer of low band-gap material sandwiched between an n-doped substrate and a p-doped layer of high band-gap materials. The difference between the smaller band gap of the well material and the larger band gap of the barriers causes a confinement potential for both electrons and holes. Current is injected into the heterostructure via suitably designed electrodes. By applying a voltage, charge carriers are pumped into the continuum of states energetically above the band edge of the barrier layers. Via Coulomb and phonon scattering some portion of these carriers is captured into the QW states where they can contribute to the lasing process. When modeling the capture process, one has to account for the Fermionic nature of electrons and holes leading to the well-known Pauli blocking of the occupied states. Since typically the holes have a significantly larger effective mass than the electrons, this phase space effect is more prominent for the electrons than for the holes giving rise to a reduced capture probability for the electrons. Naively following this line of argumentation one therefore expects a certain degree of QW charging. For the typical example of III/V semiconductor compounds under quasi-thermal lasing conditions, the low momentum states of the electrons are significantly (i.e. 2 - 5 times) more populated than those of the holes. Therefore, the capture rate of the electrons is reduced for elevated carrier densities and a positive net charge builds up. To investigate the relevance of this

effect and its possible consequences, one has to keep in mind that charging gives rise to static fields which not only affect the energetic structure of the device but also cause a redistribution of the carriers in the unconfined states. This redistribution in turn affects the capture process such that the full analysis of electric pumping-induced charging implies a complex interplay of electrostatic potentials resulting from local charge imbalances and scattering processes (see e.g. [44, 61, 67, 68]). In particular, one has to analyze the redistribution of the injected carriers between the unconfined barrier states and the confined states of the QW and its impact on the optical properties of the laser device (see e.g [58, 71]).

In this study, we present a microscopic analysis of the fundamental effects related to QW injection pumping. We show that both the carriers in the QW confined states and the unconfined barrier states have to be treated consistently in order to explain the experimentally observed absence of significant pumping-induced charging. It turns out that charge compensation occurs via the dynamic redistribution of the barrier electrons and holes in the quasi-continuum of states. Carriers in barrier states accumulate in the spatial vicinity of the QW to compensate the QW charging. This dynamic effect leads to an almost perfect overall charge neutrality. The stimulated electron-hole recombination in the QW together with the carrier replenishing and associated redistribution in the barrier states gives rise to sustained charge oscillations at the plasma frequency.

7.2 Theoretical Footing

As one of the important ingredients to analyze the characteristics of a semiconductor laser, one needs to determine how the different electronic states are excited and how they influence the optical properties. We start from the reduced single-particle density matrix of the carrier system, where the diagonal elements determine the populations and the off-diagonal elements characterize the coherences between different states and determine the optical polarization of the semiconductor[22]. In coordinate representation, the density matrix $\rho_{\lambda_1,\lambda_2}(\mathbf{r}_1,\mathbf{r}_2,t) = \langle \hat{\Psi}^\dagger_{\lambda_1}(\mathbf{r}_1,t)\hat{\Psi}_{\lambda_2}(\mathbf{r}_2,t)\rangle$ is defined by the expectation value of the product of the Fermionic field operators $\hat{\Psi}^\dagger_\lambda(\mathbf{r},t)$ and $\hat{\Psi}_\lambda(\mathbf{r},t)$ which create and annihilate an electron in the band λ at position $\mathbf{r}$, respectively.

Heisenberg's Equation of Motion

The dynamical system evolution is is governed by the Hamiltonian $\hat{H}$ via Heisenberg's equation of motion

$$i\hbar\frac{\partial}{\partial t}\langle \hat{\Psi}^\dagger_{\lambda_1}(\mathbf{r}_1,t)\hat{\Psi}_{\lambda_2}(\mathbf{r}_2,t)\rangle = \langle [\hat{\Psi}^\dagger_{\lambda_1}(\mathbf{r}_1,t)\hat{\Psi}_{\lambda_2}(\mathbf{r}_2,t),\hat{H}]_-\rangle. \tag{7.1}$$

Hamiltonian

In its simples form, the Hamiltonian of a Coulomb interacting carrier system is given as the sum of the single-particle energy H_0 and the Coulomb interaction $V(\mathbf{r},\mathbf{r}')$ [17, 22, 28, 38]

$$\hat{H} = \sum_{\nu} \int d^3r \hat{\Psi}^{\dagger}_{\nu}(\mathbf{r},t) H_0 \hat{\Psi}_{\nu}(\mathbf{r},t) + \sum_{\nu,\nu'} \frac{1}{2} \int d^3r \int d^3r' \times \hat{\Psi}^{\dagger}_{\nu}(\mathbf{r},t) \hat{\Psi}^{\dagger}_{\nu'}(\mathbf{r}',t) V(\mathbf{r},\mathbf{r}') \hat{\Psi}_{\nu'}(\mathbf{r}',t) \hat{\Psi}_{\nu}(\mathbf{r},t) \tag{7.2}$$

In the resulting equations of motion, one encounters the hierarchy problem of many-body physics since the Coulomb part of the Hamiltonian couples the dynamics of the single-particle quantity $\langle \hat{\Psi}^{\dagger}_{\lambda_1}(\mathbf{r}_1,t) \hat{\Psi}_{\lambda_2}(\mathbf{r}_2,t) \rangle$ to a two-particle expectation value $\langle \hat{\Psi}^{\dagger}_{\lambda_1}(\mathbf{r}_1,t) \hat{\Psi}^{\dagger}_{\nu}(\mathbf{r},t) \hat{\Psi}_{\nu}(\mathbf{r},t) \hat{\Psi}_{\lambda_2}(\mathbf{r}_2,t) \rangle$. The simplest approach to obtain a closed set of equations is to truncate the hierarchy using the Hartree-Fock decoupling by splitting the two-particle expectation value into products of single-particle terms and a purely correlated part ([22, 28, 38]). In the analysis in this paper, we treat all Coulomb correlations and also other effects like phonon scattering on a phenomenological level since we want to focus exclusively on the main consequences of the lack of local charge neutrality, i.e. the Hartree contribution.

7.2.1 Hartree Contribution

Equation of Motion in Hartree-Fock Approximation

In Hartree-Fock approximation, where the purely correlated part resulting from the hierarchical decoupling is neglected, the equation of motion for the density matrix is obtained as[22]

$$i\hbar \frac{\partial}{\partial t} \langle \hat{\Psi}^{\dagger}_{\lambda_1}(\mathbf{r}_1) \hat{\Psi}_{\lambda_2}(\mathbf{r}_2) \rangle \approx [H_0(\mathbf{r}_2) - H_0(\mathbf{r}_1)] \langle \hat{\Psi}^{\dagger}_{\lambda_1}(\mathbf{r}_1) \hat{\Psi}_{\lambda_2}(\mathbf{r}_2) \rangle + \int \Big[V(\mathbf{r}_2,\mathbf{r}) - V(\mathbf{r}_1,\mathbf{r}) \Big] \Big(\sum_{\nu} \langle \hat{\Psi}^{\dagger}_{\nu}(\mathbf{r}) \hat{\Psi}_{\nu}(\mathbf{r}) \rangle \langle \hat{\Psi}^{\dagger}_{\lambda_1}(\mathbf{r}_1) \hat{\Psi}_{\lambda_2}(\mathbf{r}_2) \rangle - \sum_{\nu} \langle \hat{\Psi}^{\dagger}_{\lambda_1}(\mathbf{r}_1) \hat{\Psi}_{\nu}(\mathbf{r}) \rangle \langle \hat{\Psi}^{\dagger}_{\nu}(\mathbf{r}) \hat{\Psi}_{\lambda_2}(\mathbf{r}_2) \rangle \Big) d^3r.$$

Here, the second line contains the Hartree contribution and the third line gives the Fock-exchange term which appears as a consequence of the antisymmetry of the indistinguishable electrons. In contrast to the Fock term, the Hartree contribution explicitly includes the electron density distribution

$$\sum_{\nu} n_{\nu}(\mathbf{r},t) = \sum_{\nu} \langle \hat{\Psi}^{\dagger}_{\nu}(\mathbf{r},t) \hat{\Psi}_{\nu}(\mathbf{r},t) \rangle \tag{7.3}$$

where the sum runs over all valence (v) and conduction bands (c). To identify the contribution of charging in the equation of motion, it is useful to introduce $n_e(\mathbf{r},\mathbf{r}',t) \equiv \sum_{\nu \in \{c\}} \langle \hat{\Psi}^{\dagger}_{\nu}(\mathbf{r},t) \hat{\Psi}_{\nu}(\mathbf{r}',t) \rangle$ and $n_h(\mathbf{r},\mathbf{r}',t) \equiv \sum_{\nu \in \{v\}} \langle \Psi_{\nu}(\mathbf{r},t) \Psi^{\dagger}_{\nu}(\mathbf{r}',t) \rangle$ whose diagonal $\mathbf{r} = \mathbf{r}'$ terms are the electron and hole densities. With these definitions, the sum of the electron

densities in the valence and conduction bands (7.3) can be written as

$$\sum_{\nu} n_{\nu}(\mathbf{r},t) \quad = \quad n_e(\mathbf{r},t) - n_h(\mathbf{r},t) + \sum_{\nu\in\{\mathrm{v}\}} \langle [\hat{\Psi}^{\dagger}_{\nu}(\mathbf{r},t), \hat{\Psi}_{\nu}(\mathbf{r}',t)]|_{\mathbf{r}=\mathbf{r}'} \rangle .$$

Here, the commutator of the field operators $\hat{\Psi}^{\dagger}_{\nu}(\mathbf{r},t), \hat{\Psi}_{\nu}(\mathbf{r}',t)$ appears due to the Fermionic anticommutation relation. Its contribution to the Hartree term in Jellium approximation [22] is compensated by the ionic background such that it typically does not enter the equation of motion explicitly but is included with the band energies, usually in the evaluation of the band gap.

Hartree- Term

The remaining Hartree term

$$HT(\mathbf{r}_1,\mathbf{r}_2,t) = \int \{[V(\mathbf{r}_2,\mathbf{r}) - V(\mathbf{r}_1,\mathbf{r})][n_e(\mathbf{r},t) - n_h(\mathbf{r},t)]\}\, d^3r$$

is explicitly determined by the excess charge-carrier density $\Delta n(\mathbf{r},t) = n_h(\mathbf{r},t) - n_e(\mathbf{r},t)$ to which the electrons and holes contribute, both in the confined states of the QW and the extended barrier states.

In spatially homogeneous bulk semiconductors, the Hartree term is identically vanishing due to local charge neutrality. In nanostructures such as QWs, however, the different effective masses of electrons and holes and the imperfect quantum confinement typically lead to a violation of local charge neutrality such that the Hartree term does not vanish [18].

For optically pumped QW systems, where the total density of electrons in all QW states equals the total density of holes, charging does not occur as long as the quantum confinement prevents carrier escape. For electrically pumped QW systems, however, the situation is more complicated. Here, the density of electrons and holes in the quantum confined states follows from the complex interplay of electrostatic potentials and microscopic scattering processes. Thus, the consequences of the Hartree contribution require closer investigation, especially since it includes contributions from the carriers in all bands.

Effective Hamiltonian

Due to the single-particle character of the Hartree term, an effective Hamiltonian $\hat{H}_{\mathrm{eff}}$ may be introduced which leads to the same result in the equation of motion as the Hartree contribution of the full Hamiltonian:

$$HT(\mathbf{r}_1,\mathbf{r}_2,t)\langle \hat{\Psi}^{\dagger}_{\lambda_1}(\mathbf{r}_1,t)\hat{\Psi}_{\lambda_2}(\mathbf{r}_2,t)\rangle = \langle [\hat{\Psi}^{\dagger}_{\lambda_1}(\mathbf{r}_1,t)\hat{\Psi}_{\lambda_2}(\mathbf{r}_2,t), \hat{H}_{\mathrm{eff}}(t)]_{-}\rangle .$$

In QW structures, the carrier distributions $n_{\lambda}(\mathbf{r},t)$, $\lambda = e,h$, are typically characterized by a homogeneous 2D in-pane density n^{2D}_{λ} multiplied by the confinement factor $|\,\xi_{\lambda}(z)\,|^2$ describing the spatial carrier distributions perpendicular to the well. Consequently, the

Hartree term only depends on the z coordinate, yielding an extra potential for QW carriers. Adding to the QW confinement potential, the Hartree potential thus modifies the eigenvalue problem in the confinement direction z leading to a shift in the single-particle energies and a change in the confinement functions relative to the problem without charges.

Formally, we can write the effective Hamiltonian

$$\hat{H}_{\text{eff}}(t) = \sum_{\nu} \int \hat{\Psi}^{\dagger}_{\nu}(\mathbf{r},t)\; e\Phi(t)\; \hat{\Psi}_{\nu}(\mathbf{r},t) d^3r \tag{7.4}$$

that corresponds to the Hartree potential $e\Phi$. This potential is related to the charge distribution $e\Delta n(\mathbf{r})$, via Poisson's equation

$$\nabla^2\Phi(t) = \frac{e}{\varepsilon\varepsilon_0}\Delta n(\mathbf{r},t) \tag{7.5}$$

which has to be solved self-consistently with Schrödinger's equation for the confinement problem in the direction perpendicular to the QW. In Appendix (**??**), we show that for QW structures the Hartree term basically exhibits a parabolic space dependence,

$$e\Phi \approx \frac{e^2}{2\varepsilon\varepsilon_0}\Delta n(0,t) z^2. \tag{7.6}$$

Here, e is the electron charge, ε_0 is the free space permittivity, ε is the background dielectric constant, and the excess charge carrier density at the center of the QW is denoted as $\Delta n(0,t)$.

The concept of a Hartree potential provides a convenient way to study the influence of charging on the dynamics of the system. In particular, it allows us both to easily compute the optical properties of the system using the Hartree-Fock semiconductor Bloch equations ([32, 50]), and to clearly distinguish the back coupling of the carriers in the extended barrier states.

7.2.2 Hartree-Fock Semiconductor Bloch Equations for Charged Quantum Wells

Semicnductor Bloch Equation in Two-Band Approximation

In momentum representation, (7.3) yields the well-known semiconductor Bloch equations (SBE) ([32, 50]). Within the two-band approximation we obtain from (7.3) for the off-diagonal elements of the density matrix $\rho_{\lambda_1,\lambda_2}(\mathbf{r}_1,\mathbf{r}_2,t)$, $\lambda_1 \neq \lambda_2$ the dynamic equation for the microscopic polarization $P_{\mathbf{k}}$ which defines the optical properties of the semiconductor QW [41]. Here, the index $\mathbf{k}$ denotes the momentum in the plane of the QW. Including not only purely electronic contributions, but also the dipole interaction of the carrier system with an electromagnetic field $E(t)$, we find

$$i\hbar\frac{d}{dt}P_{\mathbf{k}} = [\varepsilon_{e,\mathbf{k}}+\varepsilon_{h,\mathbf{k}}+\Delta E_{\mathrm{BGR}}]P_{\mathbf{k}} - [1-f^{e}_{\mathbf{k}}-f^{h}_{\mathbf{k}}]\Omega_{\mathbf{k}} \tag{7.7}$$

with

$$\varepsilon_{e,\mathbf{k}} = E_{e,\mathbf{k}} - \sum_{\mathbf{q}\neq\mathbf{k}} V^{\mathrm{ee}}_{|\mathbf{k}-\mathbf{q}|} f^{e}_{\mathbf{q}}, \tag{7.8}$$

$$\varepsilon_{h,\mathbf{k}} = E_{h,\mathbf{k}} - \sum_{\mathbf{q}\neq\mathbf{k}} V^{\mathrm{hh}}_{|\mathbf{k}-\mathbf{q}|} f^{h}_{\mathbf{q}} \tag{7.9}$$

and

$$\Omega_{\mathbf{k}} = \left[d_{\mathrm{eh}}E(t) + \sum_{\mathbf{q}\neq\mathbf{k}} V^{\mathrm{eh}}_{|\mathbf{k}-\mathbf{q}|} P_{\mathbf{q}} \right]. \tag{7.10}$$

Here, the Coulomb-matrix elements are defined as

$$V^{\lambda_1,\lambda_2}_{\mathbf{q}} = V^{2D}_{\mathbf{q}} \int dz_1 \int dz_2 \times \xi^{*}_{\lambda_2}(z_2)\xi^{*}_{\lambda_1}(z_1) e^{-q(|z_2-z_1|)} \xi_{\lambda_1}(z_1)\xi_{\lambda_2}(z_2).$$

At the Hartree-Fock level, the Coulomb interaction $V^{2D}_{\mathbf{q}}$ enters as a renormalization of both the single-particle energies of electrons and holes, $E_{e,\mathbf{k}}$, $E_{h,\mathbf{k}}$, and the light field $E(t)$ that couples to the carrier system via the dipole element d_{eh}.

Charging Induced Renormalizations

The charging of the QW yields an additional renormalization $\Delta E_{BGR} = \Delta E_{sub} + \Delta E_{\Sigma} + \Delta E_{HT}$ of the single-particle energies, i.e. the band gap. Since the Hartree potential modifies the confinement problem, one finds a direct change ΔE_{sub} for the energetic spacing of the subband levels of the QW. The corresponding change in the confinement functions $\xi(z)$ alters the Coulomb-matrix elements (7.11). Consequently, also the difference in the exchange self-energy [22]

$$\Delta E_{\Sigma} = \sum_{\mathbf{q}\neq 0} V^{hh}_{\mathbf{q}} - \sum_{\mathbf{q}\neq 0} V^{hh,0}_{\mathbf{q}} \tag{7.11}$$

and the difference in the Hartree contribution of the completely filled valence bands (cf. discussion of (7.4))

$$\Delta E_{HT} = n_{ion}^{2D} S \left[\left(V_0^{eh} - V_0^{eh,0} \right) - \left(V_0^{hh} - V_0^{hh,0} \right) \right]. \tag{7.12}$$

contribute to the band-gap renormalization. Here, n_{ion} denotes the homogeneous 2D density of the ionic background of the Jellium model [22] and S is the quantization area. The superscript 0 in (7.11) and (7.12) indicates that the Coulomb matrix elements $V_{\mathbf{q}}^{\lambda_1,\lambda_2,0}$ are evaluated with the confinement functions corresponding to the limit of a vanishing Hartree potential. Actually, the time dynamics of the microscopic polarization $P_{\mathbf{k}}$ couples to the dynamics of the carrier distribution functions $n_{\lambda,\mathbf{k}}$ corresponding to the momentum representation of the diagonal elements of the density matrix $\rho_{\lambda,\lambda}(\mathbf{r}_1,\mathbf{r}_2,t)$. However, assuming that the scattering processes which drive the carrier distributions to equilibrium happen on a much smaller time scale than the times of interest, we replace $n_{\lambda,\mathbf{k}}(t)$ by stationary quasi-equilibrium Fermi distributions $f_{\mathbf{k}}^{\lambda}$ for the electrons ($\lambda = e$) and holes ($\lambda = h$), respectively [10].

Time Dynamics of the Carrier Distribution Functions

Formally, the time dynamics of the carrier distribution functions $n_{\lambda,\mathbf{k}}$ is also covered by (7.3). In this investigation, however, we apply a simple rate equation model that takes into account the essential features of the full microscopic theory ([6, 20]) by phenomenological fitting parameters

$$\begin{aligned} \frac{dn_{\lambda,\mathbf{k}}}{dt} = & \eta F_{\lambda,\mathbf{k}}[1 - n_{\lambda,\mathbf{k}}] - \frac{n_{\lambda,\mathbf{k}} - f_{\lambda,\mathbf{k}}}{\tau_1} - \frac{n_{\lambda,\mathbf{k}} - f_{\lambda,\mathbf{k}}(T_{\text{lat}})}{\tau_2} \\ & - \mathscr{A} n_{\lambda,\mathbf{k}} - \mathscr{B} n_{\bar{\lambda}} n_{\lambda,\mathbf{k}} - \mathscr{C} n_{\lambda} n_{\bar{\lambda}} n_{\lambda,\mathbf{k}}. \end{aligned} \tag{7.13}$$

The first contribution describes the relaxation of carriers from the extended barrier states into the confined states of the QW. The efficiency of this process is determined by the pumping strength η and the initial state distribution $F_{\lambda,\mathbf{k}}$ of the pump-injected carriers which arrive in the active region [33]. The Pauli-blocking factor $[1 - n_{\lambda,\mathbf{k}}]$ accounts for the effective reduction of the pump efficiency due to the presence of carriers inside the QW. The carriers in the barrier states have a large excess energy determined by the electric injection. These carriers strongly scatter among each other establishing a quasi-equilibrium Fermi-Dirac distribution $F_{\lambda,\mathbf{k}}$ in the barrier states. This distribution is related to the overall 2D carrier density via $n_{bar,\lambda} = 2/S \sum_{\mathbf{k}} F_{\lambda,\mathbf{k}}$ where the factor 2 is due to the two possible spin orientations. The steady injection current ensures that these carriers are not depleted by the recombination processes. The phenomenological relaxation times τ_1 and τ_2 in the carrier rate equation (7.13) determine the equilibration of the carrier system due to Coulomb and phonon scattering, respectively. Due to the Coulomb scattering, the carrier densities develop into a Fermi-Dirac distribution $f_{\lambda,\mathbf{k}}$, which yields the same total density and kinetic energy as $n_{\lambda,\mathbf{k}}$. As a result of the phonon scattering the carrier densities relax toward a Fermi-Dirac distribution $f_{\lambda,\mathbf{k}}(T_{\text{lat}})$ at the lattice temperature T_{lat}.

Symbol	Value	Symbol	Value
m_0	1.602 $10^{-19}C$	$n_{bar,e/h}$	$10^{12}\mathrm{cm}^{-2}$
m_e	0.0665 m_0	η	1.6 $10^{9}\mathrm{s}^{-1}$
m_h	0.457 m_0	τ_1	0.2 ps
ε	13.74	τ_2	0.2 ps
n_{ion}	$6.2510^{14}cm^2$	$\mathscr{A}$	0.8 $10^{8}\mathrm{s}^{-1}$
T_{lat}	300 K	$\mathscr{B}$	0.9 $10^{-10}\mathrm{cm}^{-3}s^{-1}$
E_G	1.262 eV	$\mathscr{C}$	0.7 $10^{-29}\mathrm{cm}^{-6}s^{-1}$
a_0	12.5 nm		

Table 7.1: Model Example Parameters

The remaining terms on the right hand side of (7.13) describe the density dependence of the dominant loss mechanisms. For small densities the carrier distribution can be approximated by a Maxwell-Boltzmann distribution [19]. In this limit, we can model the density dependence of the dominant loss mechanisms in semiconductor lasers in terms of a phenomenological law [1]

$$\left[\frac{dn_{\lambda,\mathbf{k}}}{dt}\right]_{\text{loss}} = \mathscr{A} n_{\lambda,\mathbf{k}} + \mathscr{B} n_{\bar{\lambda}} n_{\lambda,\mathbf{k}} + \mathscr{C} n_{\lambda} n_{\bar{\lambda}} n_{\lambda,\mathbf{k}}. \tag{7.14}$$

Here, the coefficients $\mathscr{A}$, $\mathscr{B}$ and $\mathscr{C}$ are material specific constants. They represent non-radiative impurity recombination ($\mathscr{A}$), spontaneous emission ($\mathscr{B}$) and Auger recombination ($\mathscr{C}$). Furthermore, n_λ is the total density of electrons ($\lambda = \mathrm{e}$) and holes ($\lambda = \mathrm{h}$), respectively. The index $\bar{\lambda}$ is defined by $\bar{\mathrm{e}} = \mathrm{h}$ and $\bar{\mathrm{h}} = \mathrm{e}$. Here, n_λ denotes the total density of carriers within a given band λ. The index $\bar{\lambda}$ is defined by $\bar{e} = h$, and $\bar{h} = e$. Even though it is well-known [19] that the simple carrier density dependencies of spontaneous and Auger recombination have to be modified in realistic calculations, for the purposes of our generic model calculations it is sufficient to treat them at the presented simple level.

7.3 Numerical Results

In our numerical analysis, we consider the model system of an 8 nm GaAs QW with an asymmetric bandoffset for the valence and conduction band of approximately 168 meV and 252 meV, respectively. The relevant parameters used in our computations are summarized in Table (7.1).

7.3.1 Solution for Stationary Barrier Distributions

To estimate the effect of the Hartree term on the optical QW properties, we solve the Hartree-Fock SBE for the microscopic polarization in two-band approximation (7.7) with and without the respective corrections due to charging and compare the resulting absorption/gain spectra. The pumping-induced density of QW carriers is computed from the rate equation for the occupation probability (7.13) including carrier injection as well as scattering and recombination processes. We simplify the evaluations by considering only the lowest subband states of the valence and conduction band as relevant contributions to the Hartree term while all other band contributions are neglected. This is a commonly used approximation because optical gain mainly originates from the confined levels. However, we will show in Sec. 7.3.2 that all bands play an important role in explaining the correct charging-induced energetic shifts. In the upper frame of Fig. (7.1), we plot

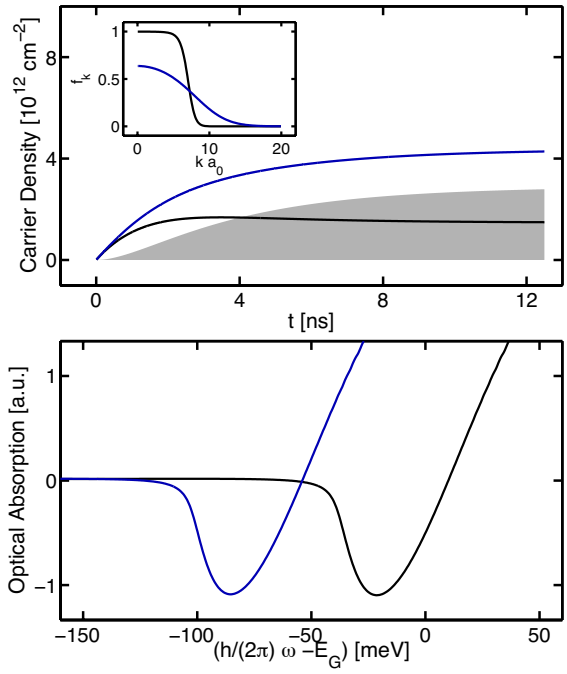

Figure 7.1: Density dynamics for injection pumping and effect of pumping-induced charging on the QW gain. (a): Time dependence of the pumping-induced electron (dashed line) and hole (solid line) densities as well as the resulting excess-carrier density (shaded area). Inset shows electron and hole distributions. (b): Gain spectra with (solid line) and without (dashed line) the renormalizations due to the Hartree potential; Both computations performed with two bands. Note, that these Hartree shifts are largely compensated by a charge redistribution in the barriers (see Fig. (7.2)).

the time evolution of the total density of electrons $n_e = 2/S\sum_{\mathbf{k}} f_{\mathbf{k}}^e$ (dashed line) and holes $n_h = 2/S\sum_{\mathbf{k}} f_{\mathbf{k}}^h$ (solid line) as well as the resulting total excess charge-carrier density $\Delta n^{QW} = n_h - n_e$ (shaded area). The inset to Fig. (7.1) shows the electron (dashed line)

and hole (solid line) distribution functions $f_{\mathbf{k}}^{\lambda}$ for the density of $n_e = n_h = 5 \cdot 10^{12}\text{cm}^{-2}$ and a lattice temperature of $T = 300\text{K}$. We clearly see that the holes have a reduced phase space filling compared with the electrons since the effective mass of the electrons m_e is considerably lower than that of the holes m_h. Accordingly, we note in the top part of Fig. (7.1) that the electron density increases slower and saturates at a lower level than the hole density on a nanosecond time scale. Eventually, more holes than electrons are captured into the QW causing a positive net charge, which is typical for small ratios m_e/m_h. To estimate the effect of charging, we compute optical gain at the steady-state conditions of Fig. (7.1) (a), i.e., at t=12.5 ns giving $\Delta n^{QW} = 2.8 \times 10^{12}\text{cm}^{-2}$. Figure (7.1) (b) presents optical gain computed using the two-band model with (solid line) and without (dashed line) the Hartree contributions. Neglecting the Hartree contributions means unchanged confinement functions and $\Delta E_{BGR} = 0$. This approximation is commonly used and it works very well to explain experiments. However, we can clearly see that the full inclusion of the Hartree terms yields an appreciable shift in the gain spectrum. Thus modeling critically depends on how the Hartree term is treated when only few confinement levels are included. Especially, our results show that typical pumping-induced charge densities shift the gain peak about 100 meV, which implies that charging is decisive in theory/experiment comparisons. At the same time, this finding conflicts with the observation that theory without charging effects produces an excellent match with experiments (see e.g. [11, 58]). From this evident discrepancy, we conclude that the two-band model is not sufficient to describe charging effects in electrically pumped QW lasers.

7.3.2 Full Dynamic Solution

Compensation Processes of Electric Puming-Induced Quantum-Well Charging

Once the QW charging due to electric pumping sets in, one also has a restoring Coulomb force which tends to attract carriers of the opposite charge and reject carriers of the same charge. Intuitively, we expect this to yield at least a partial compensation of the pumping-induced charge at the QW region. In contrast to the two-band laser model where the distribution of barrier carriers was assumed to be stationary, we now allow for a dynamic redistribution of the barrier-state carriers in reaction to the charging of the QW region.

To analyze the response of barrier electrons and holes to the Hartree potential, we make use of the parabolic approximation (7.6). Formally, within the harmonic approximation the problem of charging-induced carrier dynamics is that of a particle in a time-dependent harmonic oscillator potential. In this limit, we can set up the equation of motion of the density matrix $\rho_{\lambda,\lambda}(\mathbf{r}_1, \mathbf{r}_2, t)$ describing the density of electrons ($\lambda = e$) and holes ($\lambda = h$) in the unconfined states with a harmonic oscillator Hamiltonian $H_{\lambda}^{HO}(z)$ to compute the charging-induced dynamics

$$H_\lambda^{HO}(z,t) = -\frac{\hbar^2\nabla_z^2}{2m_\lambda} + (-1)^\lambda \frac{1}{2} m_\lambda \omega_\lambda^2(t) z^2 \tag{7.15}$$

with

$$(-1)^\lambda = \begin{cases} +1 \text{ if } \lambda = e \\ -1 \text{ if } \lambda = h. \end{cases} \tag{7.16}$$

Here, the prefactor $(-1)^\lambda$ allows for the fact that for holes the Hartree potential modifies the confinement with a sign opposite to that for electrons. The oscillator frequency ω_λ is determined by the total excess-charge-carrier density at the center of the QW, i.e. by the difference $\Delta n(t) = \Delta n(0,t)$ of hole and electron densities according to

$$\omega_\lambda^2(t) = \frac{e^2}{\varepsilon\varepsilon_0 m_\lambda} \Delta n(t). \tag{7.17}$$

It inherits the time dependence of the total excess-charge-carrier density $\Delta n = \Delta n^{QW} + \Delta n^B$, which consists of contributions from both the confined states of the QW Δn^{QW} and the unconfined states above the band edge of the barriers Δn^B. Thus, as the carriers in the quasi-continuum of states contribute to Δn as well as the carriers residing in the QW, this model takes into account the back coupling of the carriers in the unconfined states to the pumping-induced QW charge.

Theoretical Approach

For the computation of the unconfined carrier response to the pumping-induced QW charging it is particularly suitable to start from the density matrix $\rho_{\lambda,\lambda}(Z,\zeta,t)$ in center-of-mass (COM) and relative coordinates that is obtained by a Fourier transform of the Wigner function of the problem with respect to the momentum coordinate. Proceeding from the assumption that the system of carriers in the unconfined states is characterized by a Gaussian density profile and its momentum distribution follows Boltzmann statistics, the corresponding density matrix reads

$$\rho_{\lambda,\lambda}(Z,\zeta,t) = \quad N_\lambda(t) \exp\left(-\left[\frac{Z^2}{A_\lambda^2(t)} + \frac{\zeta^2}{B_\lambda^2(t)} - 2iC_\lambda(t) Z\zeta\right]\right).$$

Here, the normalization N_λ gives the total barrier charge-carrier density at the center of the QW for either electrons or holes, A_λ characterizes the Gaussian width of the spatial distribution and B_λ may be identified with the thermal wavelength of the respective carrier system. The term proportional to the product of COM- and relative coordinates ensures that propagation in time conserves the structure of the distribution function as may be

verified using insight from propagator theory. Initially, the coefficient C_λ vanishes.

Rate Equations

To derive equations of motion for the coefficients of the barrier-state carrier distribution function, it is convenient to start from the equation of motion of the full problem $\frac{\partial}{\partial t}\rho_{\lambda,\lambda}(z_1,z_2) = -\frac{i}{\hbar}[H_\lambda^{HO}(z_2) - H_\lambda^{HO}(z_1)]\rho_{\lambda,\lambda}(z_1,z_2)$. We evaluate the terms on both sides of this equation separately by differentiating the density matrix (7.18) in time on the one hand and applying the harmonic oscillator Hamiltonian to it on the other hand (cf. [29]). By comparison of the coefficients of the COM- and relative space-coordinates of both results, a system of coupled differential equations is obtained

$$\frac{\partial}{\partial t}N_\lambda = -\frac{2\hbar}{m_\lambda}C_\lambda N_\lambda \tag{7.18}$$

$$\frac{\partial}{\partial t}A_\lambda = \frac{2\hbar}{m_\lambda}C_\lambda A_\lambda \tag{7.19}$$

$$\frac{\partial}{\partial t}B_\lambda = \frac{2\hbar}{m_\lambda}C_\lambda B_\lambda \tag{7.20}$$

$$\frac{\partial}{\partial t}C_\lambda = \frac{2\hbar}{m_\lambda}\left[\left(\frac{1}{A_\lambda B_\lambda}\right)^2 - C_\lambda^2 - (-1)^\lambda \frac{m_\lambda^2}{4\hbar^2}\omega_\lambda^2\right]. \tag{7.21}$$

The connection between the original space coordinates z_1, z_2 of the density matrix and the COM- and relative coordinates Z, ζ is established via $Z = (z_1 + z_2)/2$ and $\zeta = z_2 - z_1$.

Model Exercise

We now apply our theory to describe the charging-induced dynamics of the carriers in the unconfined states. The QW charging is solved from (7.13) and the barrier-state carrier dynamics is computed from (7.18) - (7.21). As initial conditions for the carriers in barrier states, we choose wide Gaussian distributions for the electrons and holes. This choice guarantees spatial homogeneity over the sample and allows for overall charge neutrality of the system

$$\begin{aligned}
&N_\lambda(0) = 8\cdot 10^{18}\,\mathrm{cm}^{-3},\\
&A_\lambda(0) = 4000\,\mathrm{nm},\\
&B_\lambda(0) = \sqrt{\frac{2\hbar^2}{m_\lambda k_B T}}\,10^9\,\mathrm{nm}, \quad T = 900\,K,\\
&C_\lambda(0) = 0\,\mathrm{nm}^{-2}.
\end{aligned} \tag{7.22}$$

In the upper frame of Fig. (7.2) the QW charging Δn^{QW} (shaded area) and the densities of positively and negatively charged barrier carriers at the QW position N_e (dashed line) and N_h (solid line), respectively, are plotted. We note two clearly different dynamical regimes for the unconfined carrier density reacting to the QW charging. In the transient regime which lasts a few picoseconds, the barrier-state density at the center of the QW $N_\lambda(t)$ decreases simultaneously for electrons and holes. As for a normalized Gaussian profile a

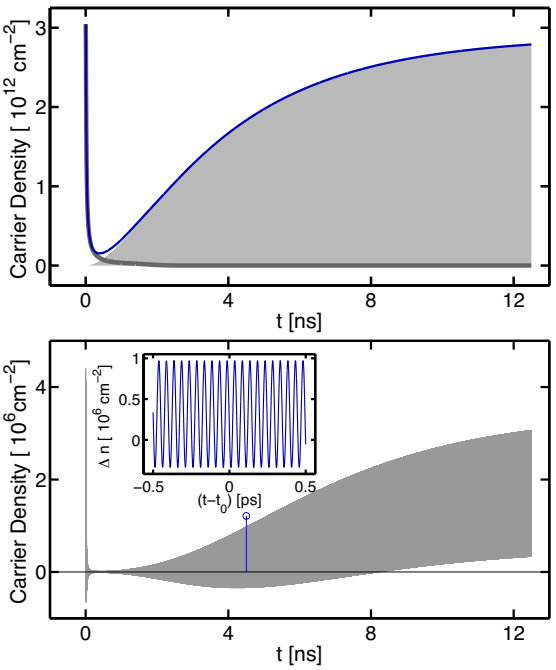

Figure 7.2: Charging induced dynamics of the carriers in the unconfined states and excess-charge-carrier density oscillations at the center of the QW. (a): Time dependence of barrier electrons (dashed line) and holes (solid line) in response to the excess-carrier density of holes inside the QW (shaded area). (b): Oscillatory motion of the total excess-carrier density at the QW position. The vertical line marks the time t_0 =4.5062 ns. In the inset the oscillations around t_0 are resolved.

smaller peak value is equivalent to a broader width, the decrease in the carrier densities corresponds to a diffusion of charge carriers. This diffusion is characteristic of the early time dynamics where the pumping-induced QW charging is negligible. In the long-time regime, the barrier electron density "follows" the positive net-charge while the barrier holes are virtually absent. The pumping-induced QW charge is compensated by an increasing number of additional barrier electrons that move in to balance the charging. In the lower frame of Fig. (7.2) the total excess carrier density $\Delta n = \Delta n^{\mathrm{QW}} + \Delta N$, $\Delta N = \Delta n^{B} = N_h - N_e$, is presented as function of time. Here, we focus on the long-time regime. The regime where the total excess-charge-carrier density assumes relatively large values is omitted. Looking at the time dynamics of the barrier carrier densities N_e and N_h in the upper frame of Fig. (7.2) we note that the barrier charge density adjusts to the QW charge. Even though this adjustment is not sufficient to completely eliminate all charging effects, they are dramatically reduced by a factor of 10^6 *such that one can neglect the charging contributions in theoretical few-band model calculations*. In the compensation process, the Gaussian distribution of the barrier-state carriers becomes increasingly narrower.

However, when the Gaussian is more localized, it disperses more quickly. This dispersion counteracts the trend for charge compensation, thus giving rise to collective charge density oscillations.

To summarize the main results of our numerical analysis, we find that (i) the carriers in barrier states redistribute to compensate for the QW charging but (ii) due to the increased localization near the QW we obtain increased wave packet dispersion. The interplay of both effects leads to sustained charge density oscillations. These oscillations are a characteristic feature of electrically pumped QW lasers with differing effective masses of electrons and holes. The particular time dependence of the total charge density and thus the extend to which barrier electrons compensate a given pumping-induced charge is a strong function of the present QW charging and the initial conditions, i.e the distribution function of pump-injected carriers.

7.3.3 Analytical Solution

To gain further insight into the oscillatory motion of the total charge at the QW position, a second-order oscillator equation for the excess-carrier density $\Delta n = \Delta n^{\mathrm{QW}} + \Delta N$ may be derived using (7.18) - (7.21) (cf. [29]). In the late-time regime which is characterized by a constant level, the equation for the excess-carrier density Δn is obtained as

$$\frac{\partial^2}{\partial t^2}\Delta n = -\left[\omega_{pl}^2 + \frac{4\hbar^2}{m_e^2}\left(\left(\frac{1}{A_e B_e}\right)^2 - 2C_e^2\right)\right]\Delta n + \frac{4\hbar^2}{m_e^2}\left(\left(\frac{1}{A_e B_e}\right)^2 - 2C_e^2\right)\Delta n^{\mathrm{QW}} \tag{7.23}$$

having the form of an inhomogeneous oscillator equation with time-dependent coefficients. From our numerical evaluations, we know that the relation

$$\left(\frac{1}{A_e(t)B_e(t)}\right)^2 \gg C_e^2(t) \tag{7.24}$$

is well fulfilled. With this input, we can find the adiabatic solution of (7.23) as

$$\Delta n(t) = \Delta\bar{n}[1 - \cos(\tilde{\omega}_{pl}t)] \tag{7.25}$$

where

$$\Delta\bar{n} = \left(\frac{2\hbar}{m_e A_e B_e \tilde{\omega}_{pl}}\right)^2 \Delta n^{QW}. \tag{7.26}$$

Here, the renormalized plasma frequency

$$\tilde{\omega}_{pl}^2(t) \equiv \omega_{pl}^2(t) + \frac{4\hbar^2}{m_e^2 A_e^2(t) B_e^2(t)} \tag{7.27}$$

has been introduced, whereas

$$\omega_{pl}^2(t) = \frac{e^2}{\varepsilon\varepsilon_0}\left(\frac{N_e(t)}{m_e} + \frac{N_h(t)}{m_h}\right) \tag{7.28}$$

is the instantaneous eigenfrequency of an electron-hole plasma. Using (7.25) we may deduce the frequency of the charge oscillations as well as their mean value, i.e the average level of total charging remaining in the QW system.

First, we compare the frequency of the analytic formula (7.27) to the frequency of the oscillations obtained by the full numerical solution to the problem of charging-induced barrier-carrier dynamics. To obtain the oscillation frequency of the full numerical solution for a particular time interval, we convolve the oscillations with a Gaussian centered at the time of interest and Fourier transform the result. In the lower frame of Fig. (7.3) the oscillation frequency of the numerical solution is shown for certain times indicated by the lines in the upper frame of Fig. (7.3) where again the total charge density Δn is plotted as function of time. The vertical lines in the lower frame of Fig. (7.3) indicate the instantaneous eigenfrequency of an electron-hole plasma ω_{pl} which is virtually indistinguishable from the renormalized plasma frequency. Thus, we verify that the analytically obtained oscillation frequency correctly reproduces the frequency encountered in the numerical solution. In particular, we note that the renormalization term in (7.27) is negligible in comparison to the original plasma frequency ω_{pl} such that in a first approximation the instantaneous eigenfrequency of the electron-hole plasma turns out to be a dependable quantity to estimate the frequency of the total charge-density oscillations. Clearly, the frequency of the charge oscillations is easily influenced by the choice of pumping strength since a given pumping rate results in a defined QW charging and so determines the barrier electron and hole densities which in turn determine the plasma frequency. In the late-time regime, we can approximate the plasma frequency by the QW charge

$$\omega_{pl}^2(t) = \frac{e^2}{\varepsilon\varepsilon_0 m_e} N_e(t) \approx \frac{e^2}{\varepsilon\varepsilon_0 m_e} \Delta n^{\mathrm{QW}}(t). \tag{7.29}$$

Thus, it becomes obvious that as Δn^{QW} saturates on a nanosecond time scale also the oscillation frequency reaches a constant value. Therefore, as typical pumping rates yield plasma frequencies in the terahertz (THz) regime, the collective oscillatory motion of

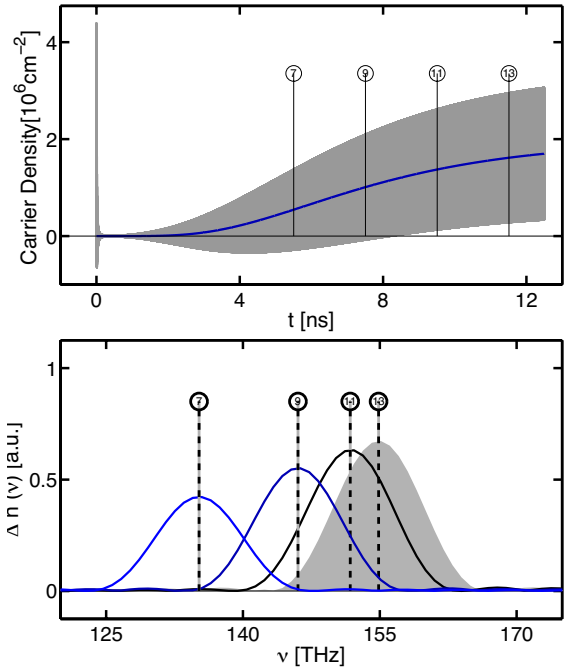

Figure 7.3: Analytical results for the excess charge carrier density oscillations at the center of the QW and time-dependent oscillation frequency in comparison to the numerically obtained solution. For further explanation see text.

barrier charge-carriers in an electrically pumped semiconductor laser device may give rise to coherent emission of THz radiation.

Beside an agreement of the analytical plasma frequency and the frequency of the numerical solution, we also find that the analytically derived formula accurately predicts the average level of total charging. To exemplify this, we compare in the upper frame of Fig. (7.3) the mean value of the oscillations of the analytically obtained total excess-charge-carrier density $\Delta\bar{n}$ (solid line) to the numerical solution (shaded area).

7.4 Summary

In summary, in this investigation we have analyzed the effect of charging on the carrier dynamics in electrically pumped QW lasers. We introduced a formulation of the problem which shows clearly that both the carriers in the quasi-continuum of states above the band edge of the barrier layers and the confined states of the QW must be treated dynamically to correctly determine the degree of charging. We have shown that the carriers in the

unconfined states try to compensate the electric pumping-induced charging at the QW position. The dynamics resulting from stimulated electron-hole recombination and carrier replenishing gives rise to collective charge oscillations and a high degree of overall charge compensation.

The observation of electromagnetic dipole radiation emitted by electrically pumped QW structures in the THz regime may be used to test the detailed properties of the induced charge oscillations. Possibly, this could provide a way to use an electrically pumped semiconductor QW laser as a source of coherent THz radiation.

III Part Three: Everything Else

8. Appended Papers

This part of the thesis provides a list of the appended papers. In addition, a brief description is given of the papers regarding their intention and content as well as of the different authors' contributions to each paper. The papers are listed in a chronological order. A more detailed positioning and references to the papers is provided in the presentation of the research results in chapterof this thesis.

8.1 List of appended Papers

- A. Bäumner, M. Kira and S.W. Koch. *Charging Dynamics in Electrically Pumped Quantum Wells*. In IEEE Journal of Quantum Electronics, Vol. 45, pages 1024-1032 (2009)
- A. Bäumner, S.W. Koch and J.V. Moloney. *Non-equilibrium analysis of the two-color operation in semiconductor quantum-well lasers*. In Phys. Status Solidi B, Vol. 248, pages 843–846 (2011)
- J. V. Moloney, I. Kilen, A. Bäumner, M. Scheller and S.W. Koch. *Nonequilibrium and thermal effects in mode-locked VECSELs*. In Opt. Express, Vol. 22, pages 422-6427 (2014)

8.2 Author's Contributions

The first research project I focused on was the problem of charging dynamics in electrically pumped quantum wells. Already when I started out as a diploma student my advisors Prof. Dr. S.W. Koch and Prof. Dr. M. Kira entrusted me with the task to test whether I could verify the proposed working hyphothesis that additional charge carriers in the extended barrier states that do not participate in the lasing process move in to ballance a possible pumping-induced net charge in the active region. Equipped with this working hypothesis and a theoretical appoach on the basis of propagator method, I have set to work in vain to find a numerically stable solution scheme as summarized in my diploma thesis. Having become acquainted with the subject-matter, towards the end of my undergraduate studies, guided thoughtfully by Prof. Dr. S.W. Koch and Prof. Dr. M. Kira I derived and applied independently an alternative strategy to solve the problem of charging dynamics in electrically pumped quantum wells. So, I introduced an numerical more stable equation of motion approach to describe the charging-induced time dynamics of barrier electrons and holes, that holds the additional advantage of providing interesting analytical insights into the inherent physical processes. The research results gained on this basis are presented in the article *Charging Dynamics in Electrically Pumped Quantum Wells* [4] .

Motivated by the experiments of Fan et al. [15], I started my second research project with the aim to develop a softwaretool to facilitate the simulation and analysis of multimode dynamics in high power laser applications. After a comprehensive literature search and intensive and enriching discussions with Prof. Dr. S.W. Koch and Prof. Dr. J.V. Moloney, I proposed a model approach on the foundation of the Maxwell Semiconductor Bloch Equations in effective scattering rate approximation which I subsequently implemented, tested and applied the problem of two-color laser emission of VECSEL systems as noted in the article *Non-Equilibrium Analysis of the Two-Color Operation in Semiconducor Quantum-Well Lasers* [5] . Prompted by the succes of this model excercise, I modified the underlying software to be applicable also for the simulation of laser structures that contain semiconductor saturable absorber mirrors in their configuration. In collaboration with the group of applied mathematics around Prof. Dr. J.V. Moloney from the College of Optical Sciences at the University of Arizona, following we started joined research efforts to optimize the program with respect to computational speed. The results of this efforts and a varied process of dialogue and fruitful discussions within the project team are reflected in the article *Non-Equilibrium and Thermal Effects in Modelocked VECSELs* [56].

While I could reach a successful solution to problem of charging dynamics in electrically pumped quantum wells, the project of modeling and simulating non-equlibrium dynamics in VECSEL applications and analyzing the influence of hole burning on stable two-color emission and modelocking is still pending and challenging. Even though most of the research of the PhD training focuses on the attempt to represent these phenomena and considerable time and effort have been invested on this subject, just a first modest

step towards an effective simulation program is made by proposing an appropriate model approach and implementation scheme. Yet, when optimized further with respect to computing speed the proposed model approach and implementation scheme promise to allow comprehensive parametric studies and to fasciliate deeper insights in the processes and mechanisms involved in the multimode dynamics of high power semiconductor laser applications as VECSELs. An initial step in this direction has been already taken with the input of the experts in applied mathematics around Prof. Dr. J.V. Moloney. So, program optimizations on the level of coding, algorithm, parallelization and initialization made the simulation of realistic structures possible and first parameter studies feasible such that in [37] it became possible to go beyond the comparativley simple model study of the earlier joint paper contribution [56].

Phys. Status Solidi B **248**, No. 4, 843–846 (2011) / **DOI** 10.1002/pssb.201000844

physica status solidi b
www.pss-b.com
basic solid state physics

Non-equilibrium analysis of the two-color operation in semiconductor quantum-well lasers

Ada Bäumner*[,1], Stephan W. Koch[1], and Jerome V. Moloney[2]

[1] Department of Physics and Material Science Center, Philipps University, Renthof 5, 35032 Marburg, Germany
[2] Arizona Center of Mathematical Science and College of Optical Science, University of Arizona, Tucson 85721, Arizona, USA

Received 13 August 2010, accepted 27 September 2010
Published online 24 December 2010

Keywords device simulation, multi-mode laser operation, semiconductor lasers

* Corresponding author: e-mail ada.baeumner@physik.uni-marburg.de, Phone: +49 6421 2822025, Fax: +49 6421 2827076

The relevance of hole burning for stable two-color operation in semiconductor quantum-well lasers is studied using a non-equilibrium laser model on the basis of the semiconductor Maxwell-Bloch equations. The field propagation is described via a traveling-wave method. The polarization dynamics is computed using the semiconductor Bloch equations for the microscopic transition and occupation probabilities. Numerical examples for single- and dual-mode operation are presented for a microresonator model system.

1 Introduction Semiconductor quantum-well (QW) lasers exist in numerous realizations. As a common feature, the gain material in all these systems has a relatively large bandwidth and a rather flat peak. This gain characteristics leads to a low mode selectivity for semiconductor laser devices with large extended cavities. Since these devices involve a very high density of longitudinal modes, usually several of the densely spaced cavity modes experience a comparable amplification. As a consequence, typical QW lasers exhibit a multi-mode emission characteristics.

Whereas this multi-mode operation is undesirable in many cases where one ideally prefers an efficient conversion of the excited carriers into a single-mode laser field, the well-defined emission at two laser modes is needed, e.g., in cases where difference frequency generation is exploited to generate light in the terahertz spectral range [1, 2]. Experimentally, such two-color operation has been observed not only in semiconductor QW lasers using spectrally filtered mirror feedback [1], but also in a traditional vertical external cavity surface emitting laser (VECSEL) system [2].

Despite the experimental realizations, a full theoretical understanding of the conditions under which semiconductor lasers can oscillate simultaneously and stable at two different frequencies is still missing. This question establishes a highly non-trivial problem since the multi-mode dynamics is determined by a complex interplay of mode competition, gain, and carrier distribution dynamics. Furthermore, the emission characteristic of the laser systems is strongly dependent on the actual geometry of the setup, the material parameters of both the dielectric structure and the gain region and the actual excitation state of the optically active material.

In this context, it is an interesting problem, to theoretically analyze the different lasing regimes that might be encountered in experiments and to correlate the observed dynamics to the system configuration in detail. Whereas previous studies [3] used quasi-equilibrium gain configurations, we include the important non-equilibrium effects using a nonlinear laser model on the basis of the semiconductor Maxwell-Bloch equations. Such a model is not limited to the dynamics of the macroscopic quantities laser field, polarization, and carrier density, which are typically studied in multi-mode problems, but, furthermore, allows insight into the underlying microscopic processes and effects. Thus, it is perfectly suited for an analysis of nonlinear processes caused by and associated with non-equilibrium effects as for example kinetic and spectral hole burning.

2 Theory To analyze the non-equilibrium dynamics of a semiconductor QW laser, we need to simulate the propagation of the light field inside the laser cavity and its nonlinear interaction with the optically active gain region, i.e., the QW layers. The problem we encounter here is a

problem of self-consistency. As the light field E(z, t) leads to a material polarization P(z, t) which in turn affects the light field, a basic building block of any laser theory is a closed set of equations for these quantities. To this aim, we apply a semi-classical theory meaning that we treat the field-induced optical excitations of the gain material microscopically, while we derive the dynamics of the light field from the classical Maxwell equations.

The relation between the macroscopic polarization P(z, t) entering the Maxwell equations and the relevant microscopic quantities is established by the summation of the so-called microscopic polarizations $p_{\boldsymbol{k}}$

$$P(t) = \sum_{\boldsymbol{k}} d_{\mathrm{cv}} p_{\boldsymbol{k}} + \mathrm{c.c.} \tag{1}$$

over the crystal momentum $\boldsymbol{k}$ in the plane of the QW. Here, the sum is weighted with the dipole-matrix element d_{cv} which is characteristic of the optically active material. Intuitively, the microscopic polarization $p_{\boldsymbol{k}}$ is a probability amplitude for the excitation of an electron from a valence-band state $\boldsymbol{k}$ into an empty conduction-band state of equal momentum. The dynamics of this transition amplitude follows from the semiconductor Bloch equations (SBE) [4]

$$\begin{aligned} \frac{\mathrm{d}}{\mathrm{d}t} p_{\boldsymbol{k}} &= -i\omega_{\boldsymbol{k}} p_{\boldsymbol{k}} - i\Omega_{\boldsymbol{k}} \left(n^e_{\boldsymbol{k}} + n^h_{\boldsymbol{k}} - 1\right) + \Gamma_{\mathrm{deph}} + \Lambda^p_{\mathrm{spont}}, \\ \frac{\mathrm{d}}{\mathrm{d}t} n^{e(h)}_{\boldsymbol{k}} &= i\left[\Omega_{\boldsymbol{k}} p^*_{\boldsymbol{k}} - \Omega^*_{\boldsymbol{k}} \mathrm{p}_{\boldsymbol{k}}\right] + \Gamma_{\mathrm{scatt}} + \Lambda^n_{\mathrm{spont}} + \Pi_{\mathrm{pump}}. \end{aligned} \tag{2}$$

The SBE clearly show the linking of the microscopic polarization $p_{\boldsymbol{k}}$ and the occupation functions $n^{e(h)}_{\boldsymbol{k}}$ defining the probability that a state $\boldsymbol{k}$ in the conduction band (valence band) is occupied by an electron (hole).

In the well-known Hartree–Fock approximation [4], the renormalized single-particle energy $\hbar\omega_{\boldsymbol{k}} = \varepsilon_r - \sum_{\boldsymbol{q}\neq\boldsymbol{k}} V_{|\boldsymbol{k}-\boldsymbol{q}|}(n^e_{\boldsymbol{q}} + n^h_{\boldsymbol{q}})$, and the renormalized Rabi frequency $\Omega_{\boldsymbol{k}} = \omega_{\mathrm{R}} + \frac{1}{\hbar}\sum_{\boldsymbol{q}\neq\boldsymbol{k}} V_{|\boldsymbol{k}-\boldsymbol{q}|} p_{\boldsymbol{q}}$ enter the SBE. Thereby, the renormalization of the single-particle energy ε_{r} and the Rabi frequency ω_{R} arises from the Coulomb interaction $V_{|\boldsymbol{k}-\boldsymbol{q}|}$ within the charge carrier system. Assuming a parabolic band structure, the single-particle energy $\varepsilon_{\mathrm{r}} = \left(\hbar^2\boldsymbol{k}^2/2m_e\right) + \left(\hbar^2\boldsymbol{k}^2/2m_h\right) + E_{\mathrm{g}}$ is determined by the effective masses of the electrons, m_e, holes, m_h, and the band-gap energy E_{g}. It defines the transition energy between the valence and conduction band for a given momentum $\boldsymbol{k}$. The Rabi frequency $\omega_{\mathrm{R}} = d_{\mathrm{cv}}E(z,t)/\hbar$ is the basic light-matter coupling parameter. In the semi-classical limit in dipole approximation it is given in terms of the exciting light field $E(z_0, t)$ at the QW position z_0 and the dipole-matrix element d_{cv}. Contributions that go beyond the Hartree–Fock approximation describe the dephasing of the polarization (Γ_{deph}), carrier scattering (Γ_{scatt}), spontaneous dipole fluctuations ($\Lambda^p_{\mathrm{spont}}$) and loss processes ($\Lambda^n_{\mathrm{spont}}$) as well as optical pumping (Π_{pump}). For qualitative model studies and in order to keep the numerics manageable it is convenient to include all these effects on the level of phenomenological rates.

The dephasing of the polarization is described by a simple decay contribution with the characteristic dephasing time τ_{deph} [5, 6]

$$\Gamma_{\mathrm{deph}} = -\frac{1}{\tau_{\mathrm{deph}}} p_{\boldsymbol{k}}. \tag{3}$$

Similarly, the carrier-scattering contribution modeling the equilibration of the carrier system follows from [5]

$$\Gamma_{\mathrm{scatt}} = -\frac{1}{\tau_{\mathrm{scatt}}}\left(n^{e(h)}_{\boldsymbol{k}} - f^{e(h)}_{\boldsymbol{k}}\right), \tag{4}$$

where τ_{scatt} introduces the characteristic time scales of scattering events. Due to Coulomb scattering the occupation probability $n^{e(h)}_{\boldsymbol{k}}$ develops into Fermi–Dirac distributions $f^{e(h)}_{\boldsymbol{k}}$ which yield the same total density and kinetic energy as the non-equilibrium distribution. As a result of phonon scattering the occupation probability $n^{e(h)}_{\boldsymbol{k}}$ develops into Fermi–Dirac distributions $f^{e(h)}_{\boldsymbol{k}}(T_{\mathrm{lat}})$ at the lattice temperature T_{lat}, conserving the particle number in the process. The relevant rate in the discussion of effects related to the spontaneous emission process is the spontaneous emission coefficient Γ_{spont}. In these terms the spontaneous emission contributions in Eq. (2) can be modeled according to $\Lambda^{\mathrm{n}}_{\mathrm{spont}} = -\Gamma_{\mathrm{spont}}(\boldsymbol{k}) n^{\lambda}_{\boldsymbol{k}} n^{\bar{\lambda}}_{\boldsymbol{k}}$ and $\Lambda^{\mathrm{p}}_{\mathrm{spont}} = \beta\Gamma_{\mathrm{spont}}(\boldsymbol{k}) n^{\lambda}_{\boldsymbol{k}} n^{\bar{\lambda}}_{\boldsymbol{k}}$ ($\lambda = e$ and $\bar{\lambda} = h$ and vice versa) [7]. Here, we use the approximation

$$\Gamma_{\mathrm{spont}}(\boldsymbol{k}) = \frac{n^3}{\pi^2\varepsilon_0\hbar^4 c_0^3} |d_{\mathrm{cv}}|^2 \left(E_{\mathrm{g}} + \frac{\hbar^2\boldsymbol{k}^2}{2m_{\mathrm{r}}}\right)^3, \tag{5}$$

where the quantities c_0, ε_0, n and m_{r} are constants describing the vacuum velocity of light, the dielectric constant, the background refractive index, and the reduced effective mass of electrons and holes, respectively. The spontaneous emission factor β is given by the ratio between the spontaneous emission radiated into the lasing mode and the total spontaneous emission such that it assumes values between zero and one. The phenomenological description of optical pumping requires the definition of a generation rate $\Pi_{\mathrm{pump}}(\boldsymbol{k})$ that enters Eq. (2). Here, we use

$$\begin{aligned} \Pi_{\mathrm{pump}}(\boldsymbol{k}) = &-\left(\frac{d_{\mathrm{cv}}}{\hbar}\right)^2 |E_0|^2 (n^e_{\boldsymbol{k}}(t) + n^h_{\boldsymbol{k}}(t) - 1) \\ &\times \left(\frac{2\eta}{(\omega_{\mathbf{k}} - \omega_{\mathrm{pump}})^2 + \eta^2}\right), \end{aligned} \tag{6}$$

where E_0, $\hbar\omega_{\mathrm{pump}}$, and η are the amplitude, the energy and the spectral width of the pump-light field, respectively.

To account for the propagation of the light field $E(z, t)$ that excites the polarization $P(z, t)$ at the QW position, we couple the Hartree–Fock SBE for the microscopic polarization $p_{\boldsymbol{k}}$ and the occupation probabilities for electrons $n^e_{\boldsymbol{k}}$ and holes $n^h_{\boldsymbol{k}}$ Eq. (2) to the transversal wave equation Eq. (7) following from the Maxwell equations. Assuming that the

cavity light-field circulates in z-direction perpendicular to the QW plane, the transversal wave equation reads

$$\left[\frac{\partial^2}{\partial z^2} - \frac{n^2}{c_0^2}\frac{\partial^2}{\partial t^2}\right] E(z,t) = \mu_0 \frac{\partial^2}{\partial t^2} P(z,t), \tag{7}$$

where the constants n and c_0 are again the background refractive index and the vacuum velocity of light and μ_0 denotes the vacuum permeability.

3 Implementation For our model analysis, we solve the semiconductor Maxwell-Bloch equations in the time domain (Eq. (2) and Eq. (7)) applying a traveling-wave method based on a direct solution of the wave equation Eq. (7). This method takes advantage of the fact that within each layer of the dielectric structure of the laser device the light field can propagate freely and thus be decomposed in forward and backward traveling field components, E^+ and E^-, respectively. Matching the forward and backward traveling field components by applying the appropriate boundary conditions and assuming that the wavelength of the laser light is large in comparison to the QW width, we obtain for the cavity field [8]

$$\begin{bmatrix} E_{j+1}^+\left(t-\frac{z_j}{c_{j+1}}\right) \\ E_j^-\left(t+\frac{z_j}{c_j}\right) \end{bmatrix} = \begin{bmatrix} \frac{2n_j}{n_j+n_{j+1}} & \frac{n_{j+1}-n_j}{n_j+n_{j+1}} \\ \frac{n_j-n_{j+1}}{n_j+n_{j+1}} & \frac{2n_{j+1}}{n_j+n_{j+1}} \end{bmatrix} \times \begin{bmatrix} E_j^+\left(t-\frac{z_j}{c_j}\right) \\ E_{j+1}^-\left(t+\frac{z_j}{c_{j+1}}\right) \end{bmatrix} - \frac{\mu_0 c_0}{2n_j} \begin{bmatrix} \frac{\partial}{\partial t}P_j(t) \\ \frac{\partial}{\partial t}P_j(t) \end{bmatrix}. \tag{8}$$

While the first term on the right hand side of Eq. (8) describes reflection and transmission at the interface of the jth dielectric layer, the second term accounts for the absorption and amplification of the light field. Here, the polarization is non-vanishing only at the QW positions. We solve Eq. (8) in the slowly varying envelope approximation. To analyze the frequency components of the outcoupled laser light field, we perform a Fourier-transform of the complex field component $E_0^-(t)$.

4 Model example To test our model, we set up an effective-mirror resonator structure with appropriate reflective boundary conditions at both ends of a linear cavity (cf. Fig. 1). The cavity length is adjusted to have several cavity modes covered by the semiconductor gain spectrum.

In order to obtain maximum overlap between the cavity light-field and the gain material and thus provide maximum light-matter coupling, the QW gain regions are positioned in the anti-nodes of the empty-cavity modes. The set of material parameters is chosen such that the cavity including the QW layers consists of a homogenous dielectric structure with constant background refractive index. This way, we avoid additional backscattering effects which may further complicate the dynamics.

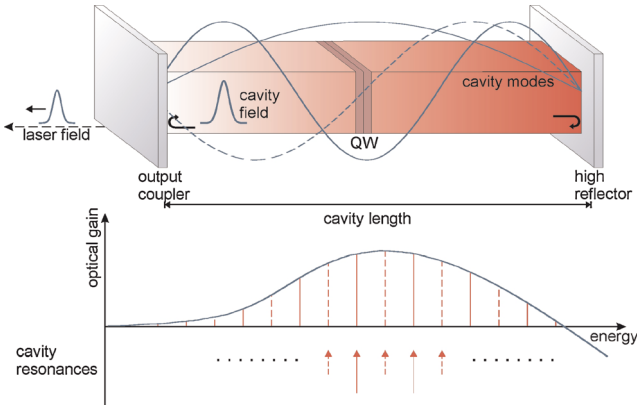

Figure 1 (online color at: www.pss-b.com) Sample setup. The upper plot depicts a schematic sketch of the effective-mirror resonator structure we use in our model calculations. The lower plot shows a typical semiconductor-gain spectrum. The vertical lines indicate the positions of the cavity resonances. While the dashed lines belong to modes leading to negligible modal gain due to the vanishing light–matter coupling, the solid lines correspond to potential lasing modes.

5 Results Our numerical results show that stable dual-mode operation is achieved for conditions where the mode spacing allows the two modes to burn separate kinetic holes into the occupation probability $n_k^{e(h)}$ as depicted schematically in Fig. 2. As can be seen in the upper panels of Fig. 3, the amplitude spectrum of the complex laser field clearly displays two dominant peaks at the position of the laser resonances with the maximum modal gain. Clearly, this situation is favored when the two modes have similar modal gain (see lower panels of Fig. 3). Interestingly, even though distinct kinetic holes are seen in the carrier distribution functions, no spectral holes can be seen in the corresponding

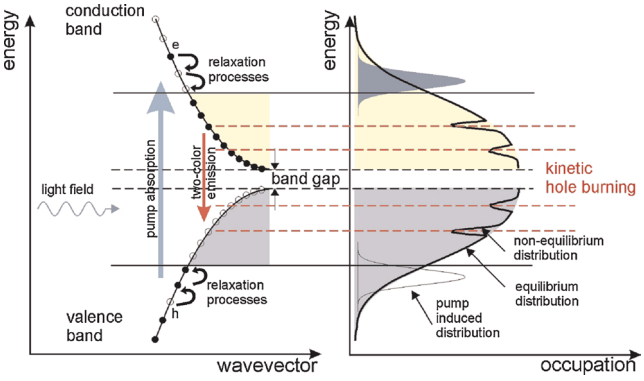

Figure 2 (online color at: www.pss-b.com) Schematic diagram of the excitations in semiconductor materials. The left plot shows the band structure in parabolic approximation. The right plot depicts the microscopic occupation probabilities for the electrons in the conduction band and the holes in the valence band.

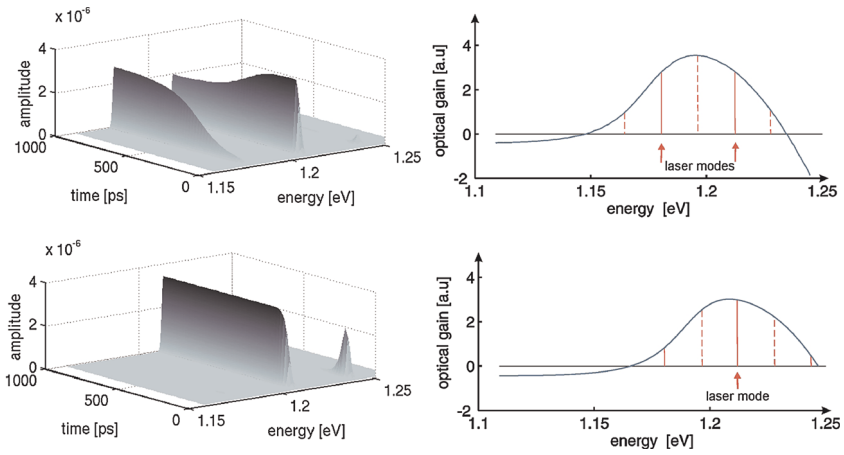

Figure 3 (online color at: www.pss-b.com) Frequency analysis of the laser field. On the left hand side, the amplitude spectrum of the complex laser field is shown in dependence of time for two different sets of material parameters. On the right hand side, corresponding gain spectra are given. For further explanations see text.

gain spectra. Due to the dephasing of the polarization there is no one-to-one correspondence between momentum values and transition energies since the dephasing of the polarization leads to an homogeneous broadening of each transition. Consequently, the distinct kinetic holes in the occupation probability only show up as a broadening and flattening of the gain spectrum.

Because of the momentum resolved treatment of the momentum-state occupation dynamics, the different elements of this distribution function are only coupled via the interaction and relaxation processes. Hence, for sufficient mode spacing, the momentum regions into which the separate holes are burned by the two-color laser operation are only weakly coupled and the influence of cross-saturation effects is relatively small. With respect to the gain, this mutual independence implies that the gain saturation caused by the amplification of a given mode reduces the available gain basically for itself and not for all other modes, as would be the case in the homogeneous limit. As a result, the separate holes in the occupation probability can compensate small inequalities in the unsaturated net gain and thus contribute to the stability of the two-color laser emission.

6 Summary We conclude that taking into account non-equilibrium effects and the corresponding inhomogeneity by coupling the dynamics of the microscopic polarization to the occupation probability is important for a detailed study of the stability of multi-mode problems. Laser simulations based on rate equations for the carrier density and the resulting quasi-equilibrium Fermi–Dirac distributions for the occupation probabilities, therefore, are not sufficient for this purpose and may be considered as the homogeneous limit of the more general model introduced here.

Acknowledgements This work was supported by the US Air Force Office of Scientific Research, contract FA9550-07-1-0573, by the Deutsche Forschungsgemeinschaft and the Humboldt Foundation.

References

[1] S. Hoffmann and M. R. Hofmann, Laser Photon. Rev. **1**(1), 44–56 (2007). See also references therein.
[2] L. Fan, M. Fallahi, J. Hader, A. R. Zakharian, J. V. Moloney, W. Stolz, S. W. Koch, R. Bedford, and J. T. Murray, Appl. Phys. Lett. **90**(18), 181124 (2007).
[3] M. Matus, M. Kolesik, J. V. Moloney, M. Hofmann, and S. W. Koch, J. Opt. Soc. Am. B **21**(10), 1758–1771 (2004).
[4] H. Haug and S. W. Koch, Quantum theory of the optical and electronic properties of semiconductors, fifth ed. (World Scientific Publishing, Singapore, 2009).
[5] W. W. Chow and S. W. Koch, Semiconductor Laser Fundamentals (Springer, Berlin, Heidelberg, New York, 1999).
[6] W. W. Chow and S. W. Koch, IEEE J. Quantum Electron. **41**(4), 495–505 (2005).
[7] O. Hess and T. Kuhn, Prog. Quantum Electron. **20**(2), 85–179 (1996).
[8] G. Khitrova, H. M. Gibbs, F. Jahnke, M. Kira, and S. W. Koch, Rev. Mod. Phys. **71**(5), 1591–1639 (1999).

Nonequilibrium and thermal effects in mode-locked VECSELs

J.V Moloney,[1,2,*] I. Kilen,[2] A. Bäumner,[3] M. Scheller,[1] and S.W. Koch[3]

[1]*College of Optical Sciences, University of Arizona, Tucson, Arizona 85721, USA*
[2]*Department of Mathematics, University of Arizona, Tucson, Arizona 85721, USA*
[3]*Department of Physics, Marburg University, Marburg 35032, Germany*
[*]*jml@acms.arizona.edu*

Abstract: Ultrafast femtosecond timescale dynamics in Vertical External Cavity Surface Emitting Lasers (VECSELs) have recently been employed to achieve record average power and duration mode-locked pulses by employing different types of saturable absorbers and Kerr Lens elements. Microscopic many-body dynamics are expected to dominate when attempting to push pulse durations below 100 fs. We present a preliminary microscopic simulation of ultrafast mode-locking in order to expose the role of hot carrier distributions in establishing ultrafast mode-locking.

OCIS codes: (140.5960) Semiconductor lasers; (250.7270) Vertical emitting lasers.

References and links

1. B. Heinen, T.-L. Wang, M. Sparenberg, A. Weber, B. Kunert, J. Hader, S. W. Koch, J. V. Moloney, M. Koch, and W. Stolz, "106W continuous-wave output power from vertical-external-cavity surface-emitting laser," Electron. Lett. **48**(9), 516 (2012).
2. A. Laurain, C. Mart, J. Hader, J.V. Moloney, B. Kunert, and W. Stolz, "15W Single frequency optically pumped semiconductor laser with sub-MHz linewidth," IEEE Photon. Tech. Lett. **26**, 131–133 (2014).
3. M. Scheller, T.-L. Wang, B. Kunert, W. Stolz, S. W. Koch, and J. V. Moloney, "Passively mode-locked VECSEL emitting 682 fs pulses with 5.1 W of average output power," Electron. Lett. **48**(10), 588–589 (2012).
4. K. G. Wilcox, A. C. Tropper, H. E. Beere, D. A. Ritchie, B. Kunert, B. Heinen, and W. Stolz, "4.35 kW peak power femtosecond pulse mode-locked VECSEL for supercontinuum generation," Opt. Express **21**(2), 1599–1605 (2013).
5. M. Hoffmann, O. D. Sieber, V. J. Wittwer, I. L. Krestnikov, D. A. Livshits, Y. Barbarin, T. Südmeyer, and U. Keller, "Femtosecond high-power quantum dot vertical external cavity surface emitting laser," Opt. Express **19**(9), 8108–8116 (2011).
6. C. A. Zaugg, Z. Sun, V. J. Wittwer, D. Popa, S. Milana, T. S. Kulmala, R. S. Sundaram, M. Mangold, O. D. Sieber, M. Golling, Y. Lee, J. H. Ahn, A. C. Ferrari, and U. Keller, "Ultrafast and widely tuneable vertical-external-cavity surface-emitting laser, mode-locked by a graphene-integrated distributed Bragg reflector," Opt. Express **21**(25), 31548–31559 (2013).
7. S. Husaini and R. A. Bedford, "Antiresonant Graphene Saturable Absorber mirror for mode-locking VECSELs," (private communication) (2013)
8. K. Seger, N. Meiser, S. Y. Choi, B. H. Jung, D. I. Yeom, F. Rotermund, O. Okhotnikov, F. Laurell, and V. Pasiskevicius, "Carbon nanotube mode-locked optically-pumped semiconductor disk laser," Opt. Express **21**(15), 17806–17813 (2013).
9. P. Klopp, U. Griebner, M. Zorn and M. Weyers, "Pulse repetition rate of 92 GHz or pulse duration shorter than 110 fs from a mode-locked semiconductor disk laser,"Appl. Phys. Lett. **98**, 071103 (2011).
10. A. H. Quarterman, K. G. Wilcox, V. Apostolopoulos, Z. Mihoubi, S. P. Elsmere, I. Farrer, D. A. Ritchie, and A. Tropper, "A passively mode-locked external-cavity semiconductor laser emitting 60-fs pulses," Nat. Photonics **3**(12), 729–731 (2009).
11. O. D. Sieber, M. Hoffmann, V. J. Wittwer, M. Mangold, M. Golling, B. W. Tilma, T. Südmeyer, and U. Keller, "Experimentally verified pulse formation model for high-power femtosecond VECSELs," Appl. Phys. B **113**(1), 133–145 (2013).
12. A. R. Albrecht, Y. Wang, M. Ghasemkhani, D. V. Seletskiy, J. G. Cederberg, and M. Sheik-Bahae, "Exploring ultrafast negative Kerr effect for mode-locking vertical external-cavity surface-emitting lasers," Opt. Express **21**(23), 28801–28808 (2013).
13. H. Haug, S. Stephan, and W. Koch, *Quantum Theory of the Optical and Electronic Properties of Semiconductors* (World Scientific, 2009).
14. A. Bäumner, S. W. Koch, and J. V. Moloney, "Non-equilibrium analysis of the two-color operation in semiconductor quantum-well lasers," Phys. Status Solidi B **248**(4), 843–846 (2011).

#204795 - $15.00 USD Received 15 Jan 2014; revised 4 Mar 2014; accepted 5 Mar 2014; published 12 Mar 2014

1. Introduction

Optically-pumped vertical external cavity surface emitting lasers (VECSELs) or disk lasers have been shown to be ideal as wavelength agile, high brightness sources for numerous applications including raw power [1], multi-Watt single frequency [2] and high average power under various mode-locking scenarios. Specifically, mode-locking has been observed with external semiconductor saturable absorber mirrors (SESAM) [3–5], with integrated quantum well and quantum dot SESAMS (MIXSEL) [6], with graphene [6,7] and carbon nanotube [8] saturable absorbers. To our knowledge, the shortest fundamental mode-locked pulse duration to date has been 107 fs albeit at very low average power [9]. While shorter 60fs pulses have been reported [10], these have been harmonically mode-locked transients within longer few picosecond "pulse molecules". Rate equation level models using parameters extracted from experiment have proved successful in capturing the mode-locking behavior for longer duration pulses [11]. As typical intraband carrier scattering times are on the order of 100 fs, it is expected that dynamically changing nonequilibrium distributions will not have a chance to relax to quasi-equilibrium Fermi-Dirac distributions during the pulse itself. The complexity of the nonequilibrium many-body dynamics has limited studies to date to a relatively simple one of multiple QW single pass geometries.

In this paper, we present what to our knowledge is the first attempt to simulate microscopic many body effects in a simple mode-locked geometry by solving the Maxwell - Semiconductor Bloch equations (MSBE) in the Hartree Fock limit using a 2-band model. Our preliminary finding is that sub 100fs mode-locking is feasible in the low gain limit where all carriers are utilized in the pulse forming stage. In higher gain situations unused carriers can destabilize the pulse by providing unused gain in spectral regions that exist external to the interacting nonequilibrium system.

In the following section we then present a brief assessment of the intriguing preliminary observation of self-Kerr Lens mode-locked pulse trains in VECSELs [12] and extend the discussion to include augmenting the ultrafast Kerr effect with a nonlinear crystal in the VECSEL cavity.

2. Microscopic theory and simulation of short-cavity mode-locking

The theoretical analysis of the VECSEL modelocking dynamics requires the simulation of the light-field $\mathrm{E}(z,t)$ propagation inside the laser cavity as well as the nonlinear interaction of this cavity field with the material polarizations $\mathrm{P}(z,t)$ of the optically active QW gain region and the QW saturable absorber (SESAM). Assuming that the cavity light-field circulates in z-direction perpendicular to the QW planes, Maxwell's wave equation can be written in the simple form

$$\left[\frac{\partial^2}{\partial z^2}-\frac{n^2}{c_0^2}\frac{\partial^2}{\partial t^2}\right]\mathrm{E}(z,t)=\mu_0\frac{\partial^2}{\partial t^2}\mathrm{P}(z,t) \tag{1}$$

where the constants n and c_0 are the background refractive index and the vacuum velocity of light and μ_0 denotes the vacuum permeability, respectively. The macroscopic polarization $\mathrm{P}(z,t)$ is obtained by the summation of the microscopic polarizations $\mathrm{p}_{\lambda,\nu,\mathbf{k}}$ over the crystal momentum $\mathbf{k}$ in the plane of the QWs. The dynamics of the microscopic polarization $\mathrm{p}_{\lambda,\nu,\mathbf{k}}$ follows from the multiband semiconductor Bloch equations [13] (SBE)

$$\begin{aligned}\frac{\partial}{\partial t}p_{\lambda,\nu,\mathbf{k}}&=-\frac{i}{\hbar}\sum_{\lambda_1,\nu_1}\left(e^{e}_{\lambda,\lambda_1,\mathbf{k}}\delta_{\nu,\nu_1}+e^{h}_{\nu,\nu_1,\mathbf{k}}\delta_{\lambda,\lambda_1}\right)p_{\lambda_1,\nu_1,\mathbf{k}}-i(\mathrm{n}^{\mathrm{e}}_{\lambda,\mathbf{k}}+\mathrm{n}^{\mathrm{h}}_{\nu,\mathbf{k}}-1)\Omega_{\lambda,\nu,\mathbf{k}}+\Gamma_{\lambda,\nu;\mathrm{deph}}\\ \frac{\partial}{\partial t}\mathrm{n}^{\mathrm{e(h)}}_{\lambda(\nu),\mathbf{k}}&=-2Im\left(\Omega_{\lambda,\nu,\mathbf{k}}(p_{\lambda,\nu,\mathbf{k}})^{\star}\right)+\Gamma^{e(h)}_{\lambda(\nu);\mathrm{scatt}}.\end{aligned} \tag{2}$$

#204795 - $15.00 USD Received 15 Jan 2014; revised 4 Mar 2014; accepted 5 Mar 2014; published 12 Mar 2014

These equations couple the dynamics of the microscopic polarization $\mathrm{p}_{\lambda,\nu,\mathbf{k}}$ and the occupation functions $\mathrm{n}^{\mathrm{e(h)}}_{\lambda(\nu),\mathbf{k}}$ determining the probability that a state $\mathbf{k}$ in the conduction band λ (valence band ν) is occupied by an electron (hole). The renormalized single-particle energies in the Hartree-Fock approximation are

$$e^{e}_{\lambda,\lambda_1,\mathbf{k}} = \varepsilon^{e}_{\lambda,\mathbf{k}}\delta_{\lambda,\lambda_1} - \sum_{\lambda_2,\mathbf{q}} V^{\lambda,\lambda_2,\lambda_1,\lambda_2}_{|\mathbf{k}-\mathbf{q}|}\mathrm{n}^{\mathrm{e}}_{\lambda_2,\mathbf{q}} e^{h}_{\nu,\nu_1,\mathbf{k}} = \varepsilon^{h}_{\nu,\mathbf{k}}\delta_{\nu,\nu_1} - \sum_{\nu_2,\mathbf{q}} V^{\nu,\nu_2,\nu_1,\nu_2}_{|\mathbf{k}-\mathbf{q}|}\mathrm{n}^{\mathrm{h}}_{\nu_2,\mathbf{q}} \qquad (3)$$

and the renormalized Rabi frequency is

$$\Omega_{\lambda,\nu,\mathbf{k}} = \omega_{\mathrm{R}} + \frac{1}{\hbar}\sum_{\lambda_1,\nu_1,\mathbf{q}\neq\mathbf{k}} V^{\lambda,\nu_1,\nu,\lambda_1}_{|\mathbf{k}-\mathbf{q}|}\mathrm{p}_{\lambda_1,\nu_1,\mathbf{q}}. \qquad (4)$$

Here, $V(|\mathbf{k}-\mathbf{q}|)$ is the Coulomb potential and $\omega_{\mathrm{R}} = d^{\lambda,\nu}_{\mathbf{k}}\mathrm{E}(z,t)/\hbar$ where $d^{\lambda,\nu}_{\mathbf{k}}$ is the dipole-matrix element.

Contributions to the SBE that go beyond the Hartree-Fock approximation describe correlation effects such as dephasing of the polarization (Γ_{deph}), carrier scattering (Γ_{scatt}), and Coulomb screening. In the equation of motion for the carrier distributions Eq. (2) the correlation effects in second-Born Markov approximation lead to Boltzmann type scattering terms.

Together with the wave equation, the SBE establish the Maxwell-semiconductor Bloch equations (MSBE). Since the numerical evaluation of the microscopic scattering terms in each time step of a numerical laser-dynamics simulation is excessively CPU-time demanding, it is often necessary to include the correlation effects on the level of effective rates expressing the net effect of the underlying microscopic processes. In this limit, the dephasing of the polarization is described by a simple decay contribution with the characteristic dephasing time τ_{dep}; $\Gamma_{\lambda,\nu;\mathrm{deph}} = -\mathrm{p}_{\lambda,\nu,\mathbf{k}}/\tau_{deph}$ and, similarly, the carrier-scattering contribution modeling the equilibration of the carrier system follows from $\Gamma_{\lambda(\nu);\mathrm{scatt}} = -\left(\mathrm{n}^{\mathrm{e(h)}}_{\lambda(\nu),\mathbf{k}} - \mathrm{f}^{\mathrm{e(h)}}_{\lambda(\nu),\mathbf{k}}\right)/\tau_{scatt}$ where $f^{e(h)}_{\lambda(\upsilon),k}$ is the background quasi-equilibrium distribution of the optically pumped QW and τ_{scatt} governs the characteristic time scales of scattering events. To test our model [14] and to study the relevance of nonequilibrium effects, we restrict ourselves to a two-band model, postulating strong confinement of electrons and holes such that only the lowest subbands need to be taken into account. In addition, we limit the consideration to a parabolic band structure where the transition energy, i.e. the difference between the conduction and valence band energy, $\hbar\omega_{\mathbf{k}} = \frac{\hbar^2\mathbf{k}^2}{2m_{\mathrm{e}}} + \frac{\hbar^2\mathbf{k}^2}{2m_{\mathrm{h}}} + \mathrm{E}_{\mathrm{g}}$ is expressible in terms of the effective masses of the electrons, m_{e}, holes, m_{h}, and the band-gap energy E_{g}. As a sanity check we employed a full multi-band microscopic simulation in a single pass setting that goes beyond the Hartree-Fock limit to assess the role of ultrafast correlations in the hot carriers (electron/hole) and carrier capture from the pumped barrier to inverted well states. In the low gain limit studied here, these correlations do not affect the results.

As a first effort we employ a simple linear one-dimensional VECSEL cavity with a 2 ps round-trip time, with an active mirror consisting of a DBR and a resonant-periodic gain medium on the one end and the SESAM attached to a 1% outcoupling mirror on the other end. We assume a 3ps (0.5 ps) relaxation time for the QW (SESAM) populations back to a reference 300 K quasi-equilibrium distribution of density 2.0e16 [1/m^2] (5.0e14 [1/m^2]) and InGaAs/AlGaAs bandstructure parameters. The gain medium consists of 10 effective 8nm QWs and the bandgap of the single SESAM QW is energetically 10 meV below that of the gain QWs. To simulate the transverse focusing onto the SESAM used in mode-locking experiments, we use a tenfold field enhancement in the SESAM. With this input, we

#204795 - $15.00 USD Received 15 Jan 2014; revised 4 Mar 2014; accepted 5 Mar 2014; published 12 Mar 2014

numerically solved the MSBE starting with a very weak initial pulse of 200 fs duration (FWHM). By changing the initial pulse duration and amplitude, we verified that the results are independent of the initialization details.

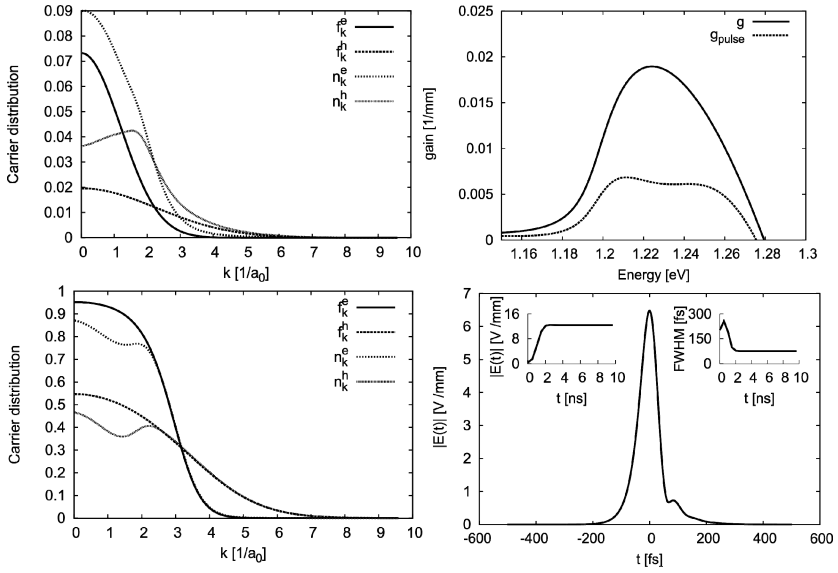

Fig. 1. Example for the results obtains by numerical solution of the MSBE for mode-locking operation. The upper left panel shows the momentum resolved reference carrier distributions $f_k^{e(h)}$ in the gain QWs together with the nonequilibrium distribution $n_k^{e(h)}$ induced by the intra-cavity circulating pulse. The corresponding nonequilibrium gain spectrum is shown in the upper right panel (dotted line) together with the reference gain spectrum of the background distributions (solid line). The SESAM carrier distribution and the converged stable pulse are plotted in the lower left and right panels, respectively. The insets show the temporal stabilization of the pulse amplitude and the FWHM.

An example of the numerical results is presented in Fig. 1. The upper left panel shows the reference carrier distribution in the gain QWs together with the nonequilibrium distribution induced by the intra-cavity circulating pulse. We clearly notice the pronounced kinetic hole-burning in the distributions. The corresponding nonequilibrium gain spectrum is shown in the upper right panel of Fig. 1. We clearly see a significant gain reduction and flattening in comparison to the quasi-equilibrium gain spectrum of the background distributions. The lower left panel depicts the SESAM carrier distribution induced by the pulse and the stable converged pulse shape is plotted in the lower right panel, respectively. From the insets, we can see that pulse amplitude and FWHM stabilize approximately 2ns after the initialization. The resulting 75 fs FWHM mode-locked pulse has a somewhat complex shape and is clearly not Fourier-transform limited since we did not implement any attempts of round-trip dispersion management.

Whereas the chosen example shows a successfully mode-locked configuration, we have encountered many situations with unstable results where the pulse develops complicated multi-peaked shapes or does not reach a stable configuration. We are in the process of mapping the parameter space to identify the best mode-locking conditions and to explore the limitations on achievable pulse durations and intensities.

3. Assessment of Kerr Lens mode-locking

As pointed out in the introduction, the intrinsic Kerr effect within the VECSEL itself might be employed to achieve mode-locking as discussed in [12]. We conducted similar experiments to study this “self-mode-locking” phenomenon and indeed observe the occurrence of a pulse train by measuring the RF signal with a fast photodiode. However, in our study we noticed that the train fluctuates over a time scale of some microseconds as also observed in [12]

#204795 - $15.00 USD Received 15 Jan 2014; revised 4 Mar 2014; accepted 5 Mar 2014; published 12 Mar 2014

which might suggest slow thermal effects or unavoidable fluctuations in the optical pump intensity. In our experimental setup we were unable to detect stable mode-locking operation in this configuration. Furthermore, it is expected that despite the high Kerr coefficient of GaAs at wavelengths around 1 micron, the tiny interaction length within the VECSEL chip will result in a Kerr-lens extremely weak compared to the thermal lens formed by the profile of the pump spot.

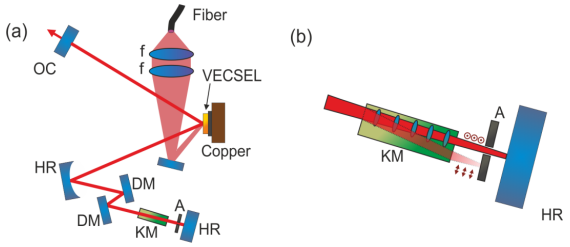

Fig. 2. (a) Schematics of the laser cavity which is formed by a highly reflective (HR) curved mirror, a flat output coupler (OC) with 1% transmission, a flat HR end mirror, the VECSEL chip as well as two dispersion compensation mirrors (DM). As Kerr-medium (KM) a YVO_4 crystal is used. (b) The YVO_4 crystal also provides polarization control: The ordinary laser beam passes the crystal directly while the orthogonal polarization is transversal displaced and is blocked by the aperture (A).

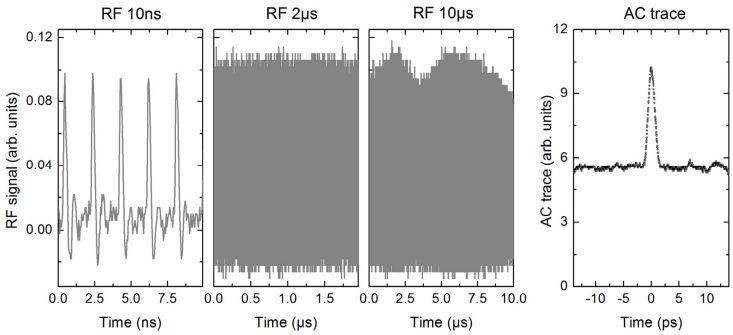

Fig. 3. RF signal for the emitted laser light for different time windows (10ns, 2µs, 10µs). Measured autocorrelation signal recorded with a background free SHG autocorrelator. A short spike is observed towering above a significant background pedestal.

We then attempted traditional Kerr-lens mode locking by adding a nonlinear crystal to the cavity – the latter should boost the Kerr nonlinearity inside the cavity to a level comparable with other Kerr-lens mode locked lasers such as titanium sapphire (TiSa) lasers. For this, we utilize an undoped yttrium orthvanadate (YVO_4) crystal which exhibits a nonlinear refractive index three times higher than that of TiSa. We built a cavity as illustrated in Fig. 2 with a VECSEL chip emitting around 1micron acting as gain element and we place the Kerr crystal close to one end mirror. The intensity induced Kerr effect will form a lens within the crystal. An aperture is inserted in the cavity such that diffraction losses occur when the laser operates in pure cw mode. Once pulses build up, the intensity increases and thus, the Kerr lens reduces the mode size at the aperture positions and saturates the losses. The AR coated 10 mm long YVO4 crystal was cut at 45° with respect to the optical axis to additionally act as beam displacer for the extraordinary beam. After passing through the crystal, both polarization components are displaced by one millimeter and the aperture can be used to select the lasing polarization. The YVO_4 crystal induces positive dispersion within the cavity. As compensation we employed two dielectric Gires-Tournois-Interferometer (GTI) mirrors with a combined negative dispersion of 5200 fs^2 per cavity round-trip. The other cavity elements including the AR-coated VECSEL chip have a relatively flat dispersion at the emission

#204795 - $15.00 USD Received 15 Jan 2014; revised 4 Mar 2014; accepted 5 Mar 2014; published 12 Mar 2014

wavelength of 1035nm. Thus, the linear dispersion of the YVO_4 crystal (about 4000 fs^2) is slightly overcompensated as is favorable for Kerr-lens mode-locking. In the experiments, we pump the VECSEL with a fiber coupled diode laser emitting around 808nm with up to 20W of pump power. We optimize the cavity for the most stable pulse train and autocorrelation trace. Under optimal conditions, the average output power is 1.5 W and we measure a RF signal as shown in Fig. 2. While the signal shows a pulse train with stability over a time frame of few μs, over longer times (tens of μs) there are significant fluctuations in the trains as also observed in attempts to achieve mode-locking employing the intrinsic Kerr effect in VECSEL [11] and thus, the system is not stably mode locked. This instability is more apparently in the measured the auto-correlation trace as shown in Fig. 3. A short pulse (with FWHM of about 850fs) sits on a high background pedestal indicating a strong quasi-CW component in the emission and thus, no stable mode-locking.

4. Summary

The research area of femtosecond pulsed mode-locking in VECSELs is a relatively young field despite the many successes demonstrated to date. Stable pulse mode-locking has been observed using saturable absorbers of various types and in varying VECSEL chip geometries. Most common is an external SESAM consisting of either a single QW or QD layer. The MIXSEL configuration provides the possibility of compact integrated high repetition rate pulsed lasers. The limitation of SESAMS is relatively slow recombination times which makes the recent demonstrations with grapheme and carbon nanotubes particularly interesting. The latter exhibits recombination times on the order of 100fs which is coincidentally the time scale on which microscopic many-body effects are expected to be influential. The challenge in modeling the latter is the extreme computational complexity of the many-body physics including carrier capture between bands including barrier states and intraband correlations involving carrier-carrier and carrier phonon scattering. The first simulation presented in this paper, while modest, is a key first step to assessing the role of nonequilibrium processes in limiting pulse duration or maximal achievable intensity or repetition rate. The next step is to move beyond the Hartree Fock limit and study the influence of ultrafast carrier scattering within individual carrier plasmas.

Kerr lens mode-locking would essentially provide an instantaneous response supplanting any need for saturable absorber solutions. However, KLM in VECSELs presents its own set of challenges due to the small loss modulation and strong sensitivity to the laser peak intensity. While our results can only be indicative of longer term instability, this behavior is likely to persist unless ways can be found to deal with noise sources such as thermal fluctuations within the VECSEL chip itself or possibly in the pump optics.

5. Conclusion

In conclusion, we have carried out the first microscopic simulation of mode-locking in a simple VECSEL cavity. Our results indicate that clean sub 100fs pulses can be generated in the low gain limit. At higher gain and consequently higher peak intensities, we have preliminary evidence that unused carriers can destabilize the pulse waveform. In parallel, we revisited the possibility of achieving KLM in such VECSEL cavities. Our experience is that the intrinsic and probably weak Kerr lens induced in the VECSEL chip causes long time instabilities of the pulse wavetrains even in the presence of a passive nonlinear crystal in the cavity.

Acknowledgment

We gratefully acknowledge funding support from the U.S Air Force Office for Scientific Research under BRI grant FA9550-14-1-0062 and from the German Science Foundation (DFG: GRK 1782). We also acknowledge fruitful discussions with Alexander Albrecht and Mansoor Sheik-Bahae at the University of New Mexico.

#204795 - $15.00 USD Received 15 Jan 2014; revised 4 Mar 2014; accepted 5 Mar 2014; published 12 Mar 2014

Charging Dynamics in Electrically Pumped Quantum Wells

Ada Bäumner, Mackillo Kira, and Stephan W. Koch

***Abstract*—Injection pumping of quantum-well lasers can lead to charging of the active region due to the different electron and hole masses. To investigate the significance and physical consequences of this effect, the consequences of electrical pumping and the associated charging phenomena are investigated microscopically. The analysis reveals the necessity to include the extended barrier states energetically above the band edge in addition to the quantum-confined well states. It is shown that the barrier-state populations compensate the quantum-well charging. The replenishing of stimulated carrier recombination under cw laser operation causes persistent charge oscillations at the plasma frequency.**

***Index Terms*—Charge carrier processes, Plasma oscillations, Quantum well lasers, Semiconductor device modeling**

I. Introduction

In its simplest form, an injection pumped quantum-well (QW) laser consists of a thin layer of low band-gap material sandwiched between an n-doped substrate and a p-doped layer of high band-gap materials. The difference between the smaller band gap of the well material and the larger band gap of the barriers causes a confinement potential for both electrons and holes. Current is injected into the heterostructure via suitably designed electrodes. By applying a voltage, charge carriers are pumped into the continuum of states energetically above the band edge of the barrier layers. Via Coulomb and phonon scattering some portion of these carriers is captured into the QW states where they can contribute to the lasing process. When modeling the capture process, one has to account for the Fermionic nature of electrons and holes leading to the well-known Pauli blocking of the occupied states. Since typically the holes have a significantly larger effective mass than the electrons, this phase space effect is more prominent for the electrons than for the holes giving rise to a reduced capture probability for the electrons. Naively following this line of argumentation one therefore expects a certain degree of QW charging. For the typical example of III/V semiconductor compounds under quasi-thermal lasing conditions, the low momentum states of the electrons are significantly (i.e. 2 - 5 times) more populated than those of the holes. Therefore, the capture rate of the electrons is reduced for elevated carrier densities and a positive net charge builds up. To investigate the relevance of this effect and its possible consequences, one has to keep in mind that charging gives rise to static fields which not only affect the energetic structure of the device but also cause a redistribution of the carriers in the unconfined states. This redistribution in turn affects the capture process such that the full analysis of electric pumping-induced charging implies a complex interplay of electrostatic potentials resulting from local charge imbalances and scattering processes (see e.g. [1]–[4]). In particular, one has to analyze the redistribution of the injected carriers between the unconfined barrier states and the confined states of the QW and its impact on the optical properties of the laser device (see e.g [5], [6]).

A. Bäumner, M.Kira and S. W. Koch are with the Department of Physics and Material Sciences Center, Philipps-University Marburg, 35032 Marburg, Germany (e-mail: ada.baeumner@physik.uni-marburg.de).

In this paper, we present a microscopic analysis of the fundamental effects related to QW injection pumping. We show that both the carriers in the QW confined states and the unconfined barrier states have to be treated consistently in order to explain the experimentally observed absence of significant pumping-induced charging. It turns out that charge compensation occurs via the dynamic redistribution of the barrier electrons and holes in the quasi-continuum of states. Carriers in barrier states accumulate in the spatial vicinity of the QW to compensate the QW charging. This dynamic effect leads to an almost perfect overall charge neutrality. The stimulated electron-hole recombination in the QW together with the carrier replenishing and associated redistribution in the barrier states gives rise to sustained charge oscillations at the plasma frequency.

II. Theoretical Approach

As one of the important ingredients to analyze the characteristics of a semiconductor laser, one needs to determine how the different electronic states are excited and how they influence the optical properties. We start from the reduced single-particle density matrix of the carrier system, where the diagonal elements determine the populations and the off-diagonal elements characterize the coherences between different states and determine the optical polarization of the semiconductor [7]. In coordinate representation, the density matrix $\rho_{\lambda_1,\lambda_2}(\mathbf{r}_1,\mathbf{r}_2,t) = \langle\hat{\Psi}^\dagger_{\lambda_1}(\mathbf{r}_1,t)\hat{\Psi}_{\lambda_2}(\mathbf{r}_2,t)\rangle$ is defined by the expectation value of the product of the Fermionic field operators $\hat{\Psi}^\dagger_\lambda(\mathbf{r},t)$ and $\hat{\Psi}_\lambda(\mathbf{r},t)$ which create and annihilate an electron in the band λ at position $\mathbf{r}$, respectively.

The dynamical system evolution is is governed by the Hamiltonian $\hat{H}$ via Heisenberg's equation of motion

$$i\hbar\frac{\partial}{\partial t}\langle\hat{\Psi}^\dagger_{\lambda_1}(\mathbf{r}_1,t)\hat{\Psi}_{\lambda_2}(\mathbf{r}_2,t)\rangle = \langle[\hat{\Psi}^\dagger_{\lambda_1}(\mathbf{r}_1,t)\hat{\Psi}_{\lambda_2}(\mathbf{r}_2,t),\hat{H}]_-\rangle. \tag{1}$$

In its simples form, the Hamiltonian of a Coulomb interacting carrier system is given as the sum of the single-particle energy

H_0 and the Coulomb interaction $V(\mathbf{r},\mathbf{r}')$ [7]–[10]

$$\hat{H} = \sum_\nu \int d^3r \hat{\Psi}^\dagger_\nu(\mathbf{r},t) H_0 \hat{\Psi}_\nu(\mathbf{r},t) + \sum_{\nu,\nu'} \frac{1}{2} \int d^3r \int d^3r' \times \hat{\Psi}^\dagger_\nu(\mathbf{r},t)\hat{\Psi}^\dagger_{\nu'}(\mathbf{r}',t) V(\mathbf{r},\mathbf{r}') \hat{\Psi}_{\nu'}(\mathbf{r}',t)\hat{\Psi}_\nu(\mathbf{r},t) \quad (2)$$

In the resulting equations of motion, one encounters the hierarchy problem of many-body physics since the Coulomb part of the Hamiltonian couples the dynamics of the single-particle quantity $\langle \hat{\Psi}^\dagger_{\lambda_1}(\mathbf{r}_1,t)\hat{\Psi}_{\lambda_2}(\mathbf{r}_2,t)\rangle$ to a two-particle expectation value $\langle \hat{\Psi}^\dagger_{\lambda_1}(\mathbf{r}_1,t)\hat{\Psi}^\dagger_\nu(\mathbf{r},t)\hat{\Psi}_\nu(\mathbf{r},t)\hat{\Psi}_{\lambda_2}(\mathbf{r}_2,t)\rangle$. The simplest approach to obtain a closed set of equations is to truncate the hierarchy using the Hartree-Fock decoupling by splitting the two-particle expectation value into products of single-particle terms and a purely correlated part ([7], [9], [10]). In the analysis in this paper, we treat all Coulomb correlations and also other effects like phonon scattering on a phenomenological level since we want to focus exclusively on the main consequences of the lack of local charge neutrality, i.e. the Hartree contribution.

A. Hartree Contribution

In Hartree-Fock approximation, where the purely correlated part resulting from the hierarchical decoupling is neglected, the equation of motion for the density matrix is obtained as [7]

$$i\hbar\frac{\partial}{\partial t}\langle \hat{\Psi}^\dagger_{\lambda_1}(\mathbf{r}_1)\hat{\Psi}_{\lambda_2}(\mathbf{r}_2)\rangle \approx [H_0(\mathbf{r}_2) - H_0(\mathbf{r}_1)]\langle \hat{\Psi}^\dagger_{\lambda_1}(\mathbf{r}_1)\hat{\Psi}_{\lambda_2}(\mathbf{r}_2)\rangle + \int \left[V(\mathbf{r}_2,\mathbf{r}) - V(\mathbf{r}_1,\mathbf{r})\right] \left(\sum_\nu \langle \hat{\Psi}^\dagger_\nu(\mathbf{r})\hat{\Psi}_\nu(\mathbf{r})\rangle \langle \hat{\Psi}^\dagger_{\lambda_1}(\mathbf{r}_1)\hat{\Psi}_{\lambda_2}(\mathbf{r}_2)\rangle - \sum_\nu \langle \hat{\Psi}^\dagger_{\lambda_1}(\mathbf{r}_1)\hat{\Psi}_\nu(\mathbf{r})\rangle \langle \hat{\Psi}^\dagger_\nu(\mathbf{r})\hat{\Psi}_{\lambda_2}(\mathbf{r}_2)\rangle \right) d^3r.$$

Here, the second line contains the Hartree contribution and the third line gives the Fock-exchange term which appears as a consequence of the antisymmetry of the indistinguishable electrons. In contrast to the Fock term, the Hartree contribution explicitly includes the electron density distribution

$$\sum_\nu n_\nu(\mathbf{r},t) = \sum_\nu \langle \hat{\Psi}^\dagger_\nu(\mathbf{r},t)\hat{\Psi}_\nu(\mathbf{r},t)\rangle \quad (3)$$

where the sum runs over all valence (v) and conduction bands (c). To identify the contribution of charging in the equation of motion, it is useful to introduce $n_e(\mathbf{r},\mathbf{r}',t) \equiv \sum_{\nu\in\{c\}}\langle \hat{\Psi}^\dagger_\nu(\mathbf{r},t)\hat{\Psi}_\nu(\mathbf{r}',t)\rangle$ and $n_h(\mathbf{r},\mathbf{r}',t) \equiv \sum_{\nu\in\{v\}}\langle \Psi_\nu(\mathbf{r},t)\Psi^\dagger_\nu(\mathbf{r}',t)\rangle$ whose diagonal $\mathbf{r}=\mathbf{r}'$ terms are the electron and hole densities. With these definitions, the sum of the electron densities in the valence and conduction bands (3) can be written as

$$\sum_\nu n_\nu(\mathbf{r},t) = n_e(\mathbf{r},t) - n_h(\mathbf{r},t) + \sum_{\nu\in\{v\}} \langle [\hat{\Psi}^\dagger_\nu(\mathbf{r},t), \hat{\Psi}_\nu(\mathbf{r}',t)]|_{\mathbf{r}=\mathbf{r}'}\rangle. \quad (4)$$

Here, the commutator of the field operators $\hat{\Psi}^\dagger_\nu(\mathbf{r},t), \hat{\Psi}_\nu(\mathbf{r}',t)$ appears due to the Fermionic anticommutation relation. Its contribution to the Hartree term in Jellium approximation [7] is compensated by the ionic background such that it typically does not enter the equation of motion explicitly but is included with the band energies, usually in the evaluation of the band gap. The remaining Hartree term

$$HT(\mathbf{r}_1,\mathbf{r}_2,t) = \int \{[V(\mathbf{r}_2,\mathbf{r}) - V(\mathbf{r}_1,\mathbf{r})][n_e(\mathbf{r},t) - n_h(\mathbf{r},t)]\}\, d^3r \quad (5)$$

is explicitly determined by the excess charge-carrier density $\Delta n(\mathbf{r},t) = n_h(\mathbf{r},t) - n_e(\mathbf{r},t)$ to which the electrons and holes contribute, both in the confined states of the QW and the extended barrier states.

In spatially homogeneous bulk semiconductors, the Hartree term is identically vanishing due to local charge neutrality. In nanostructures such as QWs, however, the different effective masses of electrons and holes and the imperfect quantum confinement typically lead to a violation of local charge neutrality such that the Hartree term does not vanish [11].

For optically pumped QW systems, where the total density of electrons in all QW states equals the total density of holes, charging does not occur as long as the quantum confinement prevents carrier escape. For electrically pumped QW systems, however, the situation is more complicated. Here, the density of electrons and holes in the quantum confined states follows from the complex interplay of electrostatic potentials and microscopic scattering processes. Thus, the consequences of the Hartree contribution require closer investigation, especially since it includes contributions from the carriers in all bands.

Due to the single-particle character of the Hartree term, an effective Hamiltonian $\hat{H}_{\text{eff}}$ may be introduced which leads to the same result in the equation of motion as the Hartree contribution of the full Hamiltonian:

$$HT(\mathbf{r}_1,\mathbf{r}_2,t)\langle \hat{\Psi}^\dagger_{\lambda_1}(\mathbf{r}_1,t)\hat{\Psi}_{\lambda_2}(\mathbf{r}_2,t)\rangle = \langle [\hat{\Psi}^\dagger_{\lambda_1}(\mathbf{r}_1,t)\hat{\Psi}_{\lambda_2}(\mathbf{r}_2,t), \hat{H}_{\text{eff}}(t)]_-\rangle. \quad (6)$$

In QW structures, the carrier distributions $n_\lambda(\mathbf{r},t)$, $\lambda = e,h$, are typically characterized by a homogeneous 2D in-pane density n^{2D}_λ multiplied by the confinement factor $\mid \xi_\lambda(z) \mid^2$ describing the spatial carrier distributions perpendicular to the well. Consequently, the Hartree term only depends on the z coordinate, yielding an extra potential for QW carriers. Adding to the QW confinement potential, the Hartree potential thus modifies the eigenvalue problem in the confinement direction z leading to a shift in the single-particle energies and a change in the confinement functions relative to the problem without charges.

Formally, we can write the effective Hamiltonian

$$\hat{H}_{\text{eff}}(t) = \sum_\nu \int \hat{\Psi}^\dagger_\nu(\mathbf{r},t)\ e\Phi(t)\ \hat{\Psi}_\nu(\mathbf{r},t) d^3r \quad (7)$$

that corresponds to the Hartree potential $e\Phi$. This potential is related to the charge distribution $e\Delta n(\mathbf{r})$, via Poisson's equation

$$\nabla^2\Phi(t) = \frac{e}{\epsilon\epsilon_0}\Delta n(\mathbf{r},t) \quad (8)$$

which has to be solved self-consistently with Schrödinger's equation for the confinement problem in the direction perpendicular to the QW. In Appendix (A), we show that for QW

structures the Hartree term basically exhibits a parabolic space dependence,

$$e\Phi \approx \frac{e^2}{2\epsilon\epsilon_0}\Delta n(0,t)z^2. \tag{9}$$

Here, e is the electron charge, ϵ_0 is the free space permittivity, ϵ is the background dielectric constant, and the excess charge carrier density at the center of the QW is denoted as $\Delta n(0,t)$.

The concept of a Hartree potential provides a convenient way to study the influence of charging on the dynamics of the system. In particular, it allows us both to easily compute the optical properties of the system using the Hartree-Fock semiconductor Bloch equations ([12], [13]), and to clearly distinguish the back coupling of the carriers in the extended barrier states.

B. Hartree-Fock Semiconductor Bloch Equations for Charged Quantum Wells

In momentum representation, (3) yields the well-known semiconductor Bloch equations (SBE) ([12], [13]). Within the two-band approximation we obtain from (3) for the off-diagonal elements of the density matrix $\rho_{\lambda_1,\lambda_2}(\mathbf{r}_1,\mathbf{r}_2,t)$, $\lambda_1 \neq \lambda_2$ the dynamic equation for the microscopic polarization $P_{\mathbf{k}}$ which defines the optical properties of the semiconductor QW [14]. Here, the index $\mathbf{k}$ denotes the momentum in the plane of the QW. Including not only purely electronic contributions, but also the dipole interaction of the carrier system with an electromagnetic field $E(t)$, we find

$$\begin{aligned} i\hbar\frac{d}{dt}P_{\mathbf{k}} &= [\epsilon_{e,\mathbf{k}}+\epsilon_{h,\mathbf{k}}+\Delta E_{\mathrm{BGR}}]\,P_{\mathbf{k}} \\ &\quad -[1-f^e_{\mathbf{k}}-f^h_{\mathbf{k}}]\Omega_{\mathbf{k}} \end{aligned} \tag{10}$$

with

$$\epsilon_{e,\mathbf{k}} = E_{e,\mathbf{k}} - \sum_{\mathbf{q}\neq\mathbf{k}} V^{\mathrm{ee}}_{|\mathbf{k}-\mathbf{q}|} f^e_{\mathbf{q}}, \tag{11}$$

$$\epsilon_{h,\mathbf{k}} = E_{h,\mathbf{k}} - \sum_{\mathbf{q}\neq\mathbf{k}} V^{\mathrm{hh}}_{|\mathbf{k}-\mathbf{q}|} f^h_{\mathbf{q}} \tag{12}$$

and

$$\Omega_{\mathbf{k}} = \left[d_{\mathrm{eh}}E(t) + \sum_{\mathbf{q}\neq\mathbf{k}} V^{\mathrm{eh}}_{|\mathbf{k}-\mathbf{q}|} P_{\mathbf{q}} \right]. \tag{13}$$

Here, the Coulomb-matrix elements are defined as

$$\begin{aligned} V^{\lambda_1,\lambda_2}_{\mathbf{q}} &= V^{2D}_{\mathbf{q}} \int dz_1 \int dz_2 \\ &\quad \times \xi^*_{\lambda_2}(z_2)\xi^*_{\lambda_1}(z_1)e^{-q(|z_2-z_1|)}\xi_{\lambda_1}(z_1)\xi_{\lambda_2}(z_2). \end{aligned} \tag{14}$$

At the Hartree-Fock level, the Coulomb interaction $V^{2D}_{\mathbf{q}}$ enters as a renormalization of both the single-particle energies of electrons and holes, $E_{e,\mathbf{k}}$, $E_{h,\mathbf{k}}$, and the light field $E(t)$ that couples to the carrier system via the dipole element d_{eh}. The charging of the QW yields an additional renormalization $\Delta E_{BGR} = \Delta E_{sub} + \Delta E_{\Sigma} + \Delta E_{HT}$ of the single-particle energies, i.e. the band gap. Since the Hartree potential modifies the confinement problem, one finds a direct change ΔE_{sub} for the energetic spacing of the subband levels of the QW. The corresponding change in the confinement functions $\xi(z)$ alters the Coulomb-matrix elements (14). Consequently, also the difference in the exchange self-energy [7]

$$\Delta E_{\Sigma} = \sum_{\mathbf{q}\neq 0} V^{hh}_{\mathbf{q}} - \sum_{\mathbf{q}\neq 0} V^{hh,0}_{\mathbf{q}} \tag{15}$$

and the difference in the Hartree contribution of the completely filled valence bands (cf. discussion of (4))

$$\Delta E_{HT} = n^{2D}_{ion} S \left[\left(V^{eh}_0 - V^{eh,0}_0 \right) - \left(V^{hh}_0 - V^{hh,0}_0 \right) \right]. \tag{16}$$

contribute to the band-gap renormalization. Here, n_{ion} denotes the homogeneous 2D density of the ionic background of the Jellium model [7] and S is the quantization area. The superscript 0 in (15) and (16) indicates that the Coulomb matrix elements $V^{\lambda_1,\lambda_2,0}_{\mathbf{q}}$ are evaluated with the confinement functions corresponding to the limit of a vanishing Hartree potential. Actually, the time dynamics of the microscopic polarization $P_{\mathbf{k}}$ couples to the dynamics of the carrier distribution functions $n_{\lambda,\mathbf{k}}$ corresponding to the momentum representation of the diagonal elements of the density matrix $\rho_{\lambda,\lambda}(\mathbf{r}_1,\mathbf{r}_2,t)$. However, assuming that the scattering processes which drive the carrier distributions to equilibrium happen on a much smaller time scale than the times of interest, we replace $n_{\lambda,\mathbf{k}}(t)$ by stationary quasi-equilibrium Fermi distributions $f^{\lambda}_{\mathbf{k}}$ for the electrons ($\lambda = e$) and holes ($\lambda = h$), respectively [15]. Formally, the time dynamics of the carrier distribution functions $n_{\lambda,\mathbf{k}}$ is also covered by (3). In this investigation, however, we apply a simple rate equation model that takes into account the essential features of the full microscopic theory ([16], [17]) by phenomenological fitting parameters

$$\begin{aligned} \frac{dn_{\lambda,\mathbf{k}}}{dt} &= \eta F_{\lambda,\mathbf{k}}[1-n_{\lambda,\mathbf{k}}] - \frac{n_{\lambda,\mathbf{k}}-f_{\lambda,\mathbf{k}}}{\tau_1} - \frac{n_{\lambda,\mathbf{k}}-f_{\lambda,\mathbf{k}}(T_{\mathrm{lat}})}{\tau_2} \\ &\quad -\mathcal{A}n_{\lambda,\mathbf{k}} - \mathcal{B}n_{\bar{\lambda}}n_{\lambda,\mathbf{k}} - \mathcal{C}n_{\lambda}n_{\bar{\lambda}}n_{\lambda,\mathbf{k}}. \end{aligned} \tag{17}$$

The first contribution describes the relaxation of carriers from the extended barrier states into the confined states of the QW. The efficiency of this process is determined by the pumping strength η and the initial state distribution $F_{\lambda,\mathbf{k}}$ of the pump-injected carriers which arrive in the active region [18]. The Pauli-blocking factor $[1-n_{\lambda,\mathbf{k}}]$ accounts for the effective reduction of the pump efficiency due to the presence of carriers inside the QW. The carriers in the barrier states have a large excess energy determined by the electric injection. These carriers strongly scatter among each other establishing a quasi-equilibrium Fermi-Dirac distribution $F_{\lambda,\mathbf{k}}$ in the barrier states. This distribution is related to the overall 2D carrier density via $n_{bar,\lambda} = 2/S\sum_{\mathbf{k}} F_{\lambda,\mathbf{k}}$ where the factor 2 is due to the two possible spin orientations. The steady injection current ensures that these carriers are not depleted by the recombination processes. The phenomenological relaxation times τ_1 and τ_2 in the carrier rate equation (17) determine the equilibration of the carrier system due to Coulomb and phonon scattering, respectively. Due to the Coulomb scattering, the carrier densities develop into a Fermi-Dirac distribution $f_{\lambda,\mathbf{k}}$, which yields the same total density and kinetic energy as $n_{\lambda,\mathbf{k}}$. As a result of the phonon scattering the carrier densities relax toward a Fermi-Dirac distribution $f_{\lambda,\mathbf{k}}(T_{\mathrm{lat}})$ at the lattice temperature T_{lat}. The remaining terms on the right hand side

TABLE I
MODEL EXAMPLE PARAMETERS

Symbol	Value	Symbol	Value
m_0	1.602 $10^{-19}C$	$n_{bar,e/h}$	10^{12}cm^{-2}
m_e	0.0665 m_0	η	1.6 10^{9}s^{-1}
m_h	0.457 m_0	τ_1	0.2 ps
ϵ	13.74	τ_2	0.2 ps
n_{ion}	$6.2510^{14}cm^2$	$\mathcal{A}$	0.8 10^{8}s^{-1}
T_{lat}	300 K	$\mathcal{B}$	0.9 $10^{-10}\text{cm}^{-3}s^{-1}$
E_G	1.262 eV	$\mathcal{C}$	0.7 $10^{-29}\text{cm}^{-6}s^{-1}$
a_0	12.5 nm		

of (17) describe the density dependence of the dominant loss mechanisms. They include the simplest model for nonradiative impurity recombination, spontaneous emission and Auger recombination in terms of phenomenological material specific constants $\mathcal{A}$, $\mathcal{B}$ and $\mathcal{C}$, respectively. Here, n_λ denotes the total density of carriers within a given band λ. The index $\bar{\lambda}$ is defined by $\bar{e} = h$, and $\bar{h} = e$. Even though it is well-known [20] that the simple carrier density dependencies of spontaneous and Auger recombination have to be modified in realistic calculations, for the purposes of our generic model calculations it is sufficient to treat them at the presented simple level.

III. NUMERICAL RESULTS

In our numerical analysis, we consider the model system of an 8 nm GaAs QW with an asymmetric bandoffset for the valence and conduction band of approximately 168 meV and 252 meV, respectively. The relevant parameters used in our computations are summarized in Table (I).

A. Solution for Stationary Barrier Distributions

To estimate the effect of the Hartree term on the optical QW properties, we solve the Hartree-Fock SBE for the microscopic polarization in two-band approximation (10) with and without the respective corrections due to charging and compare the resulting absorption/gain spectra. The pumping-induced density of QW carriers is computed from the rate equation for the occupation probability (17) including carrier injection as well as scattering and recombination processes. We simplify the evaluations by considering only the lowest subband states of the valence and conduction band as relevant contributions to the Hartree term while all other band contributions are neglected. This is a commonly used approximation because optical gain mainly originates from the confined levels. However, we will show in Sec. III-B that all bands play an important role in explaining the correct charging-induced energetic shifts.

In the upper frame of Fig. (1), we plot the time evolution of the total density of electrons $n_e = 2/S\sum_{\mathbf{k}} f^e_{\mathbf{k}}$ (dashed line) and holes $n_h = 2/S\sum_{\mathbf{k}} f^h_{\mathbf{k}}$ (solid line) as well as the resulting total excess charge-carrier density $\Delta n^{QW} = n_h - n_e$ (shaded area). The inset to Fig. (1) shows the electron (dashed line) and hole (solid line) distribution functions $f^\lambda_{\mathbf{k}}$ for the density of $n_e = n_h = 5 \cdot 10^{12}\text{cm}^{-2}$ and a lattice temperature of $T = 300$K. We clearly see that the holes have a reduced phase space filling compared with the electrons since the effective mass of the electrons m_e is considerably lower than that of the holes m_h. Accordingly, we note in the top part of Fig. (1) that the electron density increases slower and saturates at a lower level than the hole density on a nanosecond time scale. Eventually, more holes than electrons are captured into the QW causing a positive net charge, which is typical for small ratios m_e/m_h. To estimate the effect of charging, we compute optical gain at the steady-state conditions of Fig. (1) (a), i.e., at t=12.5 ns giving $\Delta n^{QW} = 2.8 \times 10^{12}\text{cm}^{-2}$. Figure (1) (b) presents optical gain computed using the two-band model with (solid line) and without (dashed line) the Hartree contributions. Neglecting the Hartree contributions means unchanged confinement functions and $\Delta E_{BGR} = 0$. This approximation is commonly used and it works very well to explain experiments. However, we can clearly see that the full inclusion of the Hartree terms yields an appreciable shift in the gain spectrum. Thus modeling critically depends on how the Hartree term is treated when only few confinement levels are included. Especially, our results show that typical pumping-induced charge densities shift the gain peak about 100 meV, which implies that charging is decisive in theory/experiment comparisons. At the same time, this finding conflicts with the observation that theory without charging effects produces an excellent match with experiments (see e.g. [6], [19]). From this evident discrepancy, we conclude that the two-band model is not sufficient to describe charging effects in electrically pumped QW lasers.

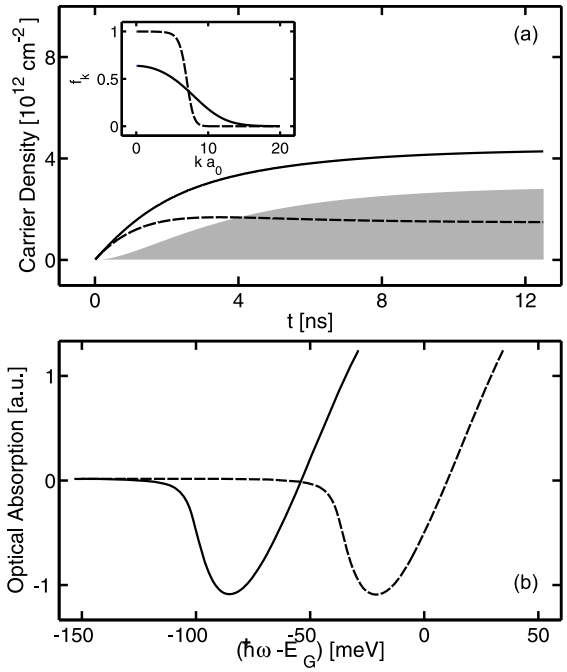

Fig. 1. Density dynamics for injection pumping and effect of pumping-induced charging on the QW gain. (a): Time dependence of the pumping-induced electron (dashed line) and hole (solid line) densities as well as the resulting excess-carrier density (shaded area). Inset shows electron and hole distributions. (b): Gain spectra with (solid line) and without (dashed line) the renormalizations due to the Hartree potential; Both computations performed with two bands. Note, that these Hartree shifts are largely compensated by a charge redistribution in the barriers (see Fig. (2)).

B. Full Dynamic Solution

Once the QW charging due to electric pumping sets in, one also has a restoring Coulomb force which tends to attract carriers of the opposite charge and reject carriers of the same charge. Intuitively, we expect this to yield at least a partial compensation of the pumping-induced charge at the QW region. In contrast to the two-band laser model where the distribution of barrier carriers was assumed to be stationary, we now allow for a dynamic redistribution of the barrier-state carriers in reaction to the charging of the QW region.

To analyze the response of barrier electrons and holes to the Hartree potential, we make use of the parabolic approximation (9). Formally, within the harmonic approximation the problem of charging-induced carrier dynamics is that of a particle in a time-dependent harmonic oscillator potential. In this limit, we can set up the equation of motion of the density matrix $\rho_{\lambda,\lambda}(\mathbf{r}_1,\mathbf{r}_2,t)$ describing the density of electrons ($\lambda = e$) and holes ($\lambda = h$) in the unconfined states with a harmonic oscillator Hamiltonian $H_\lambda^{HO}(z)$ to compute the charging-induced dynamics

$$H_\lambda^{HO}(z,t) = -\frac{\hbar^2\nabla_z^2}{2m_\lambda} + (-1)^\lambda \frac{1}{2} m_\lambda \omega_\lambda^2(t) z^2 \tag{18}$$

with

$$(-1)^\lambda = \begin{cases} +1 \text{ if } \lambda = e \\ -1 \text{ if } \lambda = h. \end{cases} \tag{19}$$

Here, the prefactor $(-1)^\lambda$ allows for the fact that for holes the Hartree potential modifies the confinement with a sign opposite to that for electrons. The oscillator frequency ω_λ is determined by the total excess-charge-carrier density at the center of the QW, i.e. by the difference $\Delta n(t) = \Delta n(0,t)$ of hole and electron densities according to

$$\omega_\lambda^2(t) = \frac{e^2}{\epsilon\epsilon_0 m_\lambda} \Delta n(t). \tag{20}$$

It inherits the time dependence of the total excess-charge-carrier density $\Delta n = \Delta n^{QW} + \Delta n^B$, which consists of contributions from both the confined states of the QW Δn^{QW} and the unconfined states above the band edge of the barriers Δn^B. Thus, as the carriers in the quasi-continuum of states contribute to Δn as well as the carriers residing in the QW, this model takes into account the back coupling of the carriers in the unconfined states to the pumping-induced QW charge.

For the computation of the unconfined carrier response to the pumping-induced QW charging it is particularly suitable to start from the density matrix $\rho_{\lambda,\lambda}(Z,\zeta,t)$ in center-of-mass (COM) and relative coordinates that is obtained by a Fourier transform of the Wigner function of the problem with respect to the momentum coordinate. Proceeding from the assumption that the system of carriers in the unconfined states is characterized by a Gaussian density profile and its momentum distribution follows Boltzmann statistics, the corresponding density matrix reads

$$\rho_{\lambda,\lambda}(Z,\zeta,t) = N_\lambda(t) \exp\left(-\left[\frac{Z^2}{A_\lambda^2(t)} + \frac{\zeta^2}{B_\lambda^2(t)} - 2iC_\lambda(t) Z\zeta\right]\right). \tag{21}$$

Here, the normalization N_λ gives the total barrier charge-carrier density at the center of the QW for either electrons or holes, A_λ characterizes the Gaussian width of the spatial distribution and B_λ may be identified with the thermal wavelength of the respective carrier system. The term proportional to the product of COM- and relative coordinates ensures that propagation in time conserves the structure of the distribution function as may be verified using insight from propagator theory. Initially, the coefficient C_λ vanishes.

To derive equations of motion for the coefficients of the barrier-state carrier distribution function, it is convenient to start from the equation of motion of the full problem $\frac{\partial}{\partial t}\rho_{\lambda,\lambda}(z_1,z_2) = -\frac{i}{\hbar}[H_\lambda^{HO}(z_2) - H_\lambda^{HO}(z_1)]\rho_{\lambda,\lambda}(z_1,z_2)$. We evaluate the terms on both sides of this equation separately by differentiating the density matrix (21) in time on the one hand and applying the harmonic oscillator Hamiltonian to it on the other hand (cf. [21]). By comparison of the coefficients of the COM- and relative space-coordinates of both results, a system of coupled differential equations is obtained

$$\frac{\partial}{\partial t} N_\lambda = -\frac{2\hbar}{m_\lambda} C_\lambda N_\lambda \tag{22}$$

$$\frac{\partial}{\partial t} A_\lambda = \frac{2\hbar}{m_\lambda} C_\lambda A_\lambda \tag{23}$$

$$\frac{\partial}{\partial t} B_\lambda = \frac{2\hbar}{m_\lambda} C_\lambda B_\lambda \tag{24}$$

$$\frac{\partial}{\partial t} C_\lambda = \frac{2\hbar}{m_\lambda}\left[\left(\frac{1}{A_\lambda B_\lambda}\right)^2 - C_\lambda^2 - (-1)^\lambda \frac{m_\lambda^2}{4\hbar^2}\omega_\lambda^2\right]. \tag{25}$$

The connection between the original space coordinates z_1, z_2 of the density matrix and the COM- and relative coordinates Z, ζ is established via $Z = (z_1 + z_2)/2$ and $\zeta = z_2 - z_1$.

We now apply our theory to describe the charging-induced dynamics of the carriers in the unconfined states. The QW charging is solved from (17) and the barrier-state carrier dynamics is computed from (22) - (25). As initial conditions for the carriers in barrier states, we choose wide Gaussian distributions for the electrons and holes. This choice guarantees spatial homogeneity over the sample and allows for overall charge neutrality of the system

$$\begin{aligned} &N_\lambda(0) = 8 \cdot 10^{18}\,\mathrm{cm}^{-3}, \\ &A_\lambda(0) = 4000\,\mathrm{nm}, \\ &B_\lambda(0) = \sqrt{\frac{2\hbar^2}{m_\lambda k_B T}}\, 10^9\,\mathrm{nm}, \quad T = 900\,K, \\ &C_\lambda(0) = 0\,\mathrm{nm}^{-2}. \end{aligned} \tag{26}$$

In the upper frame of Fig. (2) the QW charging Δn^{QW} (shaded area) and the densities of positively and negatively charged barrier carriers at the QW position N_e (dashed line) and N_h (solid line), respectively, are plotted. We note two clearly different dynamical regimes for the unconfined carrier density reacting to the QW charging. In the transient regime which lasts a few picoseconds, the barrier-state density at the center of the QW $N_\lambda(t)$ decreases simultaneously for electrons and holes. As for a normalized Gaussian profile a smaller peak value is equivalent to a broader width, the decrease in the carrier densities corresponds to a diffusion of charge carriers.

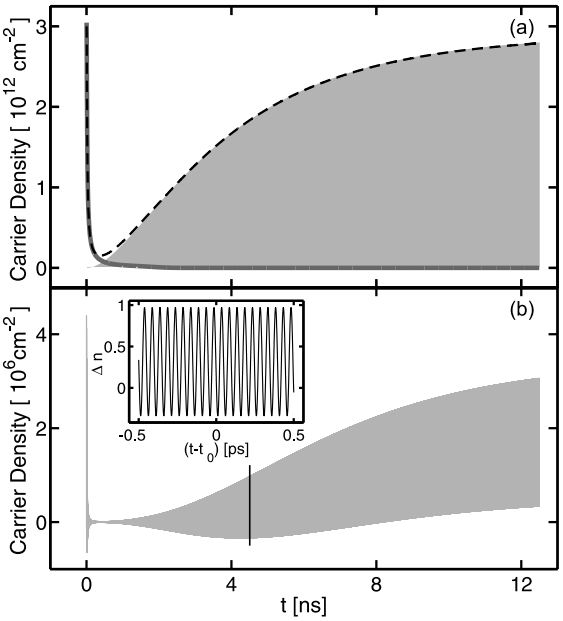

Fig. 2. Charging induced dynamics of the carriers in the unconfi ned states and excess-charge-carrier density oscillations at the center of the QW. (a): Time dependence of barrier electrons (dashed line) and holes (solid line) in response to the excess-carrier density of holes inside the QW (shaded area). (b): Oscillatory motion of the total excess-carrier density at the QW position. The vertical line marks the time t_0 =4.5062 ns. In the inset the oscillations around t_0 are resolved.

This diffusion is characteristic of the early time dynamics where the pumping-induced QW charging is negligible. In the long-time regime, the barrier electron density "follows" the positive net-charge while the barrier holes are virtually absent. The pumping-induced QW charge is compensated by an increasing number of additional barrier electrons that move in to balance the charging. In the lower frame of Fig. (2) the total excess carrier density $\Delta n = \Delta n^{\mathrm{QW}} + \Delta N$, $\Delta N = \Delta n^B = N_h - N_e$, is presented as function of time. Here, we focus on the long-time regime. The regime where the total excess-charge-carrier density assumes relatively large values is omitted. Looking at the time dynamics of the barrier carrier densities N_e and N_h in the upper frame of Fig. (2) we note that the barrier charge density adjusts to the QW charge. Even though this adjustment is not sufficient to completely eliminate all charging effects, they are dramatically reduced by a factor of 10^6 *such that one can neglect the charging contributions in theoretical few-band model calculations*. In the compensation process, the Gaussian distribution of the barrier-state carriers becomes increasingly narrower. However, when the Gaussian is more localized, it disperses more quickly. This dispersion counteracts the trend for charge compensation, thus giving rise to collective charge density oscillations.

To summarize the main results of our numerical analysis, we find that (i) the carriers in barrier states redistribute to compensate for the QW charging but (ii) due to the increased localization near the QW we obtain increased wave packet dispersion. The interplay of both effects leads to sustained charge density oscillations. These oscillations are a characteristic feature of electrically pumped QW lasers with differing effective masses of electrons and holes. The particular time dependence of the total charge density and thus the extend to which barrier electrons compensate a given pumping-induced charge is a strong function of the present QW charging and the initial conditions, i.e the distribution function of pump-injected carriers.

IV. Analytical Solution

To gain further insight into the oscillatory motion of the total charge at the QW position, a second-order oscillator equation for the excess-carrier density $\Delta n = \Delta n^{\mathrm{QW}} + \Delta N$ may be derived using (22) - (25) (cf. [21]). In the late-time regime which is characterized by a constant level, the equation for the excess-carrier density Δn is obtained as

$$\frac{\partial^2}{\partial t^2}\Delta n = -\left[\omega_{pl}^2 + \frac{4\hbar^2}{m_e^2}\left(\left(\frac{1}{A_e B_e}\right)^2 - 2C_e^2\right)\right]\Delta n + \frac{4\hbar^2}{m_e^2}\left(\left(\frac{1}{A_e B_e}\right)^2 - 2C_e^2\right)\Delta n^{\mathrm{QW}} \tag{27}$$

having the form of an inhomogeneous oscillator equation with time-dependent coefficients. From our numerical evaluations, we know that the relation

$$\left(\frac{1}{A_e(t)B_e(t)}\right)^2 \gg C_e^2(t) \tag{28}$$

is well fulfilled. With this input, we can find the adiabatic solution of (27) as

$$\Delta n(t) = \Delta\bar{n}[1 - \cos(\tilde{\omega}_{pl}t)] \tag{29}$$

where

$$\Delta\bar{n} = \left(\frac{2\hbar}{m_e A_e B_e \tilde{\omega}_{pl}}\right)^2 \Delta n^{QW}. \tag{30}$$

Here, the renormalized plasma frequency

$$\tilde{\omega}_{pl}^2(t) \equiv \omega_{pl}^2(t) + \frac{4\hbar^2}{m_e^2 A_e^2(t) B_e^2(t)} \tag{31}$$

has been introduced, whereas

$$\omega_{pl}^2(t) = \frac{e^2}{\epsilon\epsilon_0}\left(\frac{N_e(t)}{m_e} + \frac{N_h(t)}{m_h}\right) \tag{32}$$

is the instantaneous eigenfrequency of an electron-hole plasma. Using (29) we may deduce the frequency of the charge oscillations as well as their mean value, i.e the average level of total charging remaining in the QW system.

First, we compare the frequency of the analytic formula (31) to the frequency of the oscillations obtained by the full numerical solution to the problem of charging-induced barrier-carrier dynamics.

To obtain the oscillation frequency of the full numerical solution for a particular time interval, we convolve the oscillations with a Gaussian centered at the time of interest and Fourier transform the result. In the lower frame of Fig. (3) the oscillation frequency of the numerical solution is shown for certain times indicated by the lines in the upper frame of Fig. (3) where again the total charge density Δn is plotted as function of time. The vertical lines in the lower frame of Fig. (3) indicate the instantaneous eigenfrequency of an

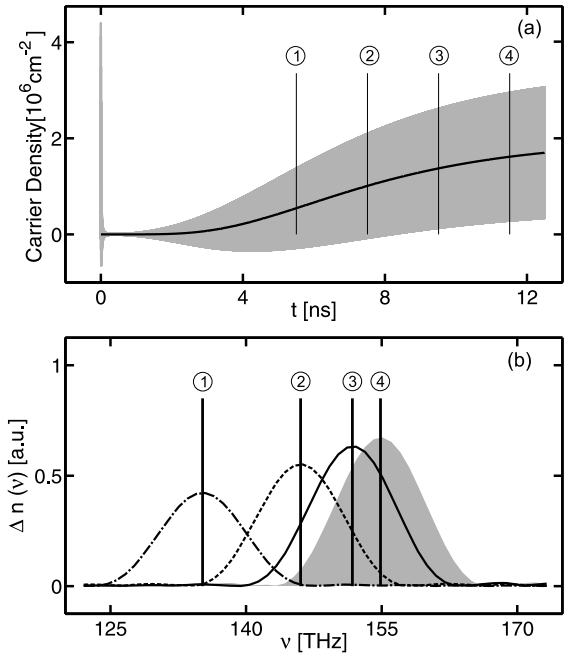

Fig. 3. Analytical results for the excess charge carrier density oscillations at the center of the QW and time-dependent oscillation frequency in comparison to the numerically obtained solution. For further explanation see text.

electron-hole plasma ω_{pl} which is virtually indistinguishable from the renormalized plasma frequency. Thus, we verify that the analytically obtained oscillation frequency correctly reproduces the frequency encountered in the numerical solution. In particular, we note that the renormalization term in (31) is negligible in comparison to the original plasma frequency ω_{pl} such that in a first approximation the instantaneous eigenfrequency of the electron-hole plasma turns out to be a dependable quantity to estimate the frequency of the total charge-density oscillations. Clearly, the frequency of the charge oscillations is easily influenced by the choice of pumping strength since a given pumping rate results in a defined QW charging and so determines the barrier electron and hole densities which in turn determine the plasma frequency. In the late-time regime, we can approximate the plasma frequency by the QW charge

$$\omega_{pl}^2(t) = \frac{e^2}{\epsilon\epsilon_0 m_e} N_e(t) \approx \frac{e^2}{\epsilon\epsilon_0 m_e} \Delta n^{\mathrm{QW}}(t). \tag{33}$$

Thus, it becomes obvious that as Δn^{QW} saturates on a nanosecond time scale also the oscillation frequency reaches a constant value. Therefore, as typical pumping rates yield plasma frequencies in the terahertz (THz) regime, the collective oscillatory motion of barrier charge-carriers in an electrically pumped semiconductor laser device may give rise to coherent emission of THz radiation.

Beside an agreement of the analytical plasma frequency and the frequency of the numerical solution, we also find that the analytically derived formula accurately predicts the average level of total charging. To exemplify this, we compare in the upper frame of Fig. (3) the mean value of the oscillations of the analytically obtained total excess-charge-carrier density $\Delta\bar{n}$ (solid line) to the numerical solution (shaded area).

V. Summary and Outlook

In summary, in this investigation we have analyzed the effect of charging on the carrier dynamics in electrically pumped QW lasers. We introduced a formulation of the problem which shows clearly that both the carriers in the quasi-continuum of states above the band edge of the barrier layers and the confined states of the QW must be treated dynamically to correctly determine the degree of charging. We have shown that the carriers in the unconfined states try to compensate the electric pumping-induced charging at the QW position. The dynamics resulting from stimulated electron-hole recombination and carrier replenishing gives rise to collective charge oscillations and a high degree of overall charge compensation.

The observation of electromagnetic dipole radiation emitted by electrically pumped QW structures in the THz regime may be used to test the detailed properties of the induced charge oscillations. Possibly, this could provide a way to use an electrically pumped semiconductor QW laser as a source of coherent THz radiation.

Appendix A
Parabolic Approximation to the Hartree Potential

Formally, the computation of the Hartree potential is based on a self-consistent solution of the Schrödinger and Poisson equations which form a set of coupled differential equations. Numerically, these equations are usually solved by successive iterations. In a first approximation, however the Hartree potential may be computed noniteratively.

To find a simple expression for the Hartree potential, we reformulate the Hartree term (5) using the following convention for the spatial three-dimensional Fourier transformation

$$f(\mathbf{r}) = \sum_{\mathbf{q}} f_{\mathbf{q}} e^{i\mathbf{qr}} \text{ and } f_{\mathbf{q}} = \frac{1}{L^3}\int d^3r f(\mathbf{r}) e^{-i\mathbf{qr}} \tag{34}$$

and the Fourier transformed Coulomb potential

$$V_{\mathbf{q}} = \frac{e^2}{L^3\epsilon\epsilon_0}\frac{1}{\mid \mathbf{q} \mid^2} \tag{35}$$

with the normalization length L, the electron charge e, the free space permittivity ϵ_0 and background dielectric constant ϵ. With these definitions, we rewrite the Hartree contribution as

$$\begin{aligned} HT(\mathbf{r}_1,\mathbf{r}_2) &= \\ &= -\int \sum_{\mathbf{q}} \frac{e^2}{\epsilon\epsilon_0 L^3}\frac{1}{\mid \mathbf{q} \mid^2}\left[e^{i\mathbf{q}\cdot(\mathbf{r}_2-\mathbf{r})} - e^{i\mathbf{q}\cdot(\mathbf{r}_1-\mathbf{r})}\right]\Delta n(\mathbf{r}) d^3r \\ &= -\sum_{\mathbf{q}} \frac{e^2}{\epsilon\epsilon_0 L^3}\frac{1}{\mid \mathbf{q} \mid^2}\left[e^{i\mathbf{q}\cdot\mathbf{r}_2} - e^{i\mathbf{q}\cdot\mathbf{r}_1}\right]\int \Delta n(\mathbf{r}) e^{-i\mathbf{qr}} d^3r \\ &= -\sum_{\mathbf{q}} \frac{e^2}{\epsilon\epsilon_0}\frac{1}{\mid \mathbf{q} \mid^2}\left[e^{i\mathbf{q}\cdot\mathbf{r}_2} - e^{i\mathbf{q}\cdot\mathbf{r}_1}\right]\Delta n_{\mathbf{q}} \end{aligned} \tag{36}$$

where in the last line we introduced the Fourier transform $\Delta n_{\mathbf{q}}$ of the mean charge carrier density $\Delta n(\mathbf{r})$. Since the Coulomb potential in reciprocal space $V_{\mathbf{q}}$ diverges when $\mathbf{q}$ approaches zero, especially small momenta contribute to

the sum. Thus, we can apply a Taylor expansion for the exponential function, which we truncate by dropping all terms above second order. In addition, we take advantage of the geometry of the QW structure to reduce the problem further. Taking into account explicitly the spatial homogeneity in the QW plane, we derive an expression for the Hartree term which is dependent only on the the crystal momentum $\mathbf{q}_\perp$ and the space coordinate z in direction perpendicular to the QW plane

$$HT(z_1,z_2) = -\sum_{\mathbf{q}_\perp} \frac{e^2}{\epsilon\epsilon_0}\frac{1}{\mid \mathbf{q}_\perp \mid^2} \times \left[i\mathbf{q}_\perp(z_2-z_1) - \frac{1}{2}(\mathbf{q}_\perp z_2)^2 + \frac{1}{2}(\mathbf{q}_\perp z_1)^2 \right] \Delta n_{\mathbf{q}_\perp}. \quad (37)$$

Obviously, the first term in (37) contributes only if $\Delta n_{\mathbf{q}_\perp}$ is antisymmetric since the q-sum runs over positive and negative values. Consequently, the contribution linear in z in (37) vanishes due to the given mirror symmetry of our problem $n_{\mathrm{e,h}}(z) = n_{\mathrm{e,h}}(-z)$. We obtain a parabolic space dependence of the Hartree term on the confinement direction z

$$\begin{aligned} HT(z_1,z_2) &= -\frac{e^2}{2\epsilon\epsilon_0}(z_1^2 - z_2^2)\sum_{\mathbf{q}_\perp}\Delta n_{\mathbf{q}_\perp} \\ &= -\frac{e^2}{2\epsilon\epsilon_0}(z_1^2 - z_2^2)\Delta n(0). \end{aligned} \quad (38)$$

Here, in the second line the relation

$$\Delta n(0) = \sum_{q_\perp} e^{iq_\perp 0}\Delta n_{\mathbf{q}_\perp} \quad (39)$$

is used. Thus, in the parabolic approximation of the Hartree contribution the charge-density distribution $\Delta n(\mathbf{r})$ is represented exclusively by its value at the point of symmetry $\mathbf{r} = 0$. Due to the obvious single-particle character of the Hartree term it may be described by an effective Hamiltonian $\hat{H}^{HO}_{\mathrm{eff}}$, which leads to the same result in the equation of motion as the direct contribution of the Coulomb interaction. It can be easily verified that in second quantization this effective Hamiltonian is given by

$$\hat{H}^{HO}_{\mathrm{eff}}(z) = \int \frac{e^2}{2\epsilon_0\epsilon}\Delta n(0) z^2 \sum_\lambda \hat{\Psi}^\dagger_\lambda(\mathbf{r})\hat{\Psi}_\lambda(\mathbf{r}) d^3r. \quad (40)$$

REFERENCES

[1] N. Tessler, R. Nagar, D. Abraham, G. Eisenstein, U. Koren, and G. Raybon, "Coupling between barrier and quantum well energy states in multiple quantum well optical amplifier", *Applied Physics Letters*, **60**, pp. 665-667, 1992.

[2] N. Tessler, G. Eisenstein, "Modelling carrier dynamics and small-signal modulation response in quantum-well lasers", *Optical and Quantum Electronics*, **26**, pp. 767-787, 1994.

[3] B. K. Ridley, "Space-charge-mediated capture of electrons and holes in a quantum well", *Physical Review B*, vol.50, no.3, pp. 1717-1724, July 1994.

[4] M. Grupen, K. Hess, "Simulation of carrier transport and nonlinearities in quantum-well laser diodes", *IEEE Journal of Quantum Electronics*, vol.34, no.1, pp. 120-139, Jan. 1998.

[5] V. L. Tolstikhin, "Carrier charge imbalance and optical properties of separate confinement heterostructure quantum well lasers", *Journal of Applied Physics*, vol.87, no.10, pp. 7342-7348, May 2000.

[6] C. Z. Ning, W. W. Chow, D. J. Bossert, R. A. Indik, and J. V. Moloney, "Influences of unconfined states on the optical properties of quantum-well structures", *IEEE Journal of Selected Topics Quantum Electronics*, vol.3, no.2, pp. 129-135, April 1997.

[7] H. Haug, S. W. Koch, *Quantum theory of the optical and electronic properties of semiconductors*, Singapore: World Scientific, 5th edition, 2009.

[8] A. Girndt, S. W. Koch, and W. W. Chow, "Microscopic theory of laser gain in semiconductor quantum wells", *Applied Physics A, Materials Science & Processing*, **66**, pp. 1-12, 1998.

[9] M. Kira, S. W. Koch, "Many-body correlations and excitonic effects in semiconductor spectroscopy", *Progress in Quantum Electronics*, **30**, pp. 155-296, 2006.

[10] W. Hoyer, M. Kira, and S. W. Koch, "Pair-correlation functions in incoherent electron-hole plasmas", *Physica Status Solidi B Basic Research*, **234**, pp. 195-206, 2002.

[11] S. Glutsch, N. T. Dan, and F. Bechstedt, "Hartree contribution to the band-gap renormalization in semiconductor microstructures", *Physical Review B*, vol.52, no.19, pp. 13776-13778, Nov. 1995.

[12] M. Lindberg, S. W. Koch, "Effective Bloch equations for semiconductors", *Physical Review B*, vol.38, no.5, pp. 3342-3350, Aug.1988.

[13] F. Jahnke, M. Kira, and S. W. Koch, "Linear and nonlinear optical properties of excitons in semiconductor quantum wells and microcavities", *Zeitschrift für Physik B*, **104**, pp. 559-572, 1997.

[14] S. W. Koch, T. Meier, W. Hoyer, and M. Kira, "Theory of optical properties of semiconductor nanostructures", *Physica E*, **14**, pp. 45-52, 2002.

[15] W. W. Chow, S. W. Koch, *Semiconductor-laser fundamentals*, Berlin, Germany: Springer-Verlag, 1999.

[16] R. Binder, D. Scott, A. E. Paul, M. Lindberg, K. Henneberger, and S. W. Koch, "Carrier-carrier scattering and optical dephasing in highly excited semiconductors", *Physical Review B*, vol.45, no.3, pp. 1107-1115, 1992.

[17] J. Hader, J. V. Moloney, and S. W. Koch, "Suppression of carrier recombination in semiconductor lasers by phase-space filling", *Applied Physics Letters*, **8**, pp. 201112, 2005.

[18] F. Jahnke, S. W. Koch, "Theory of carrier heating through injection pumping and lasing in semiconductor microcavity lasers", *Optics Letters*, vol.18, no.17, pp. 1438-1440, 1993.

[19] W. W. Chow, P. M. Smowton, P. Blood, A. Girndt, F. Jahnke, and S. W. Koch, "Comparison of experimental and theoretical GaInP quantum well gain spectra", *Applied Physics Letters*, **71**, pp. 157-159, 1997.

[20] J. Hader, J. V. Moloney, and S. W. Koch, "Microscopic evaluation of spontaneous emission- and Auger-processes in semiconductor lasers", *IEEE Journal of Quantum Electronics*, vol.41, no.10 pp. 1217-1226, Oct.2005.

[21] W. Hoyer, J. V. Moloney, E. M. Wright, M. Kira, and S. W. Koch, "Thermal wakefield oscillations of laser-induced plasma channels and their spectral signatures in luminescence", *Journal of Physics: Conference Series, Kinetic theory of Nonideal Plasmas*, **11**, pp. 153-168, 2005.

Ada Bäumner is currently working towards the Ph.D. degree in physics at the Philipps-University Marburg, Germany. The main focus of her research is on the microscopic description of the optical properties of semiconductor QW lasers.

Mackillo Kira is an associate professor at the Department of Physics at the Philipps-University Marburg, Germany. His research focuses on the development of a microscopic theory for the consistent description of quantum-optical and many-particle phenomena in semiconductors.

Stephan W. Koch has been a Professor of Physics at the Philipps-University Marburg, Germany, and a Research Professor at the Optical Sciences Center, University of Arizona, Tucson, USA, since 1993. His fields of major current interests include condensed matter theory, optical and electronic properties of semiconductors, many-body interactions, disorder effects, quantum confinement in solids, coherent and ultrafast phenomena, semiconductor laser theory, microcavity effects, and optical instabilities and nonlinearities.

9. Bibliography

Books

[1] G. P. Agrawal and N. K. Dutta. *Long-Wavelength Semiconductor Lasers*. Van Nostrand Reinhold, 1986 (cited on pages 14, 60).

[10] W. W. Chow and S. W. Koch. *Semiconductor-Laser Fundamentals, Physics of the Gain Materials*. Springer, 1999 (cited on pages 8, 16, 32, 35, 59).

[22] H. Haug and S. W. Koch. *Quantum Theory of the Optical and Electronic Properties of Semiconductors*. World Scientific, 2004 (cited on pages 8, 18, 30, 31, 35, 54–56, 58, 59).

[31] F. Jahnke. *A Many-Body Theory for Laser Emission and Excitonic Effects in Semiconductor Microcavities*. Habilitationsschrift,Philipps-University Marburg, 1996 (cited on page 28).

[47] M. Kuznetsov. *VECSEL Semiconductor Lasers: A Path to High-Power, Quality Beam and UV to IR Wavelength by Design in Semiconductor Disk Lasers: Physics and Technology (ed O. G. Okhotnikov)*. Wiley-VCH Verlag GmbH & Co. KGaA, Weinheim, Germany, 2010 (cited on pages 14, 21).

[51] K. Lüdge. *Nonlinear Laser Dynamics: From Quantum Dots to Cryptography*. Wiley-VCH, 2012 (cited on page 23).

[74] Matthias Wichmann. *Untersuchung der Multimode-Emission von optisch gepumpten Halbleiter-Scheibenlasern im Hinblick auf effiziente intrakavitäre Differenzfrequenzerzeugung*. Dissertationsschrift, 2014 (cited on page 25).

Articles

[2] R. Baets, J.P. Van de Capelle, and P. Vankwikelberge. "The modelling of semiconductor laser diodes". In: *Annales des Telecommunications* 43 (1988), pages 423–433 (cited on page 17).

[3] G. Bastard et al. "Variational Calculations on a Quantum Well in an Electric Field". In: *Physical Review B* 28 (1983), pages 3241–3245 (cited on page 52).

[4] A. Bäumner, M. Kira, and S. W. Koch. "Charging Dynamics in Electrically Pumped Quantum Wells". In: *IEEE Journal of Quantum electronics* 45 (2009), pages 1024–1032 (cited on pages 4–6, 8, 9, 53, 54, 56, 58, 60, 62, 64, 66, 68, 74).

[5] A. Bäumner, S.W. Koch, and J.V. Moloney. "Non-equilibrium analysis of the two-color operation in semiconductor quantum-well lasers". In: *Phys. Status Solidi B* 248 (2011), 843846 (cited on pages 3, 5, 6, 8, 9, 37, 39, 74).

[6] R. Binder et al. "Carrier-carrier scattering and optical dephasing in highly excited semiconductors". In: *Physical Review B* 45 (Jan. 1992), pages 1107–1115. DOI: 10.1103/PhysRevB.45.1107 (cited on pages 4, 28, 59).

[7] C. Bückers et al. "Microscopic electroabsorption line shape analysis for Ga(AsSb) /GaAs heterostructures". In: *Journal of Applied Physics* 101 (2007), page 033118 (cited on pages 28, 31).

[8] C. Bückers et al. "Microscopic calculation and measurement of the laser gain in a (GaIn)Sb quantum well structure". In: *Applied Physics Letters* 92 (2008), page 071107 (cited on pages 28, 31).

[9] C. Bückers et al. "Quantum modeling of semiconductor gain materials and vertical-external-cavity surface-emitting laser systems". In: *physica status solidi (b)* 247 (2010), pages 789–808 (cited on page 28).

[11] W. W. Chow et al. "Comparison of experimental and theoretical GaInP quantum well gain spectra". In: *Applied Physics Letters* 71 (July 1997), pages 157–159 (cited on pages 52, 62).

[12] W. W. Chow et al. "Nonequilibrium model for semiconductor laser modulation response". In: *Quantum Electronics, IEEE Journal of* 38 (2002), pages 402–409 (cited on pages 4, 17).

[13] W.W. Chow and S.W. Koch. "Theory of semiconductor quantum-dot laser dynamics". In: *IEEE Journal of Quantum Electronics* 41 (2005), pages 495–505 (cited on page 32).

[14] Sieber, O. D. et al. “Experimentally verified pulse formation model for high-power femtosecond VECSELs”. In: *Appl. Phys. B* 113 (2013), 133145 (cited on page 41).

[15] L. Fan et al. “Linear polarized dual-wavelength vertical-external-cavity surface emitting laser”. In: *Applied Physics Letters* 90 (2007), page 181124 (cited on pages 5, 8, 18, 24, 28, 37, 74).

[16] D. Gershony, C. H. Henry, and G.A. Baraff. “Calculating Optical Properties of Multidimensional Heterostructures: Application to the Modeling of Quaternary Quantum Well Lasers”. In: *IEEE Journal of Quantum Electronics* 29 (1993), pages 2433–2450 (cited on page 52).

[17] A. Girndt, S. W. Koch, and W. W. Chow. “Microscopic theory of laser gain in semiconductor quantum wells”. In: *Applied Physics A: Materials Science & Processing* 66 (1998), pages 1–12 (cited on page 54).

[18] S. Glutsch, N. T. Dan, and F. Bechstedt. “Hartree contribution to the band-gap renormalization in semiconductor microstructures”. In: *Physical Review B* 52 (Nov. 1995), pages 13776–13779. DOI: 10.1103/PhysRevB.52.13776 (cited on page 56).

[19] J. Hader, J. V. Moloney, and S. W. Koch. “Supression of carrier recombination in semiconductor lasers by phase-space filling”. In: *Applied Physics Letters* 87 (Nov. 2005), page 1112. DOI: 10.1063/1.2132524 (cited on page 60).

[21] J. Hader et al. “On the importance of radiative and Auger losses in GaN-based quantum-wells”. In: *Applied Physics Letters* 92 (2008), page 261103 (cited on page 31).

[23] B. Heinen et al. “106W continuous-wave output power from vertical-external-cavity surface-emitting laser”. In: *Electron. Lett* 48 (2012), page 516 (cited on pages 14, 40).

[24] O. Hess and T. Kuhn. “Maxwell-Bloch equations for spatially inhomogeneous semiconductor lasers. I. Theoretical formulation”. In: *Phys. Rev. A* 54 (1996), page 3347 (cited on page 17).

[25] O. Hess and T. Kuhn. “Spatio-temporal dynamics of semiconductor lasers. theory, modelling and analysis”. In: *Progress in Quantum Electronics* 20 (1996), pages 85–179 (cited on page 33).

[26] M. Hoffmann et al. “Femtosecond high-power quantum dot vertical external cavity surface emitting laser”. In: *Opt. Express* 19 (2011), 81088116 (cited on pages 26, 40).

[27] S. Hoffmann and M.R. Hofmann. “Generation of Terahertz radiation with two color semiconductor lasers”. In: *Laser & Photonics Reviews* 1 (2007), pages 44–56 (cited on pages 18, 24, 28, 37).

[28] W. Hoyer, M. Kira, and S. W. Koch. "Pair-Correlation Functions in Incoherent Electron-Hole Plasmas". In: *Physica Status Solidi B Basic Research* 234 (Nov. 2002), pages 195–206 (cited on pages 54, 55).

[29] W. Hoyer et al. "Thermal wakefield oscillations of laser-induced plasma channels and their spectral signatures in luminescence". In: *Journal of Physics: Conference Series* 11 (2005), pages 153–168 (cited on pages 64, 66).

[30] S. Husaini and R. A. Bedford. "Antiresonant Graphene Saturable Absorber mirror for mode-locking VECSELs". In: *private communication* (2013) (cited on page 40).

[32] F. Jahnke, M. Kira, and S.W. Koch. "Linear and nonlinear optical properties of excitons in semiconductor quantum wells and microcavities". In: *Zeitschrift fuer Physik B* 104 (1997), pages 559–572 (cited on pages 17, 31, 32, 57).

[33] F. Jahnke and S. W. Koch. "Theory of carrier heating through injection pumping and lasing in semiconductor microcavity lasers". In: *Optics Letters* 18 (Sept. 1993), pages 1438–1440 (cited on page 59).

[34] U. Keller. "Recent developments in compact ultrafast lasers". In: *Nature* 424 (2003), pages 831–838 (cited on page 25).

[35] U. Keller and A. C. Tropper. "Passively modelocked surface-emitting semiconductor lasers". In: *Phys. rep* 429 (2006), 67120 (cited on page 8).

[36] G. Khitrova et al. "Nonlinear optics of normal-mode coupling semiconductor microcavities". In: *Reviews of Modern Physics* 71 (1999), pages 1591–1639 (cited on page 35).

[37] I. Kilen et al. "Fully microscopic modeling of mode locking in microcavity lasers". In: *J. Opt. Soc. Am. B* 33 (2016), pages 75–80 (cited on pages 47, 75).

[38] M. Kira and S. W. Koch. "Many-body correlations and excitonic effects in semiconductor spectroscopy". In: *Progress in Quantum Electronics* 30 (2006), pages 155–296 (cited on pages 54, 55).

[39] P. Klopp et al. "Pulse repetition rate of 92 GHz or pulse duration shorter than 110 fs from a mode-locked semiconductor disk laser". In: *Appl. Phys. Lett.* 98 (2011), page 071103 (cited on page 40).

[40] A. Knorr et al. "Theory of ultrafast spatio-temporal dynamics in semiconductor heterostructures". In: *Chemical physics* 210 (1996), pages 27–47 (cited on page 18).

[41] S. W. Koch et al. "Theory of optical properties of semiconductor nanostructures". In: *Physica E* 14 (2002), pages 45–52 (cited on page 57).

[42] S.W. Koch, F. Jahnke, and W.W. Chow. "Physics of semiconductor microcavity lasers". In: *Semiconductor Science and Technology* 10 (1995), pages 739–751 (cited on pages 5, 17, 18).

[43] M. Kolesik and J. V. Moloney. “A spatial digital filter method for broad-band simulation of semiconductor lasers”. In: *IEEE Journal of Quantum Electronics* 37 (2001), pages 936–944 (cited on page 7).

[44] G. A. Kosinovsky, M. Grupen, and K. Hess. “Effect of carrier charge imbalance on the threshold current in diode lasers with thin intrinsic quantum wells”. In: *Applied Physics Letters* 65 (1994), pages 3218–3220 (cited on pages 52, 54).

[45] P. Kreuter and B. Witzigmann. “Combined analytical-finite difference time-domain full wave simulation of mode-locked vertical-extended-cavity semiconductor laser”. In: *JOSA B* 7 (2008), pages 1118–112 (cited on page 17).

[46] E. Kühn et al. “Numerical study of the influence of an antireflection coating on the operating properties of vertical-external-cavity surface-emitting lasers”. In: *Journal of Applied Physics* 106 (2009), page 063105 (cited on page 28).

[48] A. Laurain et al. “15W Single frequency optically pumped semiconductor laser with sub-MHz linewidth”. In: *IEEE Photon. Tech. Lett* 26 (2014), 131133 (cited on page 40).

[49] W.L. Li, Y. K. Su, and D.H. Jaw. “The influences of Refractive Index Dispersion on The Modal Gain of a Quantum-Well Laser ”. In: *IEEE Journal of Quantum Electronics* 33 (1997), pages 416–423 (cited on page 52).

[50] M. Lindberg and S. W. Koch. “Effective Bloch equations for semiconductors”. In: *Physical Review B* 38 (1988), pages 3342–3350 (cited on page 57).

[52] M. Matus et al. “Dynamics of two-color laser systems with spectrally filtered feedback”. In: *Journal Optical Society of America B* 21 (2004), pages 1758–1771 (cited on pages 25, 38).

[53] D. A. B. Miller et al. “Band-edge electroabsorption in quantum well structures - The quantum-confined Stark effect”. In: *Physical Review Letters* 53 (1984), pages 2173–2176 (cited on page 52).

[54] D. A. B. Miller et al. “Novel hybrid optically bistable switch: The quantum well self-electro-optic effect device”. In: *Applied Physics Letters* 45 (1984), pages 13–15 (cited on page 52).

[55] D. A. B. Miller et al. “Electric field dependence of optical absorption near the band gap of quantum well structures”. In: *Physical Review B* 32 (1985), pages 1043–1059 (cited on page 52).

[56] J. V Moloney et al. “Nonequilibrium and thermal effects in mode-locked VECSELs”. In: *Opt. Express* 22 (2014), pages 6422–6427 (cited on pages 3, 5, 6, 8, 9, 40, 41, 43, 47, 74, 75).

[57] J.V. Moloney, J. Hader, and S.W. Koch. “Quantum design of semiconductor active materials: laser and amplifier applications”. In: *Laser & Photonics Reviews* 1 (2007), pages 24–43 (cited on page 7).

[58] C. Z. Ning et al. “Influences of Unconfined States on the Optcal Properties of Quantum-Well Structures”. In: *IEEE Journal of Selected Topics in Quantum Electronics* 3 (1997), pages 129–135 (cited on pages 52, 54, 62).

[59] A.E. Paul, R. Binder, and S.W. Koch. “Spectral hole burning and light-induced band splitting in the gain region of highly excited semiconductors”. In: *Physical Review B* 45 (1992), pages 5879–5882 (cited on page 7).

[60] A. H. Quarterman et al. “A passively mode-locked external-cavity semiconductor laser emitting 60-fs pulses”. In: *Nat. Photonics* 3 (2009), 729731 (cited on page 40).

[61] B.K. Ridley. “Space-charge-mediated capture of electrons and holes in a quantum well”. In: *Physical Review B* 50 (1994), pages 1717–1724 (cited on pages 52, 54).

[62] M. Scheller et al. “Room Temperature Continuous Wave Milliwatt Terahertz Source”. In: *Optics Express* 18 (2010), page 27112 (cited on page 14).

[63] M. Scheller et al. “Passively mode-locked VECSEL emitting 682 fs pulses with 5.1 W of average output power”. In: *Electron. Lett.* 48 (2012), 588589 (cited on pages 5, 26, 40).

[64] K. Seger et al. “Carbon nanotube mode-locked optically-pumped semiconductor disk laser”. In: *Opt. Express* 21 (2013), 1780617813 (cited on page 40).

[65] J.I. Shim et al. “Refractive Index and Loss Changes Produced by Current Injection in InGaAs(P)-InGaAsP Multiple Quantum-Well (MQW) Waveguides”. In: *IEEE Journal of Selected Topics in Quantum Electronics* 1 (1995), pages 408–414 (cited on page 52).

[66] N. Tessler and G. Eisenstein. “Distributed nature of quantum-well lasers”. In: *Applied Physics Letters* 62 (1993), pages 10–12 (cited on page 52).

[67] N. Tessler and G. Eisenstein. “Modelling carrier dynamics and small-signal modulation response in quantum-well lasers”. In: *Optical and Quantum Electronics* 26 (1994), pages 767–787 (cited on pages 52, 54).

[68] N. Tessler et al. “Coupling between barrier and quantum well energy states in multiple quantum well optical amplifier”. In: *Applied Physics Letters* 60 (1992), pages 665–66 (cited on page 54).

[69] A. Thränhardt et al. “Nonequilibrium gain in optically pumped GaInNAs laser structures”. In: *Applied Physics Letters* 85 (2004), page 5526 (cited on pages 5, 27, 32).

[70] A. Thränhardt et al. “Microscopic modeling of the optical properties of semiconductor nanostructures”. In: *Journal of Non-Crystalline Solids* 352 (2006), pages 2480–2483 (cited on pages 5, 27, 32).

[71] V.I. Tolstikhin. “Carrier charge imbalance and optical properties of separate confinement heterostructure quantum well lasers”. In: *Journal of Applied Physics* 87 (2000), pages 7342–7348 (cited on pages 52, 54).

[72] E. S.-M. Tsui, P. Blood, and A. I. Kucharska. “Charge neutrality in quantum well structures ”. In: *Semiconductor Science Technology* 5 (1990), pages 333–339 (cited on page 52).

[73] T.-L. Wang et al. “Quantum design strategy pushes high-power vertical-external-cavity surface-emitting lasers beyond 100 W”. In: *Laser & Photon. Rev.* 6 (2012), 1214 (cited on page 14).

[75] K. G. Wilcox et al. “4.35 kW peak power femtosecond pulse mode-locked VECSEL for supercontinuum generation”. In: *Opt. Express* 21 (2013), 1599 1605 (cited on pages 26, 40).

[76] A.R. Zakharian et al. “Experimental and theoretical analysis of optically pumped semiconductor disk lasers”. In: *Applied Physics Letters* 83 (2003), pages 1313–1315 (cited on page 17).

[77] C. A. Zaugg et al. “Ultrafast and widely tuneable vertical- external-cavity surface-emitting laser, mode-locked by a graphene-integrated distributed Bragg reflector”. In: *Opt. Express* 21 (2013), 3154831559 (cited on pages 26, 40).